Paul Albert Harry Kastner, BSc

Consideration of Multiple Temperatures in Hybrid Linear Prediction Models of Multi-Energy Systems

Master's Thesis

to achieve the university degree of
Diplom-Ingenieur

Master degree program: Electrical Engineering

submitted to
Graz University of Technology

Supervisor
Assoc.Prof. Dipl.-Ing. Dr.techn. Markus Reichhartinger

Co-Supervisor
Dipl.-Ing. Dr.techn. Daniel Muschick

Institute of Automation and Control
Head: Univ.-Prof. Dipl.-Ing. Dr.techn. Martin Horn

Faculty of Electrical and Information Engineering

Graz, March 2021

Affidavit

I declare that I have authored this thesis independently, that I have not used other than the declared sources/resources, and that I have explicitly indicated all material which has been quoted either literally or by content from the sources used. The text document uploaded to TUGRAZonline is identical to the present master's thesis.

22.05.2021

Date

Signature

Abstract

In order to facilitate the transition towards future carbon neutral energy systems, intelligent *energy management systems* (EMS) may be employed to ensure reliable and efficient energy provision despite the volatile availability of most renewable energy carriers.

A frequently used control strategy within these EMS is *model predictive control* (MPC) in combination with hybrid linear prediction models. Although this notion of hybrid linear prediction models facilitates the derivation of rather simple, yet accurate system models for a variety of different classes of energy systems, it severely complicates the consideration of temperature-dependent behavior of components within heating and cooling systems given the inherent bilinearity of thermal energy transfer by convection. Therefore, based on recent advancements in this field [17], this thesis proposes a novel approach to compose hybrid linear prediction models of components within heating and cooling systems that facilitate the consideration of temperature-dependent behavior.

The proposed general component models were integrated into an existing optimization-based EMS framework and subsequently validated by means of numerical simulations as part of a representative case study. The obtained simulation results indicate that the proposed prediction models and their respective implementations result in reasonable EMS behavior. Furthermore, the usage of the proposed prediction models was shown to increase the available control flexibility for optimizing the operation of the investigated energy system, which is expected to entail a higher system efficiency if the developed EMS would be deployed. However, the use of the novel prediction models significantly increases the computational complexity of the control optimization problem by introducing a considerable amount of auxiliary binary optimization variables. As a result, high solving times were observed

as part of the conducted case study, a circumstance that may potentially limit the applicability of the proposed methods and models.

Kurzfassung

Die vermehrte Integration von erneuerbaren Energiequellen in die Energiesysteme der Zukunft kann durch den Einsatz von intelligenten Energiemanagementsystemen (EMS) unterstützt werden. Mithilfe dieser EMS kann ein zuverlässiger und effizienter Anlagen-/Systembetrieb trotz der typischerweise schwankenden Verfügbarkeit von erneuerbaren Energieträgern sichergestellt werden.

Eine innerhalb von EMS häufig eingesetzte Regelungsstrategie ist die modellprädiktive Regelung. Die hierfür benötigten Modelle der zu regelnden Energiesysteme werden, aus Gründen der numerischen Komplexität, häufig als hybride lineare Modelle formuliert. Dieser Umstand erschwert die präzise Modellierung des temperaturabhängigen Verhaltens von Heizsystemkomponenten, da das physikalische Phänomen der Wärmeübertragung durch Konvektion nur durch bilineare Gleichungen akkurat beschrieben werden kann.

Aufbauend auf aktuellen Forschungsarbeiten und Fortschritten im Bereich der hybriden linearen Modellierung von Heizsystemen [17], werden in dieser Arbeit neue Methoden zur hybriden linearen Modellierung verschiedenster Komponenten von Heizsystemen präsentiert. Die entwickelten Modelle sollen einerseits das temperaturabhängige Verhalten der Komponenten ausreichend genau abbilden, andererseits simpel genug sein um als Prädiktionsmodelle in modelprädiktiven Regelungen verwendet werden zu können.

Im Rahmen der vorgestellten Arbeit, wurden die entwickelten Modelle in ein bestehendes EMS Software-Framework integriert, und im Zuge einer repräsentativen Fallstudie analysiert. Die Funktionsfähigkeit und Anwendbarkeit der entwickelten Modelle und Methoden konnten anhand der erhaltenen Ergebnisse validiert werden. Darüber hinaus konnte gezeigt werden,

dass die Berücksichtigungen des temperaturabhängigen Verhaltens der modellierten Komponenten, die Möglichkeiten/Freiheitsgrade eines EMS bei der Betriebsoptimierung von Heizsystemen erhöhen kann. Diese zusätzliche Flexibilität sollte eine gesteigerte Betriebseffizienz nach sich ziehen, sollte das im Rahmen der Fallstudie entwickelte EMS tatsächlich im Realbetrieb eingesetzt werden.

Ein Nachteil der verwendeten Prädiktionsmodelle ist jedoch der merklich erhöhte Rechenaufwand für die modellprädiktive Regelung. Dieser Umstand kann je nach Anwendung die tatsächlich erreichte Effizienzsteigerung verringern, oder sogar die Anwendung der vorgestellten Methoden und Modelle an sich verhindern.

Contents

List of Figures

List of Tables

1. Introduction

The last decades have shown an increased global strive to decarbonize the global means of energy production. This was motivated by legally binding obligations defined in international treaties such as the Kyoto Protocol [24] or the Paris Agreement [25] in order to contain the detrimental consequences of global warming and climate change.

Nevertheless, within the *European Union* (EU) thermal energy for heating and cooling, which accounts for 50 % of the total final energy demand, is still mainly provided either directly or indirectly through the combustion of fossil fuels [7]. Among the renewable sources, only biomass is significantly utilized making up 12 % of the total energy demand. Alternative *renewable energy sources* (RES) and technologies, such as solar thermal energy or heat pumps, have so far only been marginally employed, accounting for a combined share of about 1 %. Following from this, it is apparent that the provision of thermal energy contributes significantly to the emission of greenhouse gases and pollutants, as well as to the depletion of fossil fuel resources within the EU.

This limited penetration of thermal energy systems by means of RES is especially noteworthy when compared to the electrical power industry where the share of RES is more than twice as high. In modern electrical energy systems, the transmission and distribution of energy between various spatially distributed and far apart energy producers and consumers is facilitated by a synchronous grid. Diverging voltage specifications and requirements of different producers, consumers and the transmission grid itself may be efficiently resolved by utilizing specific converters and transformers. This facilitates the integration of many different forms of power producers into the overall electrical energy system.

In stark contrast to that, thermal energy is typically generated individually for each process and application at the site of demand, or in small-sized local grids in the context of district heating. Different components, processes and applications typically require thermal energy in specific temperature ranges that often cannot be directly supplied by RES. This is due to the fact, that most RES provide thermal energy at a lower energy density, i.e. typically at lower temperature differences, compared to conventional energy sources. Unlike varying voltage requirements in electrical systems, these diverging temperature requirements significantly complicate the usage of RES within thermal energy systems. Considering that, depending on the application, reconciling varying temperature specifications among different producers and consumers may require significant additional (conventional) primary energy input for auxiliary heating and cooling.

Another general property of RES that impedes their large-scale integration into any form of energy systems, is the fact that they are mostly non-dispatchable, meaning that their availability is significantly influenced by ambient conditions and temporal fluctuations. It is important to note, that these fluctuations generally do not occur in tandem with variations of the energy demand. Hence, system/grid stability, i.e. stable energy provision that meets the instantaneous demand, may be compromised by large-scale integration of RES. To illustrate this, consider e.g. solar thermal energy whose availability rises with increased solar irradiance which, in turn, typically correlates with a lowered energy demand for space heating. From the above it is apparent that, if energy is generated only locally as opposed to generated decentralized and distributed over a grid, these locally occurring fluctuations may have an increased adverse effect on the stability of the energy system and hence impair the increased utilization of RES.

In order to maintain the stability and also to increase the overall efficiency of energy systems that ought to comprise a significant share of RES, suitably large energy storage capabilities to smoothen the non-concurrent fluctuations of energy demand and availability, need to be installed. However, efficient large-scale energy storage is technically difficult and typically associated with significantly increased capital expenditure and operational costs [28]. Furthermore, it may itself pose several environmental problems (see e.g. [13]).

The variety of challenges and requirements entailed by a large-scale integration of RES into existing energy systems may restrain many system operators from utilizing them. This is especially the case for thermal energy systems, where one has to consider the fact that thermal energy is typically generated at the site of demand. As a result, many thermal energy systems are embedded within processes and plants which are not primarily concerned with the production of thermal energy, but rather with the production of certain goods or services. Therefore, the significant initial economic investment, the considerable amortization period and the increased system complexity entailed by the integration of renewable energy sources/technologies may seem unfavorable. Especially considering that the resulting decrease of the environmental footprint of a respective plant, or the expected lower costs for primary energy feedstock, may be of only secondary concern to the plant operators, whose primary concern will typically always be maximized quality of service or product quality.

1.1. Energy Management Systems for Multi-Energy Systems

The operational obstacles and drawbacks associated with the increased integration of RES may be significantly mitigated by utilizing intelligent computer systems that support the monitoring, control and operation of a considered energy systems. As a result, several high-level control systems — referred to as *energy management systems* (EMS) — are currently being, or have been, developed and deployed to autonomously monitor and control the energy resource allocation within stand-alone energy provisioning plants or energy systems that are embedded within a plant or process.

The main objective of such an EMS is to devise a plan of operation defining the instantaneous and future utilization of all individual system components based on current and expected future conditions. In mathematical literature this task of devising a good operation strategy is fittingly referred to as the *unit commitment problem*. Naturally, the solution to the unit commitment problem ought to operate the respective energy system as securely, reliably and efficiently as possible. Therefore, it must ensure the stable supply of

energy demand whilst minimizing operational costs, emissions of pollutants and green house gases, and adhering to defined operational and regulatory limitations. Considering this set of requirements, the task of deriving a suitable solution to the unit commitment problem may quickly become very challenging depending on the complexity of the investigated energy system and the defined specific operational goals and constraints. This latter point is especially noteworthy considering that besides increased system complexity entailed by the integration of RES, modern (thermal) energy systems are increasingly interconnected with other energy systems and sectors.

This coupling of the energy sectors is expected to continuously increase over the next years, due to the increased deployment of technologies such as air source heat pumps, which efficiently transform electrical into thermal energy, or the utilization of industrial waste heat for residential and commercial space heating. Resulting from this, future EMS will have to consider the increased flexibility entailed by the coupling of different energy sectors in order to maximize the overall efficiency of the combined energy system as a whole.

In the following text these interconnected energy systems, which inherently may comprise multiple forms of primary energy, will be generally referred to as *multi-energy systems* (MES). Within a generic MES, energy generation and consumption may not be entirely separable into separate system components. Consider e.g. the aforementioned air source heat pump which at the same time consumes electrical energy and generates thermal energy. In order to encompass all entities that may generate and/or consume energy of one form or another they will here be referred to as *prosumers*[1].

To illustrate this newly defined class of systems by means of an example, consider a modern urban district where, apart from connections to the main electrical grid, electricity is generated by local *photovoltaic* (PV) systems on the roofs of the buildings within the district. Thermal energy for space heating and domestic hot water might be partially provided by utilizing waste heat of a neighboring industrial plant along with auxiliary heat pumps or gas boilers which are located within the district compound to function as dispatchable energy supply backup systems. Additionally, in order to handle the differences between concurrent energy demand and renewable

[1] **Pro**(ducer) + (Con)**sumer**

energy availability, and to efficiently accommodate for peaks in the energy demand or generation profiles, such a MES would also include several means of energy storage such as e.g. batteries and *thermal energy storages* (TES).

This example, whilst illustrating some of the available possibilities to integrate renewable energy sources and technologies into local thermal-electric energy systems, also exemplifies the significant increase in system complexity entailed by the resulting decentralized, multi-agent energy generation. As a consequence of this increased complexity of MES, to this day only few EMS for MES have been designed and deployed. Nevertheless, in light of the potential benefits entailed by considering MES, a substantial amount of recent research is concerned with expanding previously developed EMS strategies for single-energy systems to the general case of MES.

Whilst for the case of single-energy systems, especially electrical energy systems, many potential management strategies have been proposed (see chapter 2 for a brief review of developed and in-use methods), when considering MES all proposed energy management strategies use so-called *model predictive control* (MPC) to determine the current and future unit commitment of the investigated MES. Within MPC, the future behavior of an investigated system is analyzed generally based on a discrete-time system model, referred to as the *prediction model*, at a finite set of discrete future time instances separated by a respective time interval, referred to as the *sampling period*. The predicted system behavior is then evaluated based on a set of defined performance metrics, typically referred to as *costs*. Based on these costs an optimization problem is constructed, whereby the optimal series of system actuations over a given time horizon, referred to as *prediction horizon*, is determined by solving said optimization problem. In addition, operational constraints and heuristics, if not already considered by means of costs, may be included into the optimization problem by means of constraints on the considered optimization variables.

The finesse of MPC is rooted in the fact that optimization occurs in regular "short" time intervals, namely the sampling period, where only the first time step of each computed solution of the optimization problem — the time series of optimal actuations — is executed before the prediction and optimization process is repeated for the advanced prediction horizon. Hence, this procedure is also often fittingly referred to as *receding horizon control*.

The consideration of potential changes of current and expected conditions, performance metrics as well as operational constraints in every optimization cycle naturally renders this control strategy adaptive. This circumstance may be considered as one of the main motivations for employing MPC in EMS for MES, considering that the behavior of any MES that contains a considerable amount of renewable energy carriers is significantly influenced by varying environmental conditions, the resulting resource availabilities, and the ever-changing energy demand, that may be hard to accurately predict over a long period of time.

1.1.1. Choice of the Class of Prediction Models

The accuracy of the chosen prediction model significantly influences the derived plan of operation: Only physical phenomena that are represented within the prediction model can be considered as part of the behavioral analysis of the MES. However, increased model accuracy generally tends to entail increased model complexity, which in turn results in an increase of computational effort necessary to derive a suitable solution to the optimization problem. Considering that within MPC the defined optimization problem needs to be solved frequently, a trade-off between prediction model accuracy and optimization problem complexity usually has to be made. Important considerations in that regard are e.g. the desired sampling period, i.a. depending on the volatility of the expected conditions, and the desired length of the prediction horizon, given that both parameters significantly affect the stability and performance of the resulting controller.

One common method for reducing the complexity of the optimization problem is to represent the dynamics of the the investigated system, as well as all constraints and costs, by means of linear expressions of continuous-valued variables. This measure allows for the utilization of highly efficient numerical solvers, which have been specifically developed over the last decades for the resulting family of optimization problems, which are referred to as *linear programs* (LP).

In the context of modeling MES, however, the additional inclusion of binary system variables, representing discrete-valued system states and decisions

such as switching equipment on or off, is typically considered necessary to obtain descriptive prediction models. The resulting prediction models comprise both continuous and integer variables and are referred to as hybrid linear models. The associated MPC optimization problem is typically posed as a *mixed-integer linear program* (MILP). Similarly to LP, a variety of commercial and freely available numerical solvers that offer reasonable performance for small- to medium-scale problems have been specifically developed for MILP. Nevertheless, it is important to note that the numerical complexity of an optimization problem generally may increase exponentially with the number of included binary optimization variables. Therefore, it is generally preferable to limit the consideration of auxiliary binary variables to only the most significant cases.

The utilization of generic hybrid *non*-linear prediction models would entail that optimization problems categorized as *mixed-integer non-linear programs* (MINLP) would have to be solved. Although these days designated solvers for MINLP may be available, they usually require "long" solving times to even obtain a suitable pseudo-optimal solution, given i.a. the problem of emerging local minima and the dependency of solutions on the initial guesses. This circumstance usually precludes the usage of hybrid non-linear prediction models for MPC applications.

1.1.2. The Bilinearity of Convective Energy Transfer

Most prosumers in MES, namely most energy converters and energy consumers, can be represented by means of hybrid linear prediction models without much loss of accuracy. One reason for this being the rather long sampling periods used in MPC-driven EMS which are usually significantly higher than the time constants of the considered prosumers. Thus, most prosumer dynamics can typically be sufficiently well approximated by constant gains or first order linear systems, reducing the computational complexity of the associated optimization problem. Besides, one might add that in the context of hybrid linear systems, non-linear prosumer dynamics can be approximated as *piece-wise affine* functions by introducing additional binary variables and mixed-integer linear constraints.

However, one noteworthy problem when deriving hybrid linear prediction models for MES — and in that regard specifically hydronic heating and cooling systems — is the representation of energy transfer between prosumers by means of convection, and the associated representation of thermal energy storage by means of sensible heat storages, which are the most common form of TES within hydronic systems. In hydronic heating and cooling systems, prosumers are connected by a pipe network. A fluid, generally referred to as the *heat-transfer medium* and typically water-based, is circulated to transfer thermal energy between them by means of convection[1].

The indicated modeling problem stems from the circumstance that the rate of energy transferred by a stream of heated or cooled heat-transfer medium to a prosumer may be approximated in steady-state by:

$$\dot{E}_{\mathrm{conv}} \approx \dot{m} \cdot \left[c_p \left(T_{\mathrm{f}} \right) \cdot T_{\mathrm{f}} - c_p \left(T_{\mathrm{r}} \right) \cdot T_{\mathrm{r}} \right] . \tag{1.1}$$

Here, $\dot{E}_{\mathrm{conv}}$ denotes the temporal change of the inner energy of a prosumer due to energy transferred by convection. It is defined through the mass flow rate $\dot{m}$ into (feed path) and out of (return path) the considered prosumer, the isobaric specific heat c_p, as well as the temperature of the heat-transfer medium in the feed (T_{f}) and respective return (T_{r}) path.

From the perspective of an EMS, whose objective is to allocate a certain amount of consumed/produced thermal energy to each respective prosumer, one finds (1.1) to be bilinear. Both temperature and mass flow rate would generally be considered as degrees of freedom and, as such, optimization variables within an optimization-based EMS.

The straight-forward approach to address the apparent conflict with respect to the notion of hybrid linear prediction models is to simply define one of the variables, mass flow rate or temperature, to have a constant value. Naturally, for the case of hydronic systems where the mass flow rate is typically directly modulated by a mass flow controller, and considering that the typical operating temperatures of the utilized equipment are usually well

[1] Please note that in this thesis, contrary to nomenclature found in some classical textbooks on heat and mass transfer, the term *convection* will strictly refer to energy transfer by bulk motion of matter only, as opposed to heat transfer from a surface to a moving fluid or gas.

defined, the usual choice would be to fix both feed and return temperatures to their respective desired constant operating point for each prosumer.

The resulting linearization of (1.1) entails significant drawbacks, most notably the apparent decrease in prediction model accuracy and flexibility, i.e. flexibility for the EMS to optimize the operation of a considered system. While some flexibility still exists by changing the temperature levels differently for each optimization step, it is not clear how the temperatures should then be chosen. One would have to rely either on heuristics or on an outer optimization loop that varies the temperature levels, thus greatly increasing the computational complexity.

To illustrate the potential adverse ramifications of this circumstance, consider a heating system that comprises a solar thermal collector. The energy output of the collector — and, hence its efficiency — is known to depend on the temperature difference between the collector and the ambient surroundings [11]. An increased temperature difference entails higher thermal energy losses and, thus, reduces the efficiency of the collector. With the introduced linearization, the collector inlet and outlet temperatures are always assumed to be constant. A resulting plan of operation may not utilize the solar thermal collector in the most efficient way, given that its energy yield cannot be maximized by adjusting the inlet or outlet temperature in accordance with the current or expected environmental conditions — specifically solar irradiance and ambient temperature —, nor the operational conditions, i.e. the temperature range currently accepted by the other prosumers within the system.

In addition to not being able to account for temperature-dependent efficiencies of equipment, another issue concerns the fact that different prosumers may require thermal energy at different temperature levels to work efficiently, or even to work at all. This circumstance cannot be considered within the prediction model of a MES where different prosumers are connected to the same TES or thermal energy source, given that through the presented linearization the feed and return temperatures of every prosumer are assumed stationary and, hence necessarily equal for all connected prosumers.

In a practical application this issue might present itself if e.g. a solar thermal collector and the generator of an absorption chiller are connected to a central sensible heat storage. While a solar thermal collector is most efficient at

lower inlet and outlet temperatures, an absorption chiller typically requires thermal energy at higher temperatures to function most efficiently. As a result, the choice of inlet and outlet temperatures of the TES presents a general compromise between the different temperature specifications of the connected prosumers. This problem has to be resolved at the design stage and will, in general, inherently limit the performance of the EMS.

Besides these issues regarding optimizing the utilization of individual prosumers, it is important to note that the typically chosen prediction models to represent sensible heat storages, given the notion of constant temperatures, are very simple. The most common model is a simple first-order integrator with a linear loss term [27]. Within these simplified models the degree of temperature stratification within a sensible heat storage is only crudely approximated. However, this parameter is of fundamental importance for the efficiency of heating and cooling systems, especially when prosumers with significantly different temperature specifications are connected to the same TES.

To mitigate the illustrated issues a different approach to modeling energy transfer by convection and sensible heat storage is necessary. If temperature — not mass flow rate — is designated to be the stationary quantity, different discrete temperature levels would have to be distinguished within a sensible heat storage. As a result, energy transfer by convection could be represented as a superposition of mass streams at these discrete temperature levels. In this modeling context, however, there are several complicated questions that need to be resolved i.a.:

1. How is the temperature distribution within a sensible heat storage defined by means of discrete stationary temperature levels such that the stored energy is accurately represented?
2. How is this distribution reflected in the temperature of the in- and outflowing mass streams that charge respectively discharge a sensible heat storage?
3. How can temperature-dependent energy and exergy losses be considered?
4. If energy transfer is defined by a combination of mass streams at discrete temperature levels, how can prosumers be modeled accordingly such that their temperature-dependent behavior is represented well?

1.2. Thesis Objectives

Motivated by the preceding remarks, the main objective of this thesis is to integrate a recently developed advanced hybrid linear prediction model of sensible heat storages ([17] and [31]) into an existing modular EMS framework[1]. Within the framework, MPC with hybrid linear prediction models is utilized to devise adequate operation strategies for MES, considering potentially both economic and environmental aspects. Energy transfer by means of convection is for now represented as simple directed energy flows, i.e. the feed and return mass streams are assumed to have constant, fixed temperatures within the prediction horizon. In contrast to the simple integrator model, the newly proposed TES model distinguishes several distinct layers of constant temperature but varying height to better approximate the actual temperature distribution of the medium within a sensible heat storage. Consequently, this requires an associated re-design of the representation of connections between prosumers exchanging thermal energy by means of convection, and the extension of existing prosumer prediction models to represent prosumer behavior at varying temperature levels.

The integration of the new thermal storage model and the enhanced method for representing convective energy transfer will inevitably increase the computational complexity of the MPC optimization problem. However, it is anticipated that through these adaptations, future EMS that use the framework will facilitate a more efficient operation of MES that comprise hydronic subsystems and, hence justify the expected increase in computational complexity. This expectation is based on the following premises: First, the accuracy of the utilized prediction models of sensible heat storages is improved to better approximate their actual real-world behavior, including the physical phenomena of temperature-dependent ambient losses and exergy losses through axial conduction. Consequently, the consideration of these phenomena may allow an EMS to potentially make better decisions about when and how to charge a storage with regards to when the stored energy actually might be needed, and the losses that occur in the meantime. Second, the integration of the proposed method of representing convective energy transfer into the prediction model of a MES, i.e. the prediction models

[1] Developed at *BEST – Bioenergy and Sustainable Technologies GmbH* Graz, Austria.

of the individual prosumers, is expected to facilitate the consideration of temperature-dependent efficiencies (or performance factors) of each individual prosumer. Therefore, it may be possible to assess the most efficient, both current and future, operating temperature of each prosumer. Based on this assessment, the derived plan of operation for an investigated MES may be adjusted accordingly, such that the overall system efficiency is maximized.

Besides the discussed expansion of the existing framework, an informative case study based on actual plant data was conducted as part of this work. Its main objectives are the verification of the adapted framework, specifically the adapted prosumer prediction models, and the evaluation of the potential performance improvements and drawbacks entailed by the conducted framework adaptations.

1.3. Document Organization

The remainder of this document comprises a presentation of the conducted theoretical work and the numerical simulations which were conducted to validate the adapted prediction models and to evaluate the resulting changes in the EMS performance. It is organized as follows:

Chapter 2 contains a brief general overview over the past development of, and research into EMS, as well as an overview over the usually employed operating principles and control strategies. After that, the EMS framework that this thesis is built upon will be generally discussed. Specific emphasis will be placed on the used MPC strategy, namely the chosen class of prediction models and performance metrics. Next, the proposed novel hybrid linear prediction model to represent sensible heat storages, and the associated method of representing energy transfer by bulk motion of matter, which are the theoretical basis of this thesis, will be outlined.

Chapter 3 is concerned with the derivation of enhanced prosumer prediction models, which incorporate the mentioned novel method of representing energy transfer by convection. First, a brief review of the relevant fundamental thermodynamic principles of mass and energy balance and the resulting general physical model of a generic prosumer within a hydronic system

is given. Second, the developed enhancements of the existing prosumer prediction models, which were developed based on the notion of fixed feed and return temperatures, to now consider varying temperatures and, hence temperature-dependent prosumer behavior will be presented. Third, the integration of the enhanced prosumer models, as well as the integration of the proposed novel model of sensible heat storages into the EMS framework, will be discussed.

The functionality of the developed prediction models and the resulting EMS is analyzed in Chapter 4 by means of a representative case study. This case study is concerned with the design of an EMS for an industrial winery where heating and cooling are partially provisioned by means of a newly integrated solar thermal collector array and an absorption chiller.

After an analysis and a discussion of the obtained results. The overall potential and drawbacks of the presented prediction model enhancements are discussed in Chapter 5. Finally, to conclude the presented thesis, a brief outlook for possible improvements and necessary future work is given.

1.4. Notation

As is practice in most control theory literature bold lower case letters (e.g. $\mathbf{x}$ or $\mathbf{b}$) will denote vectors, whilst bold capital letters will be employed to represent matrices (e.g. $\mathbf{A}$). Individual values of a discrete-time series will be denoted by an appropriate time index subscript. Parentheses are used to denote functions defined over continuous-valued variables. Time derivatives will be denoted by a dot over the respective function/variable identifier.

2. Review and Background

The following chapter summarizes the necessary background information to further define the context of this thesis and to subsequently easily follow the further course of this work.

For this purpose a summary of the general development of EMS and a brief review of common operating principles of modern EMS, specifically their utilized control strategies are presented.

Subsequently, the existing control framework that this thesis expands upon is presented and discussed with respect to its general design, facilitated functionalities and underlying operating principles. The main focus in that regard is on the specifics of the utilized control strategy and the associated system representation, namely MPC with hybrid linear prediction models. Considering this notion of hybrid linear prediction models, the bilinear phenomenon of energy transfer by convection (bulk motion of matter) is represented by means of the method that was illustrated in the previous chapter, where the feed and return temperatures of a prosumer are assumed stationary over the whole prediction horizon. This representation of energy transfer by convection naturally affects how thermal energy storage, specifically sensible heat storage, may be modeled. In the presented framework sensible heat storages are represented by means of first-order integrator models with linear losses depending on their *state of charge* (SOC).

Albeit being quite simple, there are various drawbacks associated with this representation of thermal energy transfer and sensible heat storage. Therefore, alternative hybrid linear representations of the two phenomena that are proposed in literature are presented within this chapter, and analyzed with respect to their usability for prosumer prediction models in MPC-driven EMS. In particular, the thermal energy storage model proposed by Muschick et al. [17] will be examined in detail. It is this model that was analyzed

and integrated into the existing EMS framework during the course of this thesis.

2.1. Energy Management Systems

The term "energy management system" is frequently used in different contexts and with different implications, depending on the scope of the specific application or the individual field of application or research. As a result, there is no universal definition of the specific objectives, working principles or necessarily provided functionalities of an EMS.

In the context of electrical power systems an attempt in generally defining the physical appearance and scope of an EMS may be found in the IEC 61970 standard [10]. This standard defines an EMS as:

> "A computer system comprising a software platform providing basic support services and a set of applications providing the functionality needed for the effective operation of electrical generation and transmission facilities so as to assure adequate security of energy supply at minimum cost.".

The apparent focus on electrical energy systems in the above definition may stem from the historic prevalence of these systems in both research into and actual deployment of EMS. This prevalence followed from the relatively early integration of small-scale power plants and RES into the existing, formerly rather centralized, wide-area electric power grids. Today, electrical energy systems are generally characterized by distributed (decentralized) energy generation by a great number of different producers, utilizing various forms of primary energy. This circumstance naturally entails a significant increase in system complexity. As a result, a concerted research effort was and still is undertaken to address the resulting issues regarding e.g. the reliability of energy provision or grid stability by means of sophisticated control systems, i.e. EMS. Besides, an increasing amount of research nowadays is concerned with utilizing the increased system flexibility, entailed by distributed multi-agent energy generation, within the developed EMS to

increase the efficiency of the considered electrical energy systems with respect to not only economic, but also environmental criteria.

Within this context, a distinct novel area of research emerged concerned with so-called *smart grids* where the main research objective is to facilitate the optimal operation of distributed electric energy systems by intelligent, computer-supported coordination and allocation of the available resources. An important prerequisite for the success of this planning effort, however, is the availability of reliable real-time information on the current and future consumer demand, storage capabilities and environmental conditions. The efficient and reliable acquisition and provision of this data forms a distinct sub-field of smart grid related research. Subsequently, control systems process the provided data and coordinate adequate power transmission. Besides that, they may also directly set power production or consumption incentives, by e.g. adapting the bid and ask price of electrical energy in real-time, for the purpose of load balancing and load shifting.

Given the immense system complexity of modern wide-area electric synchronous grids, a hierarchical perspective emerged, whereby the focus is on the optimal operation of smaller and localized groups of consumers and distributed electrical energy resources, which are referred to as *microgrids*. Within each microgrid configuration, the operational goal is to meet local demand by optimal utilization of locally available, typically partially renewable, energy resources and energy storage capabilities. Resulting from this, each microgrid may be viewed as an individually controllable and at least partially autonomous entity with clearly defined spatial boundaries and a defined interface to the wide-area synchronous grid (*macrogrid*). In many microgrid applications this interface allows for bidirectional energy flow, i.e. energy may be purchased from the wide-area synchronous grid, whilst potential generation surpluses may be sold. Consequently, this hierarchical configuration may simplify the task of managing and optimizing entire, heavily interconnected electrical energy systems, given the reduced system size and the typically substantial degree of autonomy of the individual microgrids.

From the above discussion, it is evident that the necessary functionalities that have to be provided by an EMS vary greatly with the scope of the

individual application. They range from complete wide-area grids, to microgrids or even systems as small as individual industrial plants or residential dwellings with e.g. a locally installed PV system. Whilst EMS for the electrical power grid as a whole are concerned mainly with stability and reliability of power transmission, EMS for microgrids or smaller applications are specifically attuned to the types and numbers of included prosumers in order to optimize their respective operation, the available infrastructure regarding data acquisition and information exchange, and the type of available interfaces to the macrogrid. Resulting from this variety of application-specific objectives and requirements, most actually deployed EMS are tailor-made for a specific application.

Instead of considering only purely electrical energy systems, an increasing amount of recent research is also concerned with a more holistic perspective that focuses on the operational optimization of MES. There, different forms of energy and the coupling of different energy sectors are specifically considered, as opposed to treating every energy sector individually [12]. The coupling of different energy sectors is assumed to continuously increase over the next years and decades, considering i.a. the increasing electrification of the transport sector and the increasing deployment of technologies such as electrically powered heat pumps. Hence, the extensions of the developed methods for optimizing the operation of electrical energy systems to consider MES instead, may prove to be useful for reducing the overall operational costs and emissions of the energy industry. This conjecture may be especially valid for the case of thermal energy systems, in light of the large contribution of the heating sector to the total final energy consumption and to the emission of greenhouse gases. Besides, many modern thermal energy systems are already significantly coupled with the electrical sector by means of, among others, electrically powered space heating or domestic hot water provision. Thus, an independent treatment of operational optimization of thermal systems often may be rather meaningless.

In the context of EMS for microgrids, a large amount of research articles has been published concerning theoretical groundwork and practical implementations for both stand-alone/island and grid-connected microgrid systems. As a result, there exist several comprehensive literature reviews (see e.g. [30] or [19]), which summarize and compare the utilized control strategies, uncertainty quantification methods, i.e. the assessment of volatile future

demand and environmental conditions as well as the actual implementation and deployment with respect to the utilized software tools and general infrastructure. These reviews indicate that most EMS are based on a centralized controller utilizing an optimization-based approach. The optimization problems are typically either posed as *linear programs* (LP) or *mixed-integer linear programs* (MILP). Besides that, genetic algorithms, fuzzy control and artificial intelligence methods are repeatedly utilized.

Most reviewed EMS use externally provided or self-generated forecasts to determine uncertain quantities. These forecasts are usually treated deterministically, i.e. the forecasted quantity is assumed to occur as predicted over the investigated future time horizon. Nevertheless, some EMS employ stochastic methods to assess the stochastic properties of said forecasts in order to yield more robust operating strategies that perform well even considering the generally inevitably occurring forecast errors. The most common methods to consider these stochastic properties are Monte-Carlo analysis and bounded uncertainty methods.

In the context of EMS for MES only a limited amount of research articles related to actual implementations is yet available. Among those, all developed EMS employ an optimization-based approach based on MILP, where each MES is represented by linear dynamics and constraints of both continuous and discrete variables.

2.2. Research Object: Existing Energy Management Framework

The EMS framework that is considered in this work has been designed in a modular fashion to allow for quick and cost effective deployment for a variety of MES applications [16]. In contrast to application-specific EMS, the developed framework aims to provide a general solution for regional small- to medium-scale energy systems such as urban districts, industrial plants or individual residential or office buildings. First initial tests and simulations of the framework, for a case study of a thermal-electric energy

supply system for a modern urban district, have shown a potential decrease of operational costs by 3 % – 6 %.

The framework is designed to allow for the design of EMS for both already existing and operating, as well as newly set up MES. Hence, the developed EMS have to be agnostic to the specific type of installed infrastructure with respect to process monitoring and process control. The performance of any EMS developed with the framework will be affected and limited by the available dynamics and accuracy of the actually installed process control systems, and further by the low-level controllers of the individual system components/prosumers. Thus, knowledge about these limitations should be included at the EMS design stage within the respective prosumer prediction models to obtain overall satisfactory performance.

In order to provide the adaptability to a variety of different MES applications and the possibility to adjust an operating EMS to potential plant modifications, a MPC strategy is utilized within the framework. Consequently, a dynamic model of the respective MES is directly used when devising its respective plan or operation. Therefore, physical modifications of the MES, as well as time-varying constraints and performance metrics can be incorporated by providing updated dynamic prediction models, hence adjusting the associated optimization problem respectively. In contrast to tailor-made systems, no expensive and time-consuming re-designs of the EMS would be required. Moreover, MPC-driven controllers, in contrast to e.g. approaches based on artificial intelligence, generally require no, or at least very limited, process training data or running-in phases to yield satisfactory controller results, resulting in a generally short time to deployment.

Likewise to other EMS for MES solutions, the optimization problem associated with the controller is restricted to be a MILP in the presented framework. In spite of the entailed benefit of using efficient solvers for the MPC optimization problem, the restriction to MILP, however, naturally entails the fact that the dynamic models used to represent a MES can only comprise linear expressions of continuous and integer variables. Besides, plant heuristics and other information can only be included into the optimization problem by means of linear constraints or linear costs. As previously illustrated in Chapter1, this circumstance might compromise the accuracy of the resulting prediction models and, hence impair the performance of the devised

controller. For further information regarding the general concept of MPC and the implications of inaccurate system models the interested reader is referred to Appendix A Section A.1 and A.2.

The mentioned modularity of the presented framework stems from the fact that the prediction model of each MES is constructed through a combination of models representing individual prosumers and connections. Hence, the prediction model of any specific MES can be easily extended to include newly installed equipment or changes in the system's layout, such as modifications of the piping within a hydronic system. Furthermore, each connection and prosumer entity may be associated with individual constraints and an individual cost value. The global cost function of the MPC optimization problem is then defined by the sum of all individual cost values.

Prediction models for most typical components within a general MES, such as e.g. boilers, heat pumps, PV and solar thermal collectors, controllable sources, different energy storages and various loads, are already implemented within the presented framework. Consequently, the optimization problem can be automatically synthesized from only a set of provided prosumer parameters and schematics that illustrate the layout of the system, parametrize the pre-defined models and define the connections between them. Hence, an EMS for a given MES application may be synthesized and deployed by a system operator with little to no required knowledge of control engineering or optimization.

For further insights into the discussed framework, the following sections will discuss the utilized mathematical representation of the prosumers and connections, their associated cost values and constraints as well as the handling of uncertain model parameters, e.g. future energy demands, by means of forecasts.

2.2.1. Prosumer Models

In the context of the presented framework, a prosumer is defined as any component or piece of equipment within a MES that converts, produces, consumes, stores or determines the specific distribution — or flow — of energy or mass. Individual examples for the defined categories in the context

of hydronic heating systems are e.g. biomass boilers, biomass sources/ reservoirs, heat radiators for space heating, TES, and valves which distribute mass streams of heat-transfer medium among different prosumers.

In the discussed framework, as is the case in most optimization-based EMS, the mathematical models of the prosumers are generally kept as simple as possible, representing only the most fundamental physical phenomena and dynamics. This is necessary to minimize the computational complexity of the resulting optimization problem, considering that depending on the application a MES may comprise a large number of interacting prosumers. In addition, prediction horizons typically range from a few hours to several days, with sampling periods ranging from 15 min – 60 min. Therefore, optimization problems that comprise several thousand continuous and several hundred binary decision variables that need to be solved within a few minutes are not uncommon.

As a result, energy converters, e.g. gas boilers, are for the most part represented by a static linear function using a constant efficiency/performance coefficient linking the amount of primary energy used with the amount of end-use energy provided. This simplification is typically a reasonably accurate approximation for the behavior of most energy converters, considering the relatively small time constants of most converters compared to the sampling periods employed. However, with this simplified model it is not possible to assess noteworthy (non-linear) effects, such as load-dependent efficiency/performance, or varying behavior occurring during startup and shutdown phases of equipment.

To mitigate this issue the *mixed-logic dynamic* (MLD) system framework [3] is adopted. This framework establishes a systematic procedure for representing a broad class of hybrid linear systems in a single model, combining both system parts described by continuous and system parts described by integer variables. The central idea of this holistic modeling approach is to reformulate logic and mixed-logic propositions, which are a common way of defining binary/integer system variables or discrete operating events, as mixed-integer linear constraints of continuous and binary auxiliary variables. Among others, this framework facilitates the consideration of non-linear functions that can be approximated by *piece-wise affine* functions or *switched affine* system dynamics in a single hybrid linear system model. It is evident

that the MLD framework lends itself naturally to be used for deriving prediction models used in MPC, given that the emerging mixed-integer constraints can simply be integrated into the MPC optimization problem.

With regards to computational complexity, the MLD framework is a helpful tool when seeking to represent some relevant non-linearities within hybrid linear prediction models, considering that otherwise generally *mixed-integer non-linear programs* (MINLP) would have to be solved. However, in general the introduction of auxiliary binary variables may increase the optimization problem complexity exponentially and, thus, should be limited to only the most relevant cases. Given its facilitated functionalities, it is fair to assume that the MLD framework is a main factor for the general prevalence of MILP within optimization-based EMS, as indicated by the large number of citations of [3] in related EMS research articles. For further insights into the MLD framework, specifically on how exactly propositional logic statements may be reformulated as equivalent mixed-integer constraints, the interested reader is referred to Appendix A Section A.3.

With the adoption of the MLD framework the dynamic prediction model of each prosumer is defined by the following set of general model equations and constraints:

$$\mathbf{x}_{k+1} = \mathbf{A}\mathbf{x}_k + \mathbf{B}_\mathrm{u}\mathbf{u}_k + \mathbf{B}_\delta\boldsymbol{\delta}_k + \mathbf{B}_\mathrm{z}\mathbf{z}_k + \mathbf{B}_\mathrm{w}\mathbf{w}_k\,, \tag{2.1}$$

$$\mathbf{y}_k = \mathbf{C}\mathbf{x}_k + \mathbf{D}_\mathrm{u}\mathbf{u}_k + \mathbf{D}_\delta\boldsymbol{\delta}_k + \mathbf{D}_\mathrm{z}\mathbf{z}_k + \mathbf{D}_\mathrm{w}\mathbf{w}_k\,, \tag{2.2}$$

$$\mathbf{E}_\mathrm{x}\mathbf{x}_k + \mathbf{E}_\delta\boldsymbol{\delta}_k + \mathbf{E}_\mathrm{z}\mathbf{z}_k + \mathbf{E}_\mathrm{w}\mathbf{w}_k \leq \mathbf{g}\,, \tag{2.3}$$

with the subscript k denoting the discrete time step, $\mathbf{x} \in \mathbb{R}^{N_{\mathrm{x_c}}} \times \mathbb{Z}^{N_{\mathrm{x_d}}}$ denoting the state of the prosumer, $\mathbf{u} \in \mathbb{R}^{N_{\mathrm{u_c}}} \times \mathbb{Z}^{N_{\mathrm{u_d}}}$ representing the continuous- and integer-valued control inputs, $\boldsymbol{\delta} \in \mathbb{Z}^{N_\delta}$ and $\mathbf{z} \in \mathbb{R}^{N_\mathrm{z}}$ denoting integer- and respectively continuous-valued auxiliary variables that arise through the deployment of the MLD framework, and $\mathbf{y} \in \mathbb{R}^{N_{\mathrm{y_c}}} \times \mathbb{Z}^{N_{\mathrm{y_d}}}$ denoting the outputs of the prosumer. Additionally, in contrast to the canonical MLD system representation, known disturbances such as environmental conditions are considered in the above system representation and are denoted by $\mathbf{w} \in \mathbb{R}^{N_\mathrm{w}}$. The matrices $\mathbf{A}$, $\mathbf{B}_u$ etc. are constant matrices of appropriate dimensions.

Besides being defined by the model (2.1) – (2.3), each prosumer has a number of defined *ports*. Each port represents a unique set of internal state, output,

input or known disturbance variables. Together they represent interfaces for physical or logical interactions between prosumers, most prominently input and output interactions by means of mass or energy transfer. The specifics of these interactions are defined by so-called *connections*.

2.2.2. Connections

Representing physical interactions between prosumers mathematically means linking their internal variables by appropriate expressions or constraints. In the context of MES, these interactions mainly concern the transfer of one form of energy, or the mass transfer of a certain medium. They are represented in the EMS as *connections* between ports.

Every connection joins a single source port with a single sink port and consequently establishes a mathematical link between the prosumer variables associated with the respective ports. Both ports are required to be of the same type, meaning that the associated prosumer variables represent the same physical quantity, i.e. the same form of energy, or mass flow of the same material. The link between the associated variables is expressed by equality constraints, which enforce the underlying physical principles of mass and energy balance.

An ideal connection representing mass or energy transfer without losses can be expressed by simply enforcing equality between the variables of the source and sink port at each point in time during the whole length of the prediction horizon N_p:

$$\mathbf{y}_\mathrm{source} + \mathbf{u}_\mathrm{sink} \stackrel{!}{=} 0\,. \tag{2.4}$$

Here, $\mathbf{y}_\mathrm{source}$ and $\mathbf{u}_\mathrm{sink}$ denote the exemplary sets of output variables associated with the source port, and respectively input variables associated with the sink port. The adopted sign convention for variables is that mass or energy flow into a prosumer is said to be negative, whilst outflows are considered to be positive (producer viewpoint).

Besides ideal connections, potential losses of mass or energy along the connection may be considered by introducing a loss coefficient $\gamma \in (0, 1]$

in (2.4):

$$\gamma \cdot \mathbf{y}_{\text{source}} + \mathbf{u}_{\text{sink}} \stackrel{!}{=} 0\,. \tag{2.5}$$

Consequently, losses are always assumed to be directly proportional to the value of the port variables, i.e. most commonly to the rate of energy or mass transfer. For $\gamma = 1$, the above equation represents a lossless connection as defined by (2.4).

In addition to enforcing mass or energy balance, practical limitations of the rate at which energy or mass can be transferred over a channel can be considered. This can be easily achieved by enforcing additional inequality constraints, e.g.:

$$\mathbf{y}_{\text{source}}^{\text{min}} \leq \mathbf{y}_{\text{source}} \leq \mathbf{y}_{\text{source}}^{\text{max}}\,. \tag{2.6}$$

Here, $\mathbf{y}_{\text{source}}^{\text{min}}$ and $\mathbf{y}_{\text{source}}^{\text{max}}$ denote limits which the channel imposes on each element of $\mathbf{y}_{\text{source}}$ and, as a result of (2.4) or (2.5), likewise on each element of $\mathbf{u}_{\text{sink}}$. These limits may very well be defined time-varying, for which the specific time instance of the considered variables $\mathbf{y}_{k,\,\text{source}}$ needs to be considered in the above constraint.

The presented mathematical representation of energy and mass transfer might be troublesome in the context of hydronic systems. Considering the inherent bilinearity of energy transfer by convection, limits on the maximum or minimal pumping power within the piping network of a hydronic system, and thus on the amount of fluid that can be circulated between prosumers, cannot be meaningfully translated into limits on the minimal or maximal energy that may be transferred between connected prosumers. Conversely, mass flow of the heat-transfer medium alone does not represent energy transfer without knowledge about the temperature difference between the feed and return mass streams.

Additionally, the thermal energy losses that occur along a pipe are mainly a result of thermal conduction, and hence strongly related to the difference between the temperature of the medium inside the pipe and the ambient temperature. Considering the general case where the temperature of the heat-transfer medium within a pipe is not stationary, the resulting energy losses cannot be meaningfully represented by means of (2.5), given that

the occurring losses are dependent on the temperature of the heat-transfer medium, as opposed to the amount of transferred energy or mass.

Last, in the operation of hydronic systems one has to consider the fact that different prosumers may have different temperature specifications, i.e. they can only produce and consume thermal energy within defined temperature ranges. Therefore, energy transfer between prosumers should only be possible within a certain temperature range. Given the bilinearity of energy transfer by convection, however, this circumstance can neither be expressed by constraints on either mass flow rate nor amount or rate of transferred thermal energy.

To circumvent these issues and to describe convection within the hybrid linear modeling framework, thermal energy transfer between two prosumers in a hydronic system is assumed to always occur at a predefined constant temperature. Resulting from this, the transferred energy between two prosumers is linearly dependent on the mass flow rate only, whereby energy balance follows naturally from enforcing mass balance between source and sink ports. In this simplified context, non-ideal connections between prosumers may be considered by employing (2.5) to define static, proportional energy losses that occur when transferring energy between prosumers.

However, there are significant issues with this approach. First, the defined losses would be defined proportional to the amount of transferred energy, which does not represent the actual physical phenomenon of energy losses due to conduction well. Second, a reduced amount of energy inflow at the sink port would imply a lowered mass flow rate of the heat-transfer medium at the sink compared to the rate of outflow at the the source port. This implication is physically wrong within a hydronic systems as it violates the notion of mass balance. Hence, within an EMS for hydronic systems that is entrusted with defining mass flow rate references for the low-level flow controllers of circulation pumps, the output energy at the source ought to be used to determine the appropriate pump actuation, as otherwise the resulting pump actuation would be computed inadequately and would always be too low.

2.2.3. Forecasts

Forecasts are used to determine uncertain known disturbances, such as weather conditions or the expected volatile future energy demand and yield of prosumers. Whilst forecasts for the former are obtained from external weather service providers in the presented framework, the latter quantities are typically determined using a generalization of the methods illustrated in [18] respectively [26]. Although [18] only examines the prediction of thermal energy demand for a variety of different loads, and [26] only further extends the devised method for the prediction of solar thermal collector yield, the proposed method is easily adapted towards other types of prosumers with a volatile demand or yield of any form of energy.

The main concept, that is proposed and verified in both publications, is to determine the future energy demand and yield based on an adapted multi-linear regression method. Energy demand or yield, which are the dependent variable, are predicted on an hourly basis depending on the values of a set of independent variables, with the peculiarity that for each hour of the day a new set of linear regression coefficients is computed. At its simplest, the linear regression only consists of a constant, so these different sets represent different values for each hour of the day, and thus daily patterns. For the example of PV panels, changing coefficients can represent periodic shading from neighboring buildings. Both articles furthermore propose to optionally distinguish between different days of the week, or whether a given day is a holiday or a workday, by considering different sets of individual coefficients for those cases. The computed regression coefficients are continuously updated with the most recent measurements, whereby only a certain number of past data points are considered when recomputing the coefficients. As a result, the method neglects measurements that are too far in the past, which renders the proposed method adaptive towards changing prosumer behavior.

In order to forecast thermal energy demand, both articles recommend to consider only the ambient temperature as the independent variable, given that it can be shown to exhibit high correlation with respect to the actual thermal energy demand of various loads. The expected values of the ambient temperature at a specific location are provided by weather service providers

and are assumed to be reasonably accurate over the investigated forecast horizon and thus treated deterministically.

To forecast the energy yield from solar thermal collectors, the global solar irradiance, along with the temperature difference between the collector and the ambient surrounding and the square of said difference, are considered as independent variables. Expected future values of both global solar irradiance and ambient temperature are again provided by weather service providers. Notably, the mean collector temperature is an operational parameter that is determined by the temperatures of the in- and outflowing heat-transfer medium during stationary operation. The presented choice of the independent variable is in accordance with the steady-state energy balance of a solar thermal collector, which is defined in the EN12975:2006 standard [11] as:

$$\dot{E}_{\text{solar}} = A_{\text{coll}} \cdot \left(\eta_{\text{o}} \cdot I_{\text{g}} - k_1 \cdot (\bar{T}_{\text{fl}} - T_{\text{amb}}) - k_2 \cdot (\bar{T}_{\text{fl}} - T_{\text{amb}})^2 \right) . \tag{2.7}$$

Here, $\dot{E}_{\text{solar}}$ refers to the thermal energy output/yield of the collector, A_{coll} is the active collector area, η_{o} denotes the so-called optical efficiency of the collector, I_{g} is the global solar irradiance, whilst $\bar{T}_{\text{fl}}$ and T_{amb} denote the mean collector respectively ambient temperature. The loss coefficients k_1 and k_2 are necessarily positive and are used to assess the thermal energy losses within the collector by means of thermal conduction and radiation. By utilizing the proposed forecasting method one actually estimates the product of A_{coll} and η_{o}, as well as A_{coll} an the respective loss coefficients. Thus, the prior knowledge that all three coefficients, given their physical implications, have to be positive should to be incorporated within the forecasting algorithm to ensure physical meaningfulness of the computed linear regression coefficients.

Although $\bar{T}_{\text{fl}}$ is generally considered to be an operational parameter, it is assumed to always be constant in the context of the presented EMS framework, since the mean collector temperature of a solar thermal collector is assumed to be equal to the average of the feed and return temperatures, and these are defined to be constant. As a result of this circumstance, the forecast of the energy yield of a solar thermal collector may be treated independently from the operational optimization of the energy system it is integrated in. Hence, the expected yield may be computed prior and

independently of the current optimization cycle and subsequently simply treated as a known disturbance within the prediction model of the solar thermal collector. The mass flow rates at the inlet and outlet of the collector are then computed by the EMS as those control reference values that lead the forecasted thermal energy yield to be transferred out of the collector.

In [18] the presented method is verified with data sets for 7 different thermal loads and is shown to produce satisfactory forecast results over a 24 h forecast horizon. The solar thermal collector yield prediction is evaluated in [26] for two representative days in summer and spring. Here, the results indicate notable forecast errors for the spring day, given the typically increased fluctuations in weather conditions e.g. the cloud coverage. However, the method still produces reasonable forecast results for the total thermal energy yield over the investigated time horizon and as such still is considered to be suitable for the use within the presented EMS framework.

It is important to note that the presented methods rely on accurate weather forecasts, descriptive training data (typically for at least 30 d – 60 d, depending on whether days of the week and/or holidays ought to be distinguished) and a reasonable choice of independent variables, which is notably not addressed in the articles for the case of non-thermal prosumers. However, if these requirements are met for a given application, the discussed forecast methods are shown to provide sufficiently accurate demand and yield forecasts over forecast horizons of up to 24 h.

2.2.4. Cost Function

Similar to the overall prediction model of the investigated MES, the associated cost function is constructed in a modular fashion based on individual prosumer and connection contributions. Therefore, each prosumer and connection is associated with a time-varying cost value.

Costs may be defined based on actual economic transactions, most prominently through purchases or sales of energy or fuel, or related to the emissions of green house gases in the context of emissions trading. Additionally, behavioral costs may be defined to penalize prosumer/connection operating

points, or modes of operation that entail increased wear and tear of the utilized equipment, entail unnecessary emissions of pollutants or greenhouse gases, or that diverge from a defined operating point reference. In some instances these behavioral costs are also referred to as *soft constraints*, given that instead of imposing hard limits on the admissible range of operational parameters, they rather serve as an incentive to the optimizer to limit the divergence of said parameters from their respective admissible range, so as to reduce the associated costs. However, one should note that the specific economic implications, i.e. the implied actual operational costs, of these behavioral penalties are often very vague or cannot be meaningfully assessed. Instead, they are usually thought of as interactive means to fine-tune the EMS such that the design engineers' intuition about how an EMS should ideally behave for a given MES application may be incorporated into the optimization problem, and, hence manifest itself within the resulting derived plan of operation.

Currently the developed framework recognizes six separate ways of expressing the above considerations. The time-dependent cost value *cost* associated with each individual prosumer or connection is defined as the combination of contributions from all respective internal variables ν. Hence, the cost value of a specific prosumer or connection e with N_e internal variables, is defined as follows:

$$\begin{aligned}\text{cost}_{k,e} = \sum_{i=1}^{N_e} & \lambda^{\text{val}}_{k,\nu_i} \cdot \nu_{k,i} \cdot \Delta t_k + \lambda^{\text{abs}}_{k,\nu_i} \cdot |\nu_{k,i}| \cdot \Delta t_k \\ & + \lambda^{\text{val}_\Delta}_{k,\nu_i} \cdot \frac{\nu_{k,i} - \nu_{k-1,i}}{\Delta t_k} + \lambda^{\text{abs}_\Delta}_{k,\nu_i} \cdot \left| \frac{\nu_{k,i} - \nu_{k-1,i}}{\Delta t_k} \right| \\ & + \lambda^{\text{zone}}_{k,\nu_i} \cdot \left| \nu_{k,i} - s_{k,\nu_i} \right| \cdot \Delta t_k + \lambda^{\text{ref}}_{k,\nu_i} \cdot \left| \nu_{k,i} - r_{k,\nu_i} \right| \cdot \Delta t_k \,, \end{aligned} \tag{2.8}$$

$$\text{with} \quad s^{\min}_{k,\nu_i} \leq s_{k,\nu_i} \leq s^{\max}_{k,\nu_i} \,.$$

Here, each contribution of an internal variable ν_i at time instance k is computed based on the current value of the variable, its rate of change, its difference to a predefined range of values s_{ν_i} defined by the limits $s^{\min}_{\nu_i}$ and $s^{\max}_{\nu_i}$, and its deviation from a given reference value r_{ν_i}. Each contribution is quantified by a known/chosen, potentially time-varying, cost coefficient or price λ_{ν_i} and naturally depends on the sampling period denoted by Δt,

which may be itself defined to be time-varying to allow for the consideration of a varying prediction horizon resolution, i.e. by defining a high sampling rate for time instances in the near future and a lower sampling rate for time instances at the end of the prediction horizon. Notably, the absolute value of the internal variables is considered in (2.8), which, given the non-linearity of the absolute value operator, cannot be directly integrated into the cost function of a MILP. To circumvent this issue, additional slack variables have to be introduced along with additional constraints to represent the absolute value of a variable by means of linear expressions (see [1] for additional information).

The scalar global cost function J of the EMS optimization problem is given by the combination of all individual prosumer and connection cost values, summed up over the entire prediction horizon N_p:

$$J = \sum_{e} \sum_{k=k_0+1}^{k_0+N_\mathrm{p}} \mathrm{cost}_{k,e}\,. \tag{2.9}$$

As a result, the cost function may be easily adapted and extended if changes of the MES set-up, e.g. additionally incorporated prosumers, should be considered. Furthermore, by not only considering cost contributions based on economic expenses, such as fuel costs, but rather assigning costs to the potential emissions of pollutants or greenhouse gases, it is possible to adjust the operating strategy devised by an EMS such that a compromise between the most efficient economic and most environmental-friendly operation can be made according to the specifics of the individual application.

2.2.5. Constraints

In addition to costs, time-varying constraints may be defined for each internal prosumer or connection variable. Within the presented framework constraints may be imposed in order to limit the value or the rate of change of any generic continuous- or integer-valued internal variable ν. Internal binary variables ν_bin that represent whether prosumers are currently switched *on* or *off* can be constrained to enforce minimum on- and off-times.

The value of an internal variable ν may be limited by incorporating the following constraints into the optimization problem:

$$\nu_k^{\min} \leq \nu_k \leq \nu_k^{\max} . \tag{2.10}$$

Besides, the rate of change of a variable may be restricted within certain limits as follows:

$$\nu_k^{\Delta,\min} \leq \frac{\nu_k - \nu_{k-1}}{\Delta t_k} \leq \nu_k^{\Delta,\max} . \tag{2.11}$$

Potential constraints on the minimum on- and off-times of internal binary variables may be enforced by:

$$-\nu_{k,\text{bin}} + \nu_{k-1,\text{bin}} - \sum_{m=k-K_{\text{on}}}^{k} \frac{\nu_{m,\text{bin}}}{K_{\text{on}}} \leq 0 \tag{2.12}$$

$$\nu_{k,\text{bin}} - \nu_{k-1,\text{bin}} - \sum_{m=k-K_{\text{off}}}^{k} \frac{1 - \nu_{m,\text{bin}}}{K_{\text{off}}} \leq 0 . \tag{2.13}$$

Here, the defined minimal on- (K_{on}) and off-times (K_{off}) are expressed by means of the number of discrete time steps they encompass. Past values of the respective binary variable have to be considered in the above constraint to ensure compliance with the defined minimal on- and off-times also at the beginning of the prediction horizon. Therefore, these relevant past values have to be continuously recorded and have to be initialized prior to starting the MPC algorithm.

This concludes the overview over the operating principles of the discussed EMS framework. To illustrate how the prediction model of an actual hydronic system, along with the associated optimization problem, can be formulated within the presented framework, the fictitious example of a simplified domestic biomass heating system will be discussed in the following section.

2.2.6. Example: Simple Heating System

In the following example the modeling and control of the exemplary heating system illustrated in Figure 2.1, as it would be realized within the presented

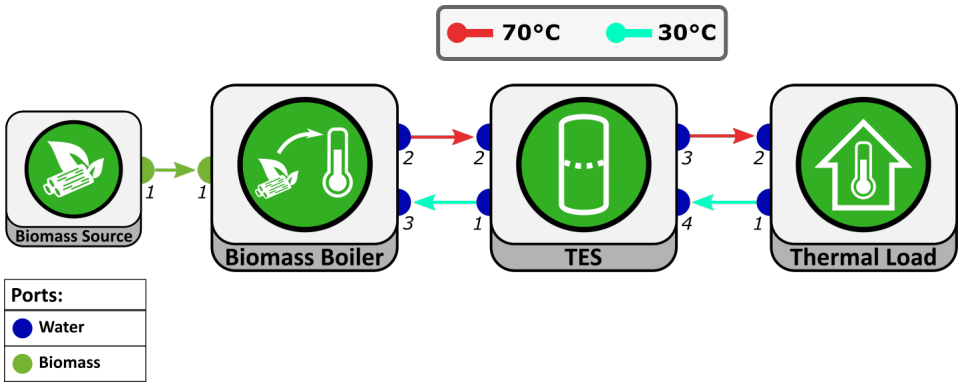

Figure 2.1.: Schematic layout of the investigated heating system.

EMS framework, will be discussed. The heating system comprises a biomass boiler with an attached biomass source, a sensible heat storage to serve as a TES, and a single thermal load that represents the thermal energy demand of a residential building.

The modeling commences by defining a set of ports for each prosumer. In the discussed example, these ports describe the mass transfer of either biomass or the heat-transfer medium, which is assumed to be water. Individual ports of a specific prosumer are identified by an associated port number as indicated in the schematic system layout.

Prior to defining the prosumer prediction models and connection constraints, the following general specifications and parameters are defined.

1. The biomass source is assumed to be inexhaustible and the current and future biomass feedstock price is assumed known.
2. The biomass boiler can be switched *on* and *off*. If switched *on*, it is assumed to operate at a constant efficiency independent of its power output. If switched *off* the power output is zero. Besides, operational limits regarding the minimum and maximum power output of the boiler are considered.
3. The TES, a sensible heat storage, has a known volume and is assumed to be very well insulated, i.e. no thermal losses due to temperature differences between the medium in the storage and the ambient surroundings are considered.

4. The future energy demand of the thermal load is assumed to be known *a priori* or is provided by accurate forecasts that can be treated deterministically.
5. The heating system is set to operate at a constant feed temperature of 70 °C and a constant return temperature of 30 °C (see Figure 2.1).
6. All connections are assumed to be ideal, i.e. energy losses are not considered. However, the maximal rate at which water can be transferred over each individual connection is assumed to be restricted. These limits are inferred from the maximum power of the circulation pumps.

With these specifications, the prediction models of the individual prosumers and the necessary connection constraints may be defined as follows:

Example 2.1. Considering that the biomass source is inexhaustible, it can be represented by a single output variable $y_{\mathrm{src},1}$, which represents the mass flow rate of the outflowing biomass at port 1. The outflow of biomass is naturally associated with an economic cost, which is represented within the cost value of the biomass source as follows:

$$\mathrm{cost}_{k,\mathrm{src}} = \lambda^{\mathrm{val}}_{k,y_{\mathrm{src},1}} \cdot y_{k,\mathrm{src},1} \cdot \Delta t_k \,. \tag{2.14}$$

The feedstock cost at each time instance k is given by the instantaneous biomass price $\lambda^{\mathrm{val}}_{k,y_{\mathrm{src},1}}$ (defined per unit of mass) and the sampling period Δt_k.

The biomass boiler is characterized by a constant conversion efficiency η_{boil} which links the consumed primary chemical energy — biomass — with the provided end-use — thermal — energy. Hence, the output of the boiler y_{boil}, the provided thermal output power, may be defined:

$$y_{k,\mathrm{boil}} = u_{k,\mathrm{on\_off}} \cdot \eta_{\mathrm{boil}} \cdot u_{k,\mathrm{boil},1} \cdot \epsilon_{\mathrm{bm}} \,. \tag{2.15}$$

Here, $u_{\mathrm{on\_off}} \in \{0, 1\}$ is a binary input variable representing whether the boiler is switched *on* ($u_{\mathrm{on\_off}} = 1$) or *off* ($u_{\mathrm{on\_off}} = 0$). The mass flow rate of the inflowing biomass stream at port 1, with known heating value ϵ_{bm}, is denoted by $u_{\mathrm{boil},1}$. The fact that the output power of the

boiler is constrained to be between a defined lower $y_{\text{boil}}^{\min}$ and upper $y_{\text{boil}}^{\max}$ bound can be expressed by enforcing:

$$\frac{y_{\text{boil}}^{\min}}{\epsilon_{\text{bm}} \cdot \eta_{\text{boil}}} \leq u_{k,\text{boil},1} \leq \frac{y_{\text{boil}}^{\max}}{\epsilon_{\text{bm}} \cdot \eta_{\text{boil}}} . \tag{2.16}$$

In its current form (2.15) cannot be used as a linear prediction model of the biomass boiler, considering the multiplication of the two input — and hence decision — variables $u_{\text{on\_off}}$ and $u_{\text{boil},1}$. However, this issue can be resolved by using a formalism described within the MLD framework, which expresses the multiplication of a binary and a continuous-valued variable by means of an auxiliary continuous-valued variable and four mixed-integer constraints (see Table A.3 in Appendix A). Thus, the auxiliary variable z_{boil} is introduced along with the following inequalities:

$$\begin{aligned}
z_{k,\text{boil}} &\leq \frac{y_{\text{boil}}^{\max}}{\epsilon_{\text{bm}} \cdot \eta_{\text{boil}}} \cdot u_{k,\text{on_off}} , \\
z_{k,\text{boil}} &\geq \frac{y_{\text{boil}}^{\min}}{\epsilon_{\text{bm}} \cdot \eta_{\text{boil}}} \cdot u_{k,\text{on_off}} , \\
z_{k,\text{boil}} &\leq u_{k,\text{boil},1} - \frac{y_{\text{boil}}^{\min}}{\epsilon_{\text{bm}} \cdot \eta_{\text{boil}}} \left(1 - u_{k,\text{on_off}}\right) , \\
z_{k,\text{boil}} &\geq u_{k,\text{boil},1} - \frac{y_{\text{boil}}^{\max}}{\epsilon_{\text{bm}} \cdot \eta_{\text{boil}}} \left(1 - u_{k,\text{on_off}}\right) .
\end{aligned} \tag{2.17}$$

With the defined auxiliary variable, (2.15) may be rewritten as:

$$y_{k,\text{boil}} = z_{k,\text{boil}} \cdot \eta_{\text{boil}} \cdot \epsilon_{\text{bm}} , \tag{2.18}$$

which now is a linear expression for the provided thermal power of the biomass boiler.

The provided thermal energy is necessarily absorbed by the in- and outflowing mass streams of heat-transfer medium. In the presented

framework this circumstance of energy balance is represented by enforcing the following equality constraint:

$$y_{k,\,\mathrm{boil}} \overset{!}{=} u_{k,\,\mathrm{boil},\,2} \cdot c_p\left(T_{\mathrm{boil},\,2}\right) \cdot T_{\mathrm{boil},\,2} + u_{k,\,\mathrm{boil},\,3} \cdot c_p\left(T_{\mathrm{boil},\,3}\right) \cdot T_{\mathrm{boil},\,3}\,. \tag{2.19}$$

Here, $u_{\mathrm{boil},\,2}$ and $u_{\mathrm{boil},\,3}$ refer to the mass flow rate of the out- and inflowing mass streams at the respective temperatures of $T_{\mathrm{boil},\,2}$ and $T_{\mathrm{boil},\,3}$. The feed and return temperatures of the boiler are known, namely $T_{\mathrm{boil},\,2} = 70\,^{\circ}\mathrm{C}$ and $T_{\mathrm{boil},\,3} = 30\,^{\circ}\mathrm{C}$. Considering that the feed and return path of the boiler are inherently connected, the mass flow rates of the heat-transfer medium have to be equal in both paths. Hence, the following equality constraint has to be met:

$$u_{k,\,\mathrm{boil},\,2} + u_{k,\,\mathrm{boil},\,3} \overset{!}{=} 0\,. \tag{2.20}$$

With this last constraint the modeling of the biomass boiler is completed, whereby its prediction model is given by (2.18) subject to the constraints defined in (2.16) – (2.17) and (2.19) – (2.20).

In the presented EMS framework a TES is represented by a first-order integrator model with linear losses that depend on the SOC of the TES. Therefore, the sensible heat storage within the investigated heating system is described by the following discrete-time state equation:

$$x_{k+1,\,\mathrm{TES}} = \alpha_{\mathrm{TES}} \cdot x_{k,\,\mathrm{TES}} - \frac{\sum_{i=1}^{4} u_{k,\,\mathrm{TES},\,i} \cdot c_p\left(T_{\mathrm{TES},\,i}\right) \cdot T_{\mathrm{TES},\,i} \cdot \Delta t_k}{H_{\mathrm{TES}}^{\mathrm{max}}}\,. \tag{2.21}$$

Here, x_{TES} denotes the state, i.e. SOC, of the sensible heat storage, $\alpha_{\mathrm{TES}} \in (0, 1]$ represents the SOC-dependent losses, and $u_{\mathrm{TES},\,i}$ denotes the mass flow rate of the in- respectively outflowing mass stream of heat-transfer medium at the i-th port of the TES at a corresponding temperature of $T_{\mathrm{TES},\,i}$. The maximum energy that may be stored within the TES is defined by means of the maximum enthalpy $H_{\mathrm{TES}}^{\mathrm{max}}$. Given the low compressibility of water, it is approximated based on the volume of the storage V_{TES} and the difference between the two defined temperature levels (70 °C

and 30 °C):

$$H_{\mathrm{TES}}^{\max} = V_{\mathrm{TES}} \cdot \rho \cdot \left[c_p(70\,^{\circ}\mathrm{C}) \cdot 70\,^{\circ}\mathrm{C} - c_p(30\,^{\circ}\mathrm{C}) \cdot 30\,^{\circ}\mathrm{C} \right] , \tag{2.22}$$

where ρ denotes the density of the medium within the storage, which for simplicity is assumed constant and independent of temperature in the discussed example. Considering that the losses of the TES are assumed to be negligible in the discussed example, the loss factor α_{TES} is set to one.

The SOC of a TES, given its definition, is naturally restricted to be between zero and one. This restriction is included by adding the constraint:

$$0 \leq x_{k,\,\mathrm{TES}} \leq 1\,. \tag{2.23}$$

The thermal load is defined by its known power demand $w_{k,\,\mathrm{load}}$. It is provisioned by means of the in- and outflowing mass streams of heat-transfer medium. Hence, similarly to (2.19) the following equality constraint is defined:

$$w_{k,\,\mathrm{load}} \overset{!}{=} u_{k,\,\mathrm{load},\,1} \cdot c_p\left(T_{\mathrm{load},\,1}\right) \cdot T_{\mathrm{load},\,1} + u_{k,\,\mathrm{load},\,2} \cdot c_p\left(T_{\mathrm{load},\,2}\right) \cdot T_{\mathrm{load},\,2}\,. \tag{2.24}$$

Here, $u_{\mathrm{load},\,1}$ and $u_{\mathrm{load},\,2}$ refer again to the out- and inflowing mass streams of heat-transfer medium with the respective temperatures of $T_{\mathrm{load},\,1}$ and $T_{\mathrm{load},\,2}$ at the respective ports 1 and 2. Given that the two ports of the load are inherently connected, the following equality constraint is defined to enforce mass balance between them:

$$u_{k,\,\mathrm{load},\,1} + u_{k,\,\mathrm{load},\,2} \overset{!}{=} 0\,. \tag{2.25}$$

With all prosumer prediction models defined, the connections between prosumer ports need to be considered by means of introducing the associated connection constraints.

Considering that all connections are defined to be lossless, the following

equality constraints are defined in accordance with (2.4):

$$\begin{aligned} y_{k,\,\text{src\_1}} + u_{k,\,\text{boil},\,1} &\stackrel{!}{=} 0\,, \\ u_{k,\,\text{boil},\,2} + u_{k,\,\text{TES},\,2} &\stackrel{!}{=} 0\,, \\ u_{k,\,\text{boil},\,3} + u_{k,\,\text{TES},\,1} &\stackrel{!}{=} 0\,, \\ u_{k,\,\text{TES},\,3} + u_{k,\,\text{load},\,2} &\stackrel{!}{=} 0\,, \\ u_{k,\,\text{TES},\,4} + u_{k,\,\text{load},\,1} &\stackrel{!}{=} 0\,. \end{aligned} \tag{2.26}$$

Given that all hydronic connections are assumed to impose a known constant maximum limit on the admissible mass flow rates, the following inequalities have to be met:

$$\begin{aligned} 0 \leq & u_{k,\,\text{boil},\,2} \leq u_{\text{boil},\,2}^{\max}\,, \\ 0 \leq & u_{k,\,\text{TES},\,3} \leq u_{\text{TES},\,3}^{\max}\,. \end{aligned} \tag{2.27}$$

Here, the connection limits are denoted by $u_{\text{boil},\,2}^{\max}$ for the connection between the boiler and the TES, and $u_{\text{TES},\,3}^{\max}$ for the connection between the TES and the thermal load.

Consequently, the model predictive EMS controller may be synthesized, with the associated optimization problem defined as follows:

$$\begin{aligned} \min_{y_{\text{src},\,1}} \quad & J = \sum_{k=k_0+1}^{k_0+N_\text{p}} \lambda_{k,\,y_{\text{src},\,1}}^{\text{val}} \cdot y_{k,\,\text{src},\,1} \cdot \Delta t_k\,, \\ \text{subject to} \quad & \text{(2.16) – (2.21), (2.23) – (2.27)} \qquad \forall\ k \in \{k_0+1,\,\ldots,\,k_0+N_\text{p}\}\,, \\ & \mathbf{x}_{k_0} \stackrel{!}{=} \mathbf{x}(t)\,. \end{aligned} \tag{2.28}$$

Notably, the defined cost function J is only dependent on the biomass source output, given that it is the only system variable for which a non-zero cost value is defined. To initialize each new optimization cycle the current prosumer state $\mathbf{x}(t)$ is determined from measurements and defined equal to the first considered state of the discrete-time prediction model $\mathbf{x}_{k_0}$.

> For this most basic example of a hydronic heating system each considered time step within the prediction horizon introduces 13 continuous-valued variables and one binary variable into the optimization problem. Therefore, for a typical prediction time horizon of 24 h with a constant sampling period of 15 min, the resulting optimization problem would comprise 1,235 continuous and 95 binary optimization variables, which, depending on the available hardware and solver algorithms, may already prove to be an optimization problem that entails non-negligible solving times.

The above example illustrates how the prediction model of a hydronic heating system and a corresponding MPC controller may be synthesized in the presented framework. In order to model the inherently bilinear phenomenon of energy transfer by convection, constant temperature values were defined for each connection within the hydronic part of the system. Notably, this measure facilitated the usage of very simple prediction models for the utilized equipment, namely the use of the presented integrator model (2.21) to represent a sensible heat storage.

As a result, it is not possible to asses temperature-dependent prosumer behavior within in the EMS optimization problem. This is due to the fact, that the modulation of the feed and return temperatures according to the instantaneous prosumer utilization or operation mode of the heating system is not possible. Besides, the chosen model to represent the TES entails several issues. These issues, along with alternative representations of thermal energy transfer and storage within a hydronic system, aiming to circumvent these issues, will be discussed in the following section.

2.3. Hybrid Linear Representations of Energy Transfer by Convection and Sensible Heat Storage

Under the assumption of constant feed and return temperatures, energy transfer by convection within hydronic systems can be reasonably well ap-

proximated as a simple linear phenomenon. Therefore, many optimization-based strategies that concern the optimal operation or design of hydronic systems or components thereof assume constant heat-transfer medium temperatures when representing energy transfer by convection.

Following from this measure, thermal energy transfer may be modeled by means of generalized energy flows, as opposed to mass flows at a particular temperature. Hence, the thermal energy output or demand of different prosumers can be combined to obtain the aggregated system output or demand. This measure may potentially significantly simplify the representation of the investigated system. Naturally, this is only possible if the feed and return temperatures are defined equally for all prosumers. Instead of using the mass flow rates of the in- and outflowing heat-transfer medium as control variables within the prediction models of prosumers (see Example 2.1), one could reformulate the derived prediction models to consider instead generalized energy flows as it is illustrated in the appendix of [16].

Represented by means of generalized energy flows, the representation of thermal energy transfer by convection is in fact equivalent to the representation of electrical energy transfer or any other generic form of energy transfer that can be expressed by means of linear equations. Hence, one may be able to define general models for certain generic classes of prosumers, i.e. energy converters or storages, independently of the specific form of considered primary or end-use energy. Considering the aforementioned historic prevalence of electrical systems in the development of EMS, one might therefore be enticed to model a TES similarly to the most prominent component for electrical energy storage, a battery. The energy stored within a battery is typically approximated by simply integrating the electric power contributions of all charging and discharging currents. Besides, a dis-/charging efficiency term and a linear loss term are typically considered to account for i.a. the internal resistance and self-discharge behavior of a generic battery.

Representing a high-temperature sensible heat storage in a similar fashion may result in the following first-order linear system:

$$\dot{H} = \alpha H + \dot{H}_{\mathrm{f}} - \dot{H}_{\mathrm{r}} \,. \tag{2.29}$$

Here, the stored thermal energy is expressed by means of the enthalpy H of the medium within the storage. The rate of change of the stored energy is described by linear losses, which are defined by means of the loss coefficient α and are proportional to the instantaneous enthalpy of the storage, as well as the overall in- and outflow of enthalpy denoted by $\dot{H}_\mathrm{f} \geq 0$ respectively $\dot{H}_\mathrm{r} \geq 0$. Notably, (2.29) is somewhat similar to (2.21) when taking the utilized sign convention that is adopted in the EMS framework into account. The sole difference between the two storage models is that within the EMS framework the generalized enthalpy flows $\dot{H}_\mathrm{f}$ and $\dot{H}_\mathrm{r}$ are approximated by mass flows at a defined temperature, and that the stored energy is represented with respect to the SOC, i.e. as a relative value with respect to a defined maximum and minimal value of energy that can be stored within the storage.

When representing specifically a fluid storage tank by (2.29) the inherent physical implications are that either the medium within the storage is ideally mixed or that there are two distinct and separable temperature layers present within the storage, i.e. the storage is ideally stratified. In other words, this means that the medium within the tank is either at a constant temperature or that there are two vertically separable volumes of matter, each with a constant though different temperature.

In the latter case, all inflowing mass streams are assumed to have a temperature equal to one of the layers and are assumed to directly enter the layer with the corresponding temperature, regardless of the specific location at which a specific inflow may actually enter the storage tank. For the case of a water-based heat-transfer medium, stratification occurs naturally considering the temperature-dependent density of water, e.g. in Example 2.1 the colder 30 °C layer was inherently assumed to be located at the bottom of the TES. It is important to note, however, that in real-world applications a certain degree of mixing and conduction between the layers cannot be avoided. Resulting from this, a certain transition zone (thermocline) with a continuous temperature gradient will always form naturally within a sensible heat storage, and hence potentially reduce the amount of usable energy within the storage. In light of this first modeling inaccuracy of the simplified model, there are additional issues entailed by using (2.29) to represent a sensible heat storage.

First, from an application perspective where prosumers with significantly different nominal temperature operating points, e.g. a biomass boiler and a solar thermal collector, are connected to the the same sensible heat storage the presented two layer model may be completely inadequate, given that there may be no output temperature that both prosumers could provide at reasonable efficiencies. Therefore, the use of the discussed simple integrator model is restricted to applications where the connected prosumers have similar temperature operating points, as otherwise the performance of the EMS might be severely impaired by e.g. continuously operating various prosumers at inefficient temperature operating points that are predefined through the chosen feed and return temperature within the prediction model of the sensible heat storage.

Second, consider the actually stored energy within a cylindrical sensible heat storage, which can be reasonably well approximated as follows, assuming that the medium within the storage is incompressible:

$$H = \int_0^L A \cdot \rho \cdot c_p \cdot (T(l) - T_0) \, \mathrm{d}l \,. \tag{2.30}$$

Here, the physical dimension of the tank are defined by L and A, denoting the height and the cross section area of the tank. Assuming that the medium within the tank is homogeneous and isotherm along the horizontal axis, the internal energy within the tank may be computed by integrating the height-dependent temperature $T(l)$ of the medium within the storage along the vertical axis[1].

The issue arising from (2.30) concerns the definition of the SOC, i.e. the main parameter that may be assessed to define minimum and maximum constraints on the amount of stored energy, with respect to the chosen reference temperature. In a typical practical application, the maximum energy that can be stored within a sensible heat storage would be defined with respect to the maximum temperature that thermal energy generating prosumers would be able to provide. A storage would be considered *full* if the medium inside would be homogeneously at this maximum temperature. In contrast to that, considering the non-zero thermal losses that occur in all

[1] In general both c_p and ρ will be temperature-dependent and, hence also dependent on l, however, this dependence is neglected in the above equation for simplicity.

practical applications, the storage would be considered *empty* if the medium within the storage would be homogeneously at ambient temperature. Hence, T_0 would have to be defined to be equal to the ambient temperature.

However, considering that thermal prosumers within hydronic systems usually have certain minimal temperature specifications, e.g. a space heater may only accept thermal energy that is provisioned at a significantly higher temperature than a defined reference room temperature, a storage might be defined to have high internal energy (with respect to T_0 being equal to the ambient temperature), but from the perspective of the connected prosumers there may be little to none usable energy stored within. In order to address this issue one might redefine T_0 to be equal to the minimal return temperature of the connected consumers, e.g. 30 °C in the previously discussed example, where now an SOC of zero would represent the case where the temperature of the internal medium is homogeneously at this minimal return temperature. Although being a more useful definition from the perspective of a connected consumer, it would potentially exclude the representation of the aforementioned state of complete cool-down to ambient temperature of a sensible heat storage. Additionally, if one considers that the ambient temperature is typically lower than the defined return temperature of consumers in heating applications, an actual sensible heat storage that would have cooled down to ambient temperature would still be defined to have an SOC of zero, given that a SOC is inherently defined to be greater or equal to zero. Hence, the necessary initial energy to bring the storage to a certain non-zero SOC would be wrongly computed within the EMS.

Considering these issues entailed by the presented integrator model when representing an actual sensible heat storage, alternative prediction models to represent sensible heat storages within hydronic systems have been devised. One method, proposed in [23], is to model a single physical thermal energy storage, within which both high and medium temperature thermal energy ought to be stored, by two separate integrator models for each considered temperature level. This allows for modeling sensible heat storages that are connected to prosumers that provide thermal energy at high temperature e.g. biomass boilers and those that generate thermal energy at a lower temperature e.g. solar thermal collectors. Naturally, this method can be easily extended if thermal energy storage ought to be considered at multiple

temperature levels, by modeling each considered temperature level by means of an individual separate integrator model.

However, within the proposed approach, interactions between the individual models that would reflect on the occurring conduction or mixing between the adjacent high and medium temperature zones, and hence the formation of a thermocline are not considered. Furthermore, each individual model is defined to have fixed physical dimensions, i.e. a fixed storage volume, hence instantaneously available capacity in one of the considered temperature zones cannot be used to store thermal energy at other temperature levels, as it would be the case in the actual single physical storage. Thus, for applications that are characterized by sudden and persisting changes of the system temperature operating points, i.e. thermal energy at medium temperature might be predominantly demanded for an extended period of time, whilst during other time periods thermal energy might be demanded exclusively at a high temperature, the presented fixed size, multi-model approach might prove to be limiting the potential benefits entailed by the deployment of an EMS.

Considering that each storage is modeled separately by an individual first-order system, energy transfer by means of convection can still be represented by mass streams at fixed temperatures, with each prosumer being connected to the storage that represents its nominal temperature operating point. However, by connecting each prosumer to several of the individual storage models and using a different prediction model depending on the storage that energy currently is drawn from or fed into, it would be possible to potentially consider varying temperature operating points of prosumers.

Another approach is proposed in [22], where a sensible heat storage is modeled by layers of constant mass and volume but considering varying layer temperatures. Given the notion of varying temperature, the authors propose to define energy transfer by means of convection to occur at a constant mass flow rate, i.e. an auxiliary binary variable is introduced to represent the activation of a pump which operates at a defined fixed pumping power. The resulting multiplication of a binary (pump activation) and continuous-valued (layer temperature) variable can then be transformed into a linear expression and several mixed-linear inequalities using the MLD framework (see e.g. (2.18) and (2.17) or Table A.3 in Appendix A). By the

same token, the authors illustrate that it is in fact possible to discretize the rate of mass flow by introducing additional auxiliary binary variables, hence several discrete operating points of a pump may be considered.

The main problem with this approach is the potential introduction of a large number of binary variables, if the rate of mass flow ought to be discretized with a sufficiently high resolution. As previously mentioned, the introduction of binary variables within prediction models generally severely increase the computational complexity of the associated optimization problem, and hence may entail significantly increased solving times. However, the illustrated approach allows to represent the occurring physical phenomena of ambient energy losses and axial conduction, that physically manifest themselves in temperature changes of the medium within the storage, in a physically accurate sense.

Besides the two mentioned approaches, a novel hybrid linear model of sensible heat storages for the use as prediction models in MPC-driven EMS has recently been proposed by Muschick et al. [17]. Considering that said novel model was in fact implemented into the previously discussed EMS framework as part of this thesis, the following section will discuss the main aspects of said proposed model in further detail.

2.3.1. The Multi-Layer Thermal Storage Model with Constant Temperature Levels

In the following, the thermal storage model proposed in [17] where it is referred to as the *multi-layer buffer model with constant temperature levels* and the associated representation of thermal energy transfer by convection will be discussed. In addition to the chosen representation of energy transfer (charge and discharge of the thermal storage), the representation of the physical phenomena of ambient energy losses and axial conduction will be illustrated.

The main concept of the proposed model is, as the name suggests, to represent the medium within a sensible heat storage by means of N (vertical) layers of varying volume but with constant temperature. Hence, the model implies ideal stratification of the physical storage with several distinct

temperature zones. The considered layers within the model are vertically ordered according to the density of the medium at the respective predefined layer temperatures. Each inflowing mass stream is defined to have a temperature that is equal to one of the layer temperatures and is defined to directly enter only said layer. Hence, temperature-dependent buoyancy of the different layers does not have to be considered specifically, as would be the case if the layer temperatures would be assumed varying as e.g. in [22]. However, mixing effects due to natural convection are therefore not considered, i.e. neglected, within the proposed model.

In order to accurately represent the complete loss of internal energy due to ambient energy losses, one of the layer temperatures and the reference temperature T_0 are defined to be equal to the ambient temperature. The layer at ambient temperature does therefore not contribute to the amount of energy stored inside of the storage.

For the following explanations, the considered thermal storage tank is assumed to be cylindrical, as illustrated in Figure 2.2. Following from this assumption, the volume of each layer is sufficiently defined by its respective height. Therefore, the layer heights are considered as states within the state-space model representation of the thermal storage tank. One fundamental assumption that is made in the following is that the sum of all layer heights stays constant, namely equal to the height of the storage tank L. Hence, for each outflow there ought to occur an equivalent inflow of fluid, which may be enforced by defining mass balance constraints for the set of inlets and outlets of the storage. Additionally, the density of the medium within the storage needs to be considered constant over the entire temperature range, and the medium inside the storage is assumed to be incompressible, which typically is a valid assumption for most liquids. As a consequence of these assumptions, the height of the layer with ambient temperature can be neglected within the state-space representation of the storage, given that its height can always be computed through the other system states.

For simplicity it is further assumed that the medium within the storage is of equivalent chemical composition as the heat-transfer medium within the hydronic system that the storage is integrated in. Therefore, direct mass exchange between prosumers and the storage tank occurs such that no internal heat exchangers or similar components have to be considered.

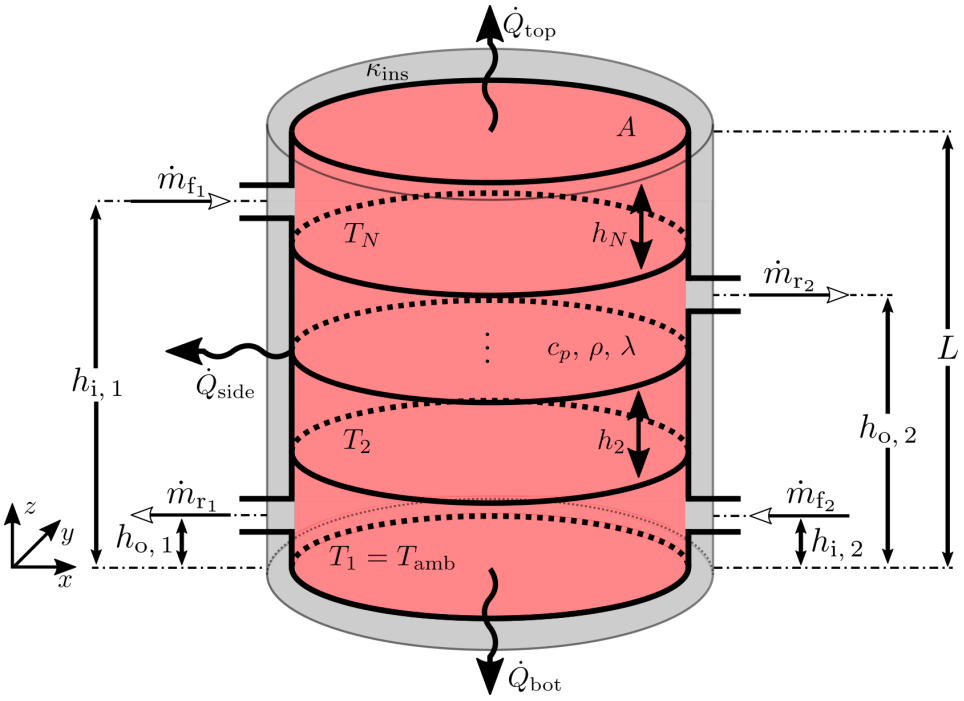

Figure 2.2.: Schematic of the multi-layer constant temperature representation of a cylindrical sensible heat storage.

Energy Transfer

Within the multi-layer constant temperature context, energy transfer by convection is represented such that every in- and outflowing stream of heat-transfer medium is represented by a superposition of at most N parallel mass streams whose respective temperatures are constant and equal to one of the defined layer temperatures. This is depicted in Figure 2.3 for the example of a generic mass stream with mass flow rate $\dot{m}$ and temperature T. Following from this representation, the rate of change of the energy $\dot{E}_{\text{ms}}$ transferred by the mass stream by means of convection may be approximated as follows:

$$\dot{E}_{\text{ms}} \approx \dot{m} \cdot c_p(T) \cdot T \overset{!}{=} \sum_{i=1}^{N} \dot{m}_i \cdot c_p\left(T_i\right) \cdot T_i\,. \tag{2.31}$$

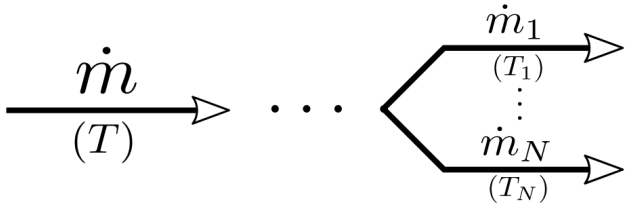

Figure 2.3.: Illustration of the proposed approximation method to represent energy transfer by convection. A mass stream with mass flow rate $\dot{m}$ and a variable temperature T is approximated as a mixture of at most N mass streams with mass flow rates $\dot{m}_i$ at pre-defined, constant temperatures T_i, $i = 1, \ldots, N$.

Here, $\dot{m}_i$ denotes the mass flow rate of the i-th parallel mass stream, which is defined to have the respective temperature T_i of the i-th layer of the sensible heat storage model. Naturally, the following condition regarding the individual mass flow rates of the introduced N fictitious parallel mass streams ought to hold:

$$\dot{m} \stackrel{!}{=} \sum_{i=1}^{N} \dot{m}_i \,. \tag{2.32}$$

In contrast to the previously discussed fixed temperature representation of energy transfer by convection, the proposed representation (2.31) facilitates the representation of mass streams with varying temperatures by means of adjusting the respective mass flow rates $\dot{m}_i$ of the parallel, constant temperature mass streams. The actual temperature T of the original mass stream is preserved as the mixed/aggregated temperature T_m of the N parallel mass streams:

$$T \stackrel{!}{=} T_\mathrm{m} := \frac{\sum\limits_{i=1}^{N} \dot{m}_i \cdot T_i}{\sum\limits_{i=1}^{N} \dot{m}_i} \,. \tag{2.33}$$

However, only temperature values within the range spanned by the extreme layer temperatures of the storage model can be represented by the illustrated method.

As mentioned before, each mass stream entering the storage is defined to only increase the size of the associated layer of equal temperature, regardless of the actual location where the mass stream enters the storage. Consequentially, the height changes of the layers within the storage resulting from inflowing mass streams may be expressed as follows:

$$\dot{h}_{\mathrm{in},\,l} = \frac{1}{\rho \cdot A} \cdot \sum_{j=1}^{N_\mathrm{i}} \dot{m}_{\mathrm{f}_j,\,l} \quad \forall\; l \in \{2,\,\ldots,\,N\}\,. \tag{2.34}$$

Here, the rate of change of the height of the l-th layer due to inflows of heat-transfer medium $\dot{h}_{\mathrm{in},\,l}$ is defined by all respective mass streams $\dot{m}_{\mathrm{f}_j,\,l}$ entering the respective layer through one of the N_i inlets of the storage. In the above equation A denotes the inner cross section area of the storage and ρ denotes the mean heat-transfer medium density. The height change of the first layer is not specifically considered, given the previously illustrated fact that its height can be determined from all other layer heights.

In contrast to the inflowing mass streams, the representation of outflowing mass streams is more involved in the multi-layer context, considering that for a specific outlet energy/mass may only be drawn from the specific layer that currently is located at the same height as said outlet. In order to express this restriction, N binary indicator variables $\mathrm{at}(l,k)$ are introduced for each of the N_o outlets of the storage to represent whether the l-th layer is currently accessible at the k-th outlet. With regards to the heights of all layers which are not at ambient temperature — the states of the multi-layer storage prediction model — these indicator variables are defined by the following mixed-logical proposition:

$$\begin{aligned} \mathrm{at}(l,\,k) \iff \left[L - \sum_{i=l+1}^{N} h_i > h_{\mathrm{o},k}\right] \wedge \left[L - \sum_{i=l}^{N} h_n \leq h_{\mathrm{o},k}\right] \quad \forall\; l \in \{2,\,\ldots,\,N\}\,, \\ \mathrm{at}(1,\,k) \iff \left[L - \sum_{i=2}^{N} h_i > h_{\mathrm{o},k}\right]\,. \end{aligned} \tag{2.35}$$

Here, h_i and $h_{\mathrm{o},k}$ denote the height of the i-th layer and respectively the height of the k-th outlet, as indicated in Figure 2.2.

In the article, the introduction of N additional auxiliary binary variables $\mathrm{ab}(l,\, k)$ for each outlet is proposed, which are defined as follows:

$$\mathrm{ab}(l,\, k) \iff \left[L - \sum_{i=l+1}^{N} h_i > h_{\mathrm{o},k} \right] \quad \forall\, l \in \{1,\, \ldots,\, N-1\}\,. \tag{2.36}$$

The introduced auxiliary variables indicate whether the upper boundary of the l-th layer exceeds, i.e. is *above*, the height of the k-th outlet. Naturally for the top-most layer, whose upper boundary coincides with the top of the storage, this would always be the case, hence:

$$\mathrm{ab}(N,\, k) = \texttt{true} \quad \forall\, k \in \{1,\, \ldots\, , N_\mathrm{o}\}\,. \tag{2.37}$$

With the introduced auxiliary variables it is possible to transform the mixed-logical propositions (2.35) into strictly logical propositions, namely:

$$\mathrm{at}(l,\, k) \iff \mathrm{ab}(l,\, k) \wedge \neg \mathrm{ab}(l-1,\, k) \quad \forall\, l \in \{2,\, \ldots,\, N\}\,, \tag{2.38}$$

or, for the case of the bottom layer:

$$\mathrm{at}(1,\, k) \iff \mathrm{ab}(1,\, k)\,. \tag{2.39}$$

With the discussed propositions that define the introduced binary variables, the restriction that each outlet may only draw from the layer that currently resides at the same height as the respective outlet, may be expressed by enforcing the following constraint for each outlet:

$$\dot{m}_{\mathrm{r}_k,\, l} \leq \mathrm{at}(l,\, k) \cdot \dot{m}^{\max}_{\mathrm{r}_k,\, l}\,. \tag{2.40}$$

Here, $\dot{m}_{\mathrm{r}_k,\, l}$ denotes the mass flow rate of the mass stream exiting the k-th outlet and drawing from the l-th layer. The variable $\dot{m}^{\max}_{\mathrm{r}_k}$ in the above equations denotes a chosen upper bound for the maximum mass flow rate that may pass through said outlet. In the above equation the binary variable $\mathrm{at}(l,\, k)$ is interpreted as either 1 or 0 depending on whether its value is `true` or `false`. Hence, the mass streams through the outlets of the storage are restricted to draw only from the layer currently residing at the respective outlet, as all other $\mathrm{at}(l, k)$ variables are naturally `false`, and hence through 2.40 define all other mass streams drawing from different layers to be zero.

With the illustrated outlet constraints, height changes of the storage layers due to outflowing mass streams may be computed similarly to (2.34) as follows:

$$\dot{h}_{\text{out},l} = -\frac{1}{\rho \cdot A} \cdot \sum_{k=1}^{N_\text{o}} \dot{m}_{\text{r}_k,l} \quad \forall\, l \in \{2, \ldots, N\}\,. \tag{2.41}$$

Ambient losses

For sensible heat storage tanks, losses of internal energy are assumed to mainly occur by means of conduction through the outer shell of the storage. Hence, in accordance with *Fourier's Law of Conduction*, the occurring thermal energy losses $\dot{Q}_{\text{loss},l}$ for the l-th layer of the storage model may be approximated by:

$$\dot{Q}_{\text{loss},l} = \kappa_{\text{ins}} \cdot A_l \cdot (T_l - T_{\text{amb}})\,. \tag{2.42}$$

Here, κ_{ins} is defined as the mean thermal conductance of the casing and insulation layer of the storage, A_l is the area of the outer surface of the storage that is in contact with the respective l-th layer, whilst T_l and T_{amb} represent the temperature of the l-th layer and the ambient surroundings respectively. Therefore, ambient thermal energy losses by conduction are directly dependent on the specific geometry of a considered sensible heat storage. This approximation of the occurring thermal energy losses by (2.42) is only valid if the sensible heat storage is in fact sufficiently well insulated, considering the inherent assumption that the outer surface of the insulation layer of the storage is actually at ambient temperature.

Given the assumed cylindrical shape of the storage, it is evident that one has to distinguish between thermal energy losses through the side and the top and bottom faces of the storage. Whilst losses through the side of the storage occur continuously and are directly proportional to the respective height of a layer, losses through the top and bottom occur only for the layer that currently is in contact with the top respectively the bottom of the storage.

In order to account for the latter phenomenon, similarly to the previously discussed phenomenon of storage discharge by means of outflowing mass

streams, two binary indicator variables are introduced for each layer, except for the layer with ambient temperature for which per definition no ambient thermal energy losses occur. The introduced binary variables indicate whether an individual layer is currently in contact with any of the two face sides of the storage. This measure allows to model the occurring ambient energy losses for each layer as follows:

$$\begin{aligned}\dot{Q}_{\text{loss},l} &= \dot{Q}_{\text{side},l} + \dot{Q}_{\text{top},l} + \dot{Q}_{\text{bot},l} \\ &= \kappa_{\text{ins}} \cdot (T_l - T_{\text{amb}}) \cdot \left(\underbrace{\frac{2 \cdot \pi}{\ln(r_{\text{o}}) - \ln(r_{\text{i}})} \cdot \dot{h}_l}_{\text{side}} + \underbrace{\text{adj}_{\text{t}}(l) \cdot A}_{\text{top}} + \underbrace{\text{adj}_{\text{b}}(l) \cdot A}_{\text{bottom}} \right) .\end{aligned} \tag{2.43}$$

Here, the total ambient losses for the l-th layer $\dot{Q}_{\text{loss},l}$ are determined by a combination of terms describing the losses through the side and the face sides of the storage. The energy losses through the side are computed based on the current height of the l-th layer h_l and the inner and outer radii of the storage, which are denoted by r_{i} respectively r_{o}. Energy losses through the face sides of the storage are defined directly proportional to the cross section area of the storage denoted by A, whereby the introduced binary indicator variables, $adj_{\text{t}}(l)$ for the top and $adj_{\text{b}}(l)$ for the bottom, express whether the l-th layer is currently in contact with one of the face sides.

In the above the inherent assumption is made that the insulating layer of the storage is of equal thickness and composition at both the wall and at the face sides. Hence, only a single general mean thermal conductance κ_{ins} needs to be defined/determined.

The introduced binary indicator variables are defined by the following propositions:

$$\begin{aligned}\text{adj}_{\text{t}}(l) &\iff \left[\sum_{i=l+1}^{N} h_i = 0 \right] \quad \forall\, l \in \{2, \ldots, N\} , \\ \text{adj}_{\text{b}}(l) &\iff \left[L - \sum_{i=l}^{N} h_i = 0 \right] \quad \forall\, l \in \{2, \ldots, N\} .\end{aligned} \tag{2.44}$$

With the energy losses quantitatively defined for each layer, the occurring thermal energy losses, that physically would manifest themselves in a temperature decrease of the medium within the storage, have to be translated into the multi-layer constant temperature context. In said context, energy losses for a specific layer have to be expressed by decreasing the respective height and hence the volume of the layer. However, considering that the sum of all layer heights is set to remain constant, every height decrease of a particular layer has to result in a equivalent height increase of another layer. Therefore, thermal losses of a particular layer are considered by an associated height decrease and a equal height increase of that adjacent layer whose temperature is closer to the ambient temperature, and hence its specific usable energy is lower.

To denote the index of the layer that is adjacent to the l-th layer, the indicator τ_l is introduced and defined as follows:

$$\tau_l := \begin{cases} -1 & T_l > T_{\text{amb}} \\ 1 & T_l < T_{\text{amb}} \end{cases}, \tag{2.45}$$

The height change of the l-th layer due to ambient thermal energy losses $\dot{h}_{\text{amb},l}$ can then be computed as the ratio between the total ambient losses per layer and the energy difference between the l-th and its adjacent layer per unit height:

$$\begin{aligned} \dot{h}_{\text{amb},l} &= -\frac{\dot{Q}_{\text{loss},l}}{\rho \cdot A \cdot \left(c_p\left(T_l\right) \cdot T_l - c_p\left(T_{l+\tau_l}\right) \cdot T_{l+\tau_l}\right)} \quad \forall\, l \in \{2, \ldots, N\}\,, \\ \dot{h}_{\text{adj},l+\tau_l} &= -\dot{h}_{\text{amb},l} \quad \forall\, l + \tau_l \in \{2, \ldots, N\}\,. \end{aligned} \tag{2.46}$$

Axial Conduction

The term axial conduction, in the context of sensible heat storages, refers to the physical phenomenon where if two layers of liquid, each with uniform though different temperature, are brought into contact, the layer with the higher temperature will overtime transfer thermal energy by means of conduction to the layer of lower temperature, hence increasing its respective temperature and forming the aforementioned thermocline. This process

continues naturally until both layers reach a uniform equilibrium temperature, whereupon no further energy transfer between the layers occurs. Thus, in the context of sensible heat storages this phenomenon does not entail a decrease of internal energy, but rather a potential decrease in usable energy (exergy). For the considered storage, the phenomenon of axial conduction can be shown to be reasonably well described by the following partial differential equation (see e.g. [31]):

$$\frac{\partial T}{\partial t} = \frac{\lambda}{c_p \cdot \rho} \cdot \frac{\partial^2 T}{\partial z^2} \,. \tag{2.47}$$

Here, T denotes the height- and time-dependent temperature, λ the thermal conductivity and c_p the isobaric specific heat of the medium within the storage[1].

Equation (2.47) supports the intuition that the effects of axial conduction, i.e. the smoothing of the vertical temperature profile $T(z)$ within the storage, are particularly pronounced if $T(z)$ contains sharp changes, e.g. as they would occur in a well stratified storage. Considering that in the context of the presented modeling approach layer temperatures are set constant, the following proceedings will discuss how the phenomenon of axial conduction described by (2.47) may be captured by means of layer height variations.

To derive a representation/approximation of axial conduction in the multi-layer constant temperature context, consider the medium within the storage to be uniformly spatially discretized in z-direction with a step width of Δz, resulting in equal-sized cells/slabs of volume. The enthalpy H_c stored within such a cell of constant volume $V_c = \Delta z \cdot A$ is then defined by:

$$\dot{H}_\mathrm{c} = \Delta z \cdot A \cdot \rho \cdot c_p \cdot \dot{T}_\mathrm{c} \,. \tag{2.48}$$

Here, T_c denotes the temperature of the medium within the cell, which is assumed to be uniform within the enclosed volume V_c. In the multi-layer constant temperature context, this change in enthalpy needs to be expressed by means of varying layer heights. This may be achieved by means of the following equation:

$$\dot{H}_\mathrm{l} \approx \dot{h}_\mathrm{l} \cdot A \cdot \rho \cdot c_p \cdot (T_\mathrm{l} - T_0) \,, \tag{2.49}$$

[1] Considering the assumption that the medium within the buffer is incompressible, the isobaric specific heat is in fact equal to the isochoric specific heat.

where $\dot{H}_\mathrm{l}$ denotes the temporal change of the enthalpy of a considered layer, $\dot{h}_\mathrm{l}$ denotes the equivalent change in layer height, and T_l denotes the constant layer temperature.

The temporal change of the temperature $\dot{T}_\mathrm{c}$ within each cell, due to axial conduction, can be approximated by utilizing the central difference formula to rewrite the second spatial derivative in (2.47) s.t.:

$$\dot{T}_\mathrm{c} = \frac{\lambda}{c_p \cdot \rho} \cdot \frac{T_{\mathrm{c}-1} - 2T_\mathrm{c} + T_{\mathrm{c}+1}}{\Delta z^2} \,. \tag{2.50}$$

Here, $T_{\mathrm{c}-1}$ and $T_{\mathrm{c}+1}$ denote the temperatures of the adjacent lower respectively adjacent upper cell. An appropriate approximation of the central difference formula in the context of layers with varying heights, i.e. space is not discretized uniformly, is proposed in the article as follows:

$$\frac{\partial^2 T_l}{\partial z^2} \approx \frac{1}{h_l} \cdot \left(\frac{T_{l-1} - T_l}{\frac{1}{2}\left(h_{l-1} + h_l\right)} - \frac{T_l - T_{l+1}}{\frac{1}{2}\left(h_l + h_{l+1}\right)} \right) . \tag{2.51}$$

Here, the second partial derivative of the temperature of the l-th layer with respect to z is defined by the temperatures of the adjacent layers and their respective layer heights. Consequently, inserting (2.51) into (2.47) and subsequently into (2.48), and equating (2.48) and (2.49) yields:

$$\dot{h}_l \cdot A \cdot \rho \cdot c_p \cdot \left(T_l - T_0\right) \approx 2\lambda A \left(\frac{T_{l-1} - T_l}{h_{l-1} + h_l} - \frac{T_l - T_{l-1}}{h_{l+1} + h_l} \right) . \tag{2.52}$$

Notably, the above equation is non-linear with respect to the layer heights, following the natural intuition that a smaller adjacent layer would entail a faster energy transfer. The resulting inverse proportionality cannot be included into the state-space representation of the multi-layer constant temperature storage model, given the previously stated notion of hybrid linear models.

The classical approach to circumvent this issue of non-linearity would be to linearize the inverse proportionality by means of a tangent through an operating point x_0 s.t.:

$$\frac{1}{x} \approx \frac{1}{x_0} - \frac{1}{x_0^2}\left(x - x_0\right) . \tag{2.53}$$

However, depending on the chosen x_0, the above linearization may become negative for large values of x which would compromise the stability of the multi-layer storage model as it would have the effect of growing extreme temperature layers as opposed to shrinking them. This stability issue, however, could be resolved by setting $x_0 = \frac{L}{2}$ and hence preventing negative values, considering that x — the sum of two layer heights — is naturally limited between 0 and L. However, as pointed out in the article, any linearization will result in a non-linear expression if the differential equations ought to be discretized in time, which is necessary if the discussed model ought to be utilized as a prediction model for MPC. Thus, the inverse proportionality may only be approximated by a constant which will result in at least an accurate approximation of the steady-state of the phenomenon of axial conduction.

Following from the above remarks, axial conduction evidently cannot be accurately represented within the context of modeling a sensible heat storage by means of multiple layers at constant temperatures. Therefore, if one requires a prediction model that accurately represents the phenomenon of axial conduction within a sensible heat storage (e.g. when modeling large seasonal TES), the proposed model may not be suitable. However, the authors of the article propose the following method in order to at least approximately capture the occurring exergy losses caused by axial conduction.

As mentioned previously, the phenomenon of axial conduction manifests itself in the fact that overtime layers of extreme temperature within a stratified storage scenario will transfer energy by means of conduction to layers of lower temperature. Representing this fact in the multi-layer constant temperature context implies that layers of higher temperature will decrease in size, whilst adjacent layers of lower temperature will increase in size. However, in contrast to the representation of ambient losses, the phenomenon of axial conduction will not result in a decrease of enthalpy, hence requiring the consideration of layer triplets as opposed to pairs. Within such a layer triplet configuration the two outer layers will reduce in size whilst the central one will increase by the same amount. This behavior is somewhat coherent with the steady-state of the axial conduction process, where the medium within the storage would be at a uniform temperature preserving all previously contained enthalpy. With regards to the proposed triplet perspective, this

final steady-state is represented, depending on the initially stored energy within the storage and the defined layer temperatures, either accurately by a single layer occupying the whole volume of the storage, or approximately by two adjacent layers whose relative size would match the initially stored energy within the storage.

For the proposed method, the following constraints need to be enforced for each designated layer triplet.

$$\dot{h}_{l-1} + \dot{h}_l + \dot{h}_{l+1} \stackrel{!}{=} 0\,, \tag{2.54}$$

$$\dot{h}_{l-1} \cdot (T_{l-1} - T_0) + \dot{h}_l \cdot (T_l - T_0) + \dot{h}_{l+1} \cdot (T_{l+1} - T_0) \stackrel{!}{=} 0\,. \tag{2.55}$$

Here, an exemplary layer triplet is considered with the l-th storage layer in the center and the adjacent layers at the top respectively at the bottom. The constraints (2.54) and (2.55) imply the preservation of the energy stored within the buffer and the preservation of the combined layer height.

By reformulating the above constraints, the respective height changes of the layers might be expressed as follows:

$$\dot{h}_l = -\dot{h}_{l-1} - \dot{h}_{l+1}\,, \tag{2.56}$$

$$\dot{h}_{l+1} = \frac{T_l - T_{l-1}}{T_{l+1} - T_l} \cdot \dot{h}_{l-1}\,. \tag{2.57}$$

The height change of the top layer of the triplet, that occurs given the occurring energy transfer from the top layer to the central layer, may be defined in accordance with Fourier's Law of Conduction s.t.:

$$\dot{h}_{l+1} = -\kappa_{l+1,l} \cdot A \cdot (T_{l+1} - T_l)\,, \tag{2.58}$$

where $\kappa_{l+1,l}$ symbolizes the thermal conductance between the top and central layer. This thermal conductance, however, would be generally defined as inversely proportional to the layer heights h_{l+1} and h_l. Given that this inverse proportionality cannot be expressed by means of hybrid linear equations, $\kappa_{l+1,l}$ may be set equal to:

$$\kappa_{l+1,l} = \frac{\lambda}{L/N}\,. \tag{2.59}$$

where L denotes the height of the storage and N is the number of considered storage layers. Depending on the typical layer configuration within, and operation of a respective storage, $\kappa_{l+1,l}$ may be chosen differently or individually for each layer pair as to approximate the actual temporal progression of axial conduction better.

It is evident from (2.56) and (2.57) that energy transfer within a triplet configuration may only occur whilst the two extreme layers have a height greater than zero. If one of the extreme layers reaches zero height, a different layer might come into contact with the central layer driving its continuing height increase or the former central layer may turn into an extreme layer of a different triplet configuration. Similarly to the previous discussions on representing the ambient losses occurring at the face sides of the storage, this circumstance can be represented by a set of discrete states, hence binary indicator variables are introduced which represent whether a distinct layer triplet configuration is currently active within the storage. Considering the high number of binary variables that would have to to be introduced if all viable triplet combinations would be considered, the inherent redundancy within the choice of triplet combinations can be used to reduce the amount of introduced binary variables. Hence, within the article, the authors restrict the considered triplet combinations by considering only consecutive pairs of layers making up the top and central layer, with the next lower layer of non-zero height forming the bottom layer of an active triplet.

For each triplet constructed in this way, the respective binary indicator variable $tri(c+1,\, c,\, b)$, indicates whether the height of the top $(c+1)$ and bottom (b) layer are non-zero. Therefore it is defined by the following mixed-logic propositional statement:

$$\mathrm{tri}(c+1,\, c,\, b) \iff [h_{c+1} > 0] \wedge [h_b > 0] \wedge \bigwedge_{i=b+1}^{c-1} [h_i = 0]\,. \tag{2.60}$$

By integrating these indicator variables into (2.58) and using (2.56) as well as (2.57), the phenomenon of axial conduction is represented in the multi-layer constant temperature context for each triplet, by means of the following

height changes:

$$\begin{aligned}
\dot{h}_{\text{top, tri}(c+1,c,b)} &= -\text{tri}(c+1,\, c,\, b) \cdot \frac{\lambda}{L/N} \cdot A \cdot (T_{c+1} - T_c)\,, \\
\dot{h}_{\text{mid, tri}(c+1,c,b)} &= -\dot{h}_{\text{top, tri}(c+1,c,b)} - \dot{h}_{\text{bot, tri}(c+1,c,b)}\,, \\
\dot{h}_{\text{bot, tri}(c+1,c,b)} &= \dot{h}_{\text{top, tri}(c+1,c,b)} \cdot \frac{T_{c+1} - T_c}{T_c - T_b}\,.
\end{aligned} \tag{2.61}$$

Given that each layer may be part of several triplet configurations, the following combined height changes for each layer are defined:

$$\begin{aligned}
\dot{h}_{\text{cond},N} &= \sum_{i=1}^{N-2} \dot{h}_{\text{top, tri}(N,N-1,i)}\,, \\
\dot{h}_{\text{cond},N-1} &= \sum_{i=1}^{N-3} \dot{h}_{\text{top, tri}(N-1,N-2,i)} + \sum_{i=1}^{N-2} \dot{h}_{\text{mid, tri}(N,N-1,i)}\,, \\
\dot{h}_{\text{cond},l} &= \sum_{i=1}^{l-2} \dot{h}_{\text{top, tri}(l,l-1,i)} + \sum_{i=1}^{l-1} \dot{h}_{\text{mid, tri}(l+1,l,i)} + \sum_{i=l+1}^{N} \dot{h}_{\text{bot, tri}(i+1,i,l)} \\
&\qquad \forall\, l \in \{3,\, \ldots,\, N-2\}\,, \\
\dot{h}_{\text{cond},2} &= \dot{h}_{\text{mid, tri}(3,2,1)} + \sum_{i=3}^{N} \dot{h}_{\text{bot, tri}(i+1,i,2)}\,, \\
\dot{h}_{\text{cond},1} &= \sum_{i=2}^{N} \dot{h}_{\text{bot, tri}(i+1,i,1)}\,.
\end{aligned} \tag{2.62}$$

Although it is not possible to accurately represent axial conduction within the multi-layer constant temperature context by means of the above equations, they do entail a similar steady-state behavior. Therefore, by utilizing the presented layer triplet method, indications as to the occurring loss of exergy are present within the storage prediction model and may thus be assessed within the EMS optimization problem when determining the optimal plan of operation for the considered storage and the MES that the storage is integrated in.

2.3.2. Complete Model

With the discussed representations of the dominant physical phenomena of energy transfer by convection, ambient losses and axial conduction, the complete multi-layer constant temperature thermal storage prediction model can be assembled. The height changes of the layers within the storage are determined by the combined contributions of the individual physical effects, resulting in the following state-space model:

$$\dot{h}_l = \dot{h}_{\text{in},l} + \dot{h}_{\text{out},l} + \dot{h}_{\text{amb},l} + \dot{h}_{\text{adj},l} + \dot{h}_{\text{cond},l} \quad \forall\, l \in \{2, \ldots, N\}\,. \tag{2.63}$$

The following chapter is concerned with the implications of the introduced method of representing convective energy transfer by means of a set of parallel mass streams at fixed temperatures. Specifically, the effects of applying this method to the existing prosumers models, and how the added flexibility may be used to improve the performance of an EMS by considering temperature-dependent prosumer behavior, will be discussed.

Second, the most important aspects regarding the actual implementation of the presented TES model into the existing framework will be briefly summarized.

3. Modeling Prosumers Within Hydronic Systems

The physical analysis and modeling of hydronic systems typically commences by formulating fundamental energy and mass balance equations for all individual components of the investigated system, and subsequently linking those equations to describe interactions (energy/mass transfer) between the components.

For each component, these balance equations describe how and by which means energy or mass is consumed from, and provided back to, the environment of the component. Hence, they provide an abstraction of the inner-workings of a component by means of energy interactions with its environment. Considering that in EMS only these kind of interactions are of interest when modeling prosumers, energy and mass balance equations serve as the starting point when deriving prediction models for specific prosumers.

In the following, the fundamental energy and mass balance equations for a generic prosumer in a hydronic system will be derived. To do this, a generic prosumer will be treated as a so-called *control volume* or *open system*, a thermodynamic term that simply describes a closed volume of space at whose boundaries energy and mass transfer occurs. In the context of hydronic systems, the derived balance equations can be significantly simplified under a few basic assumptions. The simplified equations allow the interpretation that the energy interactions of a prosumer with its environment in a hydronic system are driven by energy transfer by convection, which is described by (1.1) — the equation whose bilinearity motivated the deliberations presented in this thesis.

Subsequently, the derived balance equations will be reformulated to consider the previously introduced notion of representing mass streams at varying temperatures, by means of sets of parallel mass streams at fixed temperatures. Based on this, simple prediction models for common classes of prosumers in hydronic systems will be derived that utilize this notion of varying temperature to capture temperature-dependent prosumer behavior. The considered prosumer classes are namely, generic consumers, generic producer, solar thermal collectors and heat pumps. Additionally, the representation of flow diverters in the form of valves (switches) and multi-port tee pieces (distributors) as well as the updated representation of connections will be briefly discussed.

Last, the main aspects concerning the integration of the previously discussed multi-layer constant temperature model of sensible heat storages into the EMS framework will be summarized.

3.1. Control Volume Analysis

The following analysis of the energy and mass balance equations of a generic control volume will serve as the foundation for the subsequent derivation of prosumer prediction models. This analysis will be conducted for the simplified control volume depicted in Figure 3.1. Notably, the depicted control volume — bounded by the dashed line — comprises only one inlet, and one outlet, with the mass stream through each being assumed to be strictly one-dimensional. Although shown for this simplified example, the following deliberations can be easily extended to more sophisticated configurations and applications that involve e.g. multi-dimensional mass flow through multiple inlets and outlets. However, this general derivation is omitted here, as to not obstruct the important fundamental assertions by mathematical intricacies. Nevertheless, the developed insights may serve as a general starting point when deriving generic models for prosumers within hydronic systems.

For the depicted control volume the *first law of thermodynamics* — the energy conservation principle — defines the rate of change of the energy contained

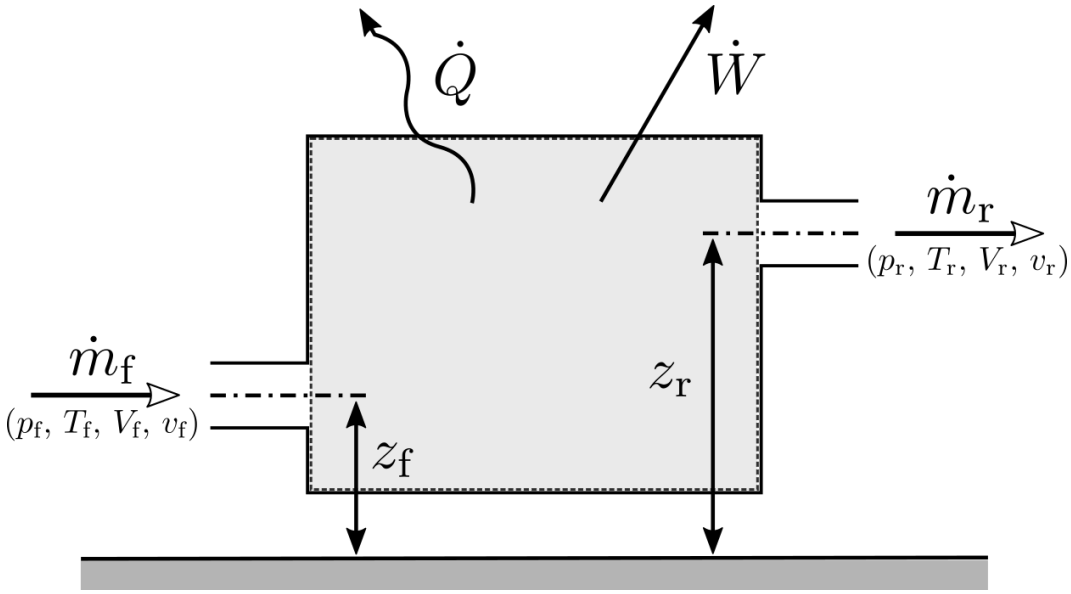

Figure 3.1.: Considered control volume with a single inlet and outlet, and one-dimensional mass streams.

within the control volume E_cv, as follows:

$$\dot{E}_\mathrm{cv} = -\dot{Q} - \dot{W} + \dot{E}_\mathrm{f} - \dot{E}_\mathrm{r}\,. \tag{3.1}$$

The terms $\dot{Q}$ and $\dot{W}$ refer to the net rate of energy transfer by heat respectively work along the boundary of the control volume. Besides energy transfer by means of heat or work, energy transfer by means of bulk motion of matter of the entering and exiting mass streams needs to be considered. The resulting contributions of this form of energy transfer to the total internal, kinetic or potential energy of the control volume are comprised in the terms $\dot{E}_\mathrm{f}$ for the inflowing (feed path), and in $\dot{E}_\mathrm{r}$ for the outflowing mass stream respectively.[1]

By introducing the specific internal energy u [$\mathrm{J\,kg^{-1}}$] of a medium, the transfer of kinetic, potential and internal energy entailed by a one-dimensional

[1]The sign convention adopted in the above and the remainder of this section is in accordance with the arrows indicated in Figure3.1. Work done by and heat transfer from the control volume are defined to be positive, whilst work done to and heat transfer into the control volume are defined to be negative.

stream of mass crossing a control volume boundary can be expressed as follows:

$$\dot{E}_{\mathrm{ms}} = \dot{m}_{\mathrm{ms}} \cdot \left(u_{\mathrm{ms}} + \frac{V_{\mathrm{ms}}^2}{2} + g_{\mathrm{ms}} \cdot z_{\mathrm{ms}} \right) . \tag{3.2}$$

In the above equation, the energy transfer $\dot{E}_{\mathrm{ms}}$, entailed by a stream of matter crossing the boundary of the control volume at a mass flow rate of $\dot{m}_{\mathrm{ms}}$, is expressed by means of the associated changes of internal, kinetic and potential energy. The change in internal energy is defined with respect to the specific internal energy of the conveyed medium u_{ms}. The change in kinetic energy is defined by the normal velocity V_{ms} of the mass stream, which is defined with respect to the orientation of the control volume boundary. The change in potential energy is defined by the gravitational acceleration g_{ms} and the height z_{ms} at which the mass stream enters or exits the control volume.

Using (3.2) to describe the transfer of energy entailed by the in- and outflowing mass streams, $\dot{E}_{\mathrm{r}}$ respectively $\dot{E}_{\mathrm{f}}$, within the energy balance equation (3.1) of the considered control volume, results in the following:

$$\dot{E}_{\mathrm{cv}} = -\dot{Q} - \dot{W} + \dot{m}_{\mathrm{f}} \cdot \left(u_{\mathrm{f}} + \frac{V_{\mathrm{f}}^2}{2} + g_{\mathrm{f}} \cdot z_{\mathrm{f}} \right) - \dot{m}_{\mathrm{r}} \cdot \left(u_{\mathrm{r}} + \frac{V_{\mathrm{r}}^2}{2} + g_{\mathrm{r}} \cdot z_{\mathrm{r}} \right) . \tag{3.3}$$

Considering the fact that mass flowing over the boundary of a control volume is always associated with so-called flow work, due to the pressure of the entering and exiting medium, the rate of energy transfer by work $\dot{W}$ can be expressed with respect to the mass flow rate at the inlet and outlet s.t.:

$$\dot{W} = \dot{W}_{\mathrm{cv}} + \dot{m}_{\mathrm{r}} \cdot p_{\mathrm{r}} \cdot v_{\mathrm{r}} - \dot{m}_{\mathrm{f}} \cdot p_{\mathrm{f}} \cdot v_{\mathrm{f}} . \tag{3.4}$$

In (3.4) the term $\dot{W}_{\mathrm{cv}}$ comprises the combined net energy transfer by work along the boundary of the control volume with the exception of energy transfer by flow work, which is defined by the mass flow rate $\dot{m}$, the specific volume v and the pressure p of the medium at the inlet and at the outlet respectively. By introducing the specific enthalpy h:

$$h = u + p \cdot v , \tag{3.5}$$

and substituting (3.4) and (3.5) into (3.3), the following expression for E_{cv} is obtained:

$$\dot{E}_{cv} = -\dot{Q} - \dot{W}_{cv} + \dot{m}_f \cdot \left(h_f + \frac{V_f^2}{2} + g_f \cdot z_f \right) - \dot{m}_r \cdot \left(h_r + \frac{V_r^2}{2} + g_r \cdot z_r \right) . \tag{3.6}$$

The above equation (3.6) is typically referred to as as the *one-dimensional flow form of the control volume energy rate balance* in literature (see e.g. [15]). For simplicity (3.6) has been defined as if h, g, V and z are uniform quantities within the respective mass streams crossing the control volume boundary, which for most hydronic systems is considered a sufficient approximation of the actual physical reality.

Besides the principle of energy conservation, the rate of change of the mass contained within the control volume $\dot{m}_{cv}$ is defined by the principle of *mass conservation* which states that:

$$\dot{m}_{cv} = \dot{m}_f - \dot{m}_r . \tag{3.7}$$

With the balance equations (3.6) and (3.7) it is possible to quantitatively express energy conversion within, and mass and energy transfer between components of a hydronic system. These balancing equations are applicable to every generic prosumer with one inlet and one outlet, whereas the specific behavior or physical properties of each prosumer are comprised within the respective work and heat terms $\dot{W}_{cv}$ respectively $\dot{Q}$.

Considering the large sampling times which usually occur within an optimization-based EMS, it is typically sufficient to reduce the above equations to their steady-state forms. These are widely employed for the general thermodynamic analysis of components within a hydronic system, where the main focus of the analysis is on periods of steady operation, as opposed to transient startup and shutdown periods. For a control volume, steady-state operation infers that the mass within the control volume does not vary with time. Additionally, the mass flow rates and all rates of energy transfer by means of heat or work are similarly set constant with time. The balance

equations (3.7) and (3.6) can, thus, be simplified:

$$\dot{m}_\mathrm{f} = \dot{m}_\mathrm{r} = \dot{m}\,, \tag{3.8}$$

$$\dot{Q} + \dot{W}_\mathrm{cv} = \dot{m} \cdot \left((h_\mathrm{f} - h_\mathrm{r}) + \left(\frac{V_\mathrm{f}^2}{2} - \frac{V_\mathrm{r}^2}{2} \right) + g \cdot (z_\mathrm{f} - z_\mathrm{r}) \right) . \tag{3.9}$$

Notably, (3.9) allows the natural interpretation that in steady-state operation the net energy transferred along the boundary of the control volume by means of heat and work is completely provided, respectively absorbed, by the entering and exiting mass streams. Considering the fact that within a hydronic system the main means of energy transfer between components is the circulation of the heated or cooled heat-transfer medium, the differences in kinetic and potential energy between the mass streams at the inlet and at the outlet of prosumers are negligible for most applications. Thus, (3.9) may be further simplified to:

$$\dot{Q} + \dot{W}_\mathrm{cv} = \dot{m} \cdot (h_\mathrm{f} - h_\mathrm{r})\,, \tag{3.10}$$

where now all energy transfer by means of heat or work along the boundary of the control volume is enabled only by the difference in specific enthalpy, and as such mainly by the difference in temperature and pressure of the mass streams of heat-transfer medium at the inlet and outlet.

In hydronic systems the heat-transfer medium at the inlet and outlet of any component is typically of equal chemical composition. Furthermore, by assuming that the heat-transfer medium within a given hydronic system is a subcooled liquid, the heat-transfer medium may be idealized to be incompressible, i.e. its specific volume v is assumed to be constant. Using the isobaric specific heat, defined as:

$$c_p = \left(\frac{\partial h}{\partial T} \right)_p , \tag{3.11}$$

the difference in specific enthalpy between the mass stream at the inlet and outlet in (3.10) may therefore be rewritten as:

$$\dot{E}_\mathrm{conv} = \dot{Q} + \dot{W}_\mathrm{cv} = \dot{m} \cdot \left(\int_{T_\mathrm{r}}^{T_\mathrm{f}} c_p \,\mathrm{d}T + v\,(p_\mathrm{r} - p_\mathrm{f}) \right) . \tag{3.12}$$

Here, the energy transferred as a result of the difference in temperature and pressure of the heat-transfer medium at the inlet and outlet is denoted by E_{conv}. The temperature of the heat-transfer medium at the inlet is denoted by T_{f} respectively T_{r} for the outlet.

Notably, if the pressure difference between the inlet and outlet can be assumed to be negligible, the above equation (3.12) is further simplified[1] s.t.:

$$\dot{E}_{\text{conv}} = \dot{m} \left(\int_{T_{\text{r}}}^{T_{\text{f}}} c_p \, \mathrm{d}T \right) . \tag{3.13}$$

To even further simplify (3.13), one may consider that in the context of incompressible media [15]:

> "Over limited temperature intervals the variation of c can be small. In such instances the specific heat c can be treated as constant without serious loss of accuracy.".

Thus, depending on the considered temperature range and the chemical composition of the heat-transfer medium, one may either assume the specific heat to be constant or use the relevant endpoints of the isobaric specific heat as to simplify (3.13) s.t.:

$$\dot{E}_{\text{conv}} = \dot{m} \cdot \left[c_p(T_{\text{f}}) \cdot T_{\text{f}} - c_p(T_{\text{r}}) \cdot T_{\text{r}} \right] . \tag{3.14}$$

Notably, (3.14) is equal to (1.1) and represents the typical approximation for energy transfer by bulk motion of matter within a hydronic system.

[1] For the sake of completeness, please note that by representing the heat-transfer medium by means of the incompressible substance model, which is one of the fundamental assumptions for the derivation of (3.13), there is no need to emphasize the use of the isobaric specific heat c_p, considering that both isobaric and isochoric specific heat c_v, defined as:

$$c_v = \left(\frac{\partial u}{\partial T} \right)_v ,$$

are equal, and may thus be represented by a general indicator such as c. The specific denotation by c_p was preferred in this text over a more general denotation, considering that then (3.12) and potentially (3.13) are also valid for the steady-state energy transfer by bulk motion of matter if the respective heat-transfer medium were to be modeled as an ideal gas.

Based on the derived approximation, the following section will elaborate on how the previously illustrated method of representing a general mass stream with varying temperature by means of a superposition of parallel mass streams at constant temperatures (see equations (2.32) and (2.31)) may be used to extend the existing thermal prosumer prediction models within the discussed EMS framework, in order to be able to consider temperature-dependent prosumer behavior within the EMS.

3.2. Multi-Flow Constant Temperature Prediction Models

Including the proposed multi-flow constant temperature representation of a mass stream into the derived, simplified mass and energy balance equations ((3.8) and (3.14)) yields:

$$\sum_{i=1}^{N_\mathrm{f}} \dot{m}_{\mathrm{f},i} = \sum_{i=1}^{N_\mathrm{r}} \dot{m}_{\mathrm{r},i}\,, \tag{3.15}$$

$$\dot{E}_\mathrm{conv} \approx \sum_{i=1}^{N_\mathrm{f}} \dot{m}_{\mathrm{f},i} \cdot c_p\left(T_{\mathrm{f},i}\right) \cdot T_{\mathrm{f},i} - \sum_{i=1}^{N_\mathrm{r}} \dot{m}_{\mathrm{r},i} \cdot c_p\left(T_{\mathrm{r},i}\right) \cdot T_{\mathrm{r},i}\,. \tag{3.16}$$

Here, the one-dimensional mass stream at the single inlet and single outlet is each represented by N_f respectively N_r parallel mass streams $\dot{m}_{\mathrm{f},i}$ respectively $\dot{m}_{\mathrm{r},i}$, which each are defined to have a constant temperature of $T_{\mathrm{f},i}$ respectively $T_{\mathrm{r},i}$. Naturally, the following constraints, according to (2.32), need to be imposed to ensure sensible approximation results:

$$\dot{m}_\mathrm{f} \overset{!}{=} \sum_{i=1}^{N_\mathrm{f}} \dot{m}_{\mathrm{f},i}\,, \qquad \dot{m}_\mathrm{r} \overset{!}{=} \sum_{i=1}^{N_\mathrm{r}} \dot{m}_{\mathrm{r},i}\,. \tag{3.17}$$

In the following, this multi-flow constant temperature approximation of energy transfer by convection (3.16) for the one-dimensional flow, single inlet, single outlet control volume will be used as the foundation for deriving enhanced prediction models for prosumers within hydronic systems that will be integrated into the previously presented EMS framework.

3.2.1. General Prosumer Modeling Considerations

The following deliberations are valid for all kinds of prosumers. They concern: First, the choice of the number of considered parallel mass streams with fixed temperatures to represent a mass stream with varying temperature at the inlet or outlet of a prosumer. Second, the choice of the mass flow rates of the considered parallel mass streams, given that they are generally not uniquely determined by the temperature of the mass stream they represent. Last, considering that the heat-transfer medium inlet and outlet of prosumers are inherently connected, mass balance needs to be enforced between them, i.e. between the associated ports.

Temperature operating ranges

Most common prosumers within hydronic systems have defined temperature operating ranges, given by minimum and maximum bounds on the respective admissible temperatures at their inlets and outlets. Consider the case, where a prosumer is connected to a sensible heat storage that is represented by means of N layers of constant temperature. With respect to (3.16), it is evident that the set of $N_\mathrm{f} = N$ respectively $N_\mathrm{r} = N$ parallel mass streams $\{\dot{m}_1, \ldots, \dot{m}_N\}$ at the considered layer temperatures $\{T_1, \ldots, T_N\}$, that is defined for each in- and outflowing mass stream of a prosumer, thus, may be potentially unnecessarily large. This circumstance is noteworthy considering that each mass flow rate $\dot{m}_i$ is a control/optimization variable of the EMS optimization problem, hence increasing the computational complexity of the optimization problem. Following from this, only the minimal set of parallel mass streams useful in representing the defined temperature operating range of each respective prosumer inlet and outlet should be considered within the final prediction model of the prosumer.

To illustrate this by means of an example, consider an absorption chiller where the admissible temperature range at the inlet of its generator is defined to be 70 °C – 90 °C. The temperature of the mass stream at the outlet is internally controlled to always be at 50 °C. The generator is connected to a sensible heat storage which is represented by $N = 6$ layers at the temperatures of $T_l \in \{15\,°\mathrm{C}, 30\,°\mathrm{C}, 45\,°\mathrm{C}, 60\,°\mathrm{C}, 75\,°\mathrm{C}, 90\,°\mathrm{C}\}$. Consequentially,

it would be sensible to consider only a set of parallel mass streams at the latter three temperatures, respectively at the third and fourth temperature, to represent the actual mass stream entering respectively exiting the inlet and outlet of the generator. For the usual case that a prosumer is connected to a TES, the choice of considered temperatures at the inlets and outlets is, thus, dependent on the set of defined layer temperatures. Hence, the number of layers and the respective temperatures need to be carefully chosen considering the specifications of the connected prosumers in order to ensure that the whole temperature operating range of each connected prosumer can be represented as accurately as necessary.

Handling the ambiguity of the choice of mass flow rates of the parallel mass streams

Besides this limitation of the number of considered parallel mass streams, another important aspect concerns the *ambiguity* within the specific choice of the individual mass flow rates $\dot{m}_i$ when representing a mass stream of mass flow rate $\dot{m}$ and temperature T.

According to (2.32), the sum of all mass flow rates $\dot{m}_i$ is restricted to be equal to the mass flow rate $\dot{m}$ of the represented mass stream. However, with respect to (2.33), it is evident that the mass flow rates $\dot{m}_i$ are generally not uniquely determined by the temperature T of the represented mass stream. It is generally advantageous to assign non-zero values to only the mass flow rates $\dot{m}_i$ of those mass streams whose temperature T_i just exceeds, respectively is just inferior to, the actual temperature T of the original mass stream. This gives the best approximation of the transported energy, given that the isobaric specific heat c_p at temperature T is better approximated by values at temperatures close to it. More importantly, this eliminates the possibility for the solver to choose physically implausible values for the mass flow rates. For example, consider a boiler delivering a certain amount of thermal energy $\dot{E}$ at a temperature T_{hot} to a TES. Its feed stream could be represented by two mass streams at temperatures close to T_{hot}, but it also could by represented by two mass streams of greatly differing temperatures, one very hot and one close to the temperature at the inlet of the boiler. As a result, however, a temperature layer at low temperature

and a temperature layer at very high temperature within the storage would increase in height. The actual temperature distribution in the storage would, hence, be represented very inaccurately resulting in i.a. faulty estimates of the occurring thermal energy losses and the contained exergy within the storage. Such non-physical behavior could be the result of optimization if no restrictions are imposed.

The necessary restrictions can be applied within an optimization problem by enforcing so-called *special order set of type 2* (SOS2) constraints on the set of considered mass flow rates at each prosumer inlet and outlet. These SOS2 constraints are defined for a given ordered set of optimization variables and enforce that only two consecutive elements of said set can be non-zero. With respect to the considered mass flow rates, these ordered sets are obtained by sorting the mass flow rates $\dot{m}_i$ by their respective temperature T_i. The imposed SOS2 constraints then only allow for two consecutive mass flow rates, i.e. mass streams with adjacent temperatures, to be non-zero at any time.

Fluid circulation and mass balance

Considering that within a hydronic system a heat-transfer medium is circulated among prosumers, and that typically most prosumers do not have the capability to store mass, mass balance for the set of inlets and outlets of each prosumer has to be enforced at each time step. Hence, within the prediction model of a generic prosumer with N_i inlets and N_o outlets the following constraint needs to be enforced:

$$\sum_{m=1}^{N_\mathrm{i}} \sum_{i=1}^{N_{\mathrm{f},m}} \dot{m}_{\mathrm{f}_m,i} \overset{!}{=} -\sum_{m=1}^{N_\mathrm{o}} \sum_{i=1}^{N_{\mathrm{r},m}} \dot{m}_{\mathrm{r}_m,i}\,. \tag{3.18}$$

Here, $N_{\mathrm{f},m}$ and $N_{\mathrm{r},m}$ refer to the number of considered parallel mass streams to represent the mass stream entering the m-th inlet respectively outlet. Contrary to the sign convection used within the preceding derivations, here, inflowing mass streams are set to be negative as they were defined to be within the previously discussed EMS framework.

Aside from these general remarks on integrating the multi-flow constant temperature method into the prosumer prediction models of the existing EMS framework, the following sections will discuss prediction models for specific types of prosumers, as well as the representation of connections between them in further detail.

3.2.2. Generic Consumers

Generic thermal energy consumers within hydronic systems, such as heat radiators, are typically modeled to have only a single inlet and a single outlet. Their individual dynamics are typically negligible in light of the utilized large sampling periods, rather they are assumed to be completely specified by only their instantaneous thermal energy demand, which is assumed to be known or provided by means of forecasts.

Consumers are therefore represented by equality constraints ensuring adequate energy provision that meets their instantaneous demand $\dot{E}_{\mathrm{gc}}$ by means of the in- and outflowing mass stream of heat-transfer medium. With the multi-flow constant temperature approach to modeling general mass streams, these equality constraints can be formulated as follows:

$$\dot{E}_{\mathrm{gc}} \overset{!}{=} -\eta_{\mathrm{gc}} \cdot \left(\sum_{i=1}^{N_{\mathrm{f}}} \dot{m}_{\mathrm{f},i} \cdot c_p \left(T_{\mathrm{f},i} \right) \cdot T_{\mathrm{f},i} + \sum_{i=1}^{N_{\mathrm{r}}} \dot{m}_{\mathrm{r},i} \cdot c_p \left(T_{\mathrm{r},i} \right) \cdot T_{\mathrm{r},i} \right) . \tag{3.19}$$

In the above equation, $\eta_{\mathrm{gc}} \in (0, 1]$ denotes a general efficiency coefficient that defines the amount of primary (thermal) energy that has to be absorbed from the in- and outflowing mass stream to yield the end-use energy demand $\dot{E}_{\mathrm{gc}}$, which, given the established sign convention within the existing EMS framework, is positive for heating, respectively negative for cooling, applications.

From (3.19) it is apparent, that for the more general case of a consumer with multiple inlets and outlets, additional sum terms for each additional inlet and outlet have to be included in (3.19). For the case that a specific consumer may be able to use multiple forms of primary energy to meet its overall end-use energy demand, additional energy input terms, e.g. representing

electrical energy, along with potentially an energy form specific efficiency have to be added to the right side of (3.19).

In the event that the efficiency of energy conversion η_{gc} is dependent on the inlet temperature, individual efficiency coefficients can be introduced for each energy transfer contribution by one of the considered parallel inlet mass streams. Hence, (3.19) may be reformulated s.t.:

$$\dot{E}_{\mathrm{gc}} \stackrel{!}{=} -\sum_{i=1}^{N_{\mathrm{f}}} \eta_{\mathrm{gc,\,in},\,T_{\mathrm{f},\,i}} \cdot \dot{m}_{\mathrm{f},\,i} \cdot c_p\left(T_{\mathrm{f},\,i}\right) - \sum_{i=1}^{N_{\mathrm{r}}} \dot{m}_{\mathrm{r},\,i} \cdot c_p\left(T_{\mathrm{r},\,i}\right) \cdot T_{\mathrm{r},\,i}\,. \tag{3.20}$$

Here, $\eta_{\mathrm{gc,\,in},\,T_{\mathrm{f},\,i}} \in (0, 1]$ represents the individual efficiency factor defined for each considered inlet mass stream temperature $T_{\mathrm{f},\,i}$.

Similarly to the above, if applicable for a given consumer, one may also define individual efficiency factors depending on the temperature of the outlet mass streams s.t.:

$$\dot{E}_{\mathrm{gc}} \stackrel{!}{=} -\sum_{i=1}^{N_{\mathrm{f}}} \dot{m}_{\mathrm{f},\,i} \cdot c_p\left(T_{\mathrm{f},\,i}\right) \cdot T_{\mathrm{f},\,i} - \sum_{i=1}^{N_{\mathrm{r}}} \eta_{\mathrm{gc,\,out},\,T_{\mathrm{r},\,i}} \cdot \dot{m}_{\mathrm{r},\,i} \cdot c_p\left(T_{\mathrm{r},\,i}\right) \cdot T_{\mathrm{r},\,i}\,. \tag{3.21}$$

Here, contrary to the remarks on inlet temperature-dependent efficiencies, $\eta_{\mathrm{gc,\,out},\,T_{\mathrm{r},\,i}} \geq 1$, considering that the outflowing energy is subtracted from the inflowing energy to yield the net absorbed energy of the consumer.

The treatment of the circumstance where the efficiency of a consumer is not dependent on either the inlet nor the outlet temperature, but rather on the temperature difference between them, requires the introduction of continuous-valued auxiliary variables to represent the mass flow rates of the heat-transfer medium at each inlet–outlet temperature combination. Considering the particular relevance of this circumstance for the representation of solar thermal collectors, its mathematical representation in the multi-flow constant temperature context will be discussed in Section 3.2.4.

For most thermal energy consumers the admissible inlet temperature ranges are defined within the data sheet of the consumer or known to the system operator. Therefore, the set of considered inlet temperatures ought to be defined to span the whole defined range with as many intermediate temperature points as necessary depending on the required modeling accuracy. For

the case that a consumer is connected to a TES, the temperatures must match those of the layers in the TES. If the outlet temperature of a respective consumer can be modulated, the same reasoning as for the inlet temperatures applies to the outlet temperatures.

If the nominal ranges are undefined, they may be chosen with respect to the typical temperature setpoint of the consumer, e.g. 20 °C for a space-heating consumer. The considered inlet temperatures ought to be higher, the return temperatures ought to be lower than the defined setpoint for heating, and vice versa for cooling.

If the inlet and outlet temperature ranges intersect, additional limits on the sign of the inlet and outlet mass flow rates must be enforced. Otherwise a consumer could use energy from the return stream and pump it into the feed stream, which would make no physical sense.

3.2.3. Generic Producers

Producers are modeled similar to consumers. However, instead of a known/forecast demand, producers are defined by their controllable output power:

$$\dot{E}_{\mathrm{gp}} = u_{\mathrm{gp}} \cdot y_{\mathrm{gp}}^{\max} \overset{!}{=} \sum_{i=1}^{N_{\mathrm{f}}} \dot{m}_{\mathrm{f},i} \cdot c_p\left(T_{\mathrm{f},i}\right) \cdot T_{\mathrm{f},i} + \sum_{i=1}^{N_{\mathrm{r}}} \dot{m}_{\mathrm{r},i} \cdot c_p\left(T_{\mathrm{r},i}\right) \cdot T_{\mathrm{r},i}\,. \quad (3.22)$$

Here, the power output of the producer $\dot{E}_{\mathrm{gp}}$ is defined by the control variable $u_{\mathrm{gp}} \in [0,1]$ and with respect to the maximum producer output power $y_{\mathrm{gp}}^{\max}$. The instantaneous output power is then set equal to the thermal energy that is transferred by means of the in- and outflowing mass streams.

Minimal output power specifications can be included by introducing auxiliary variables, one binary, one real-valued, and corresponding constraints as illustrated in equations (2.16) - (2.18).

In order to provide the desired output power, a generic producer consumes primary energy $\dot{E}_{\mathrm{gp,in}}$ in a defined form, hence requiring:

$$-\eta_{\mathrm{gp}} \cdot \left(\sum_{i=1}^{N_{\mathrm{f}}} \dot{m}_{\mathrm{f},i} \cdot c_p\left(T_{\mathrm{f},i}\right) \cdot T_{\mathrm{f},i} + \sum_{i=1}^{N_{\mathrm{r}}} \dot{m}_{\mathrm{r},i} \cdot c_p\left(T_{\mathrm{r},i}\right) \cdot T_{\mathrm{r},i} \right) \overset{!}{=} \dot{E}_{\mathrm{gp,in}}\,. \quad (3.23)$$

In the above equations, η_{gp} represents a general conversion efficiency with which primary energy $E_{\mathrm{gp,in}}$ is converted into end-use thermal energy E_{gp}. Naturally, for generic producers that generate thermal energy for heating applications $\eta_{\mathrm{gp}} \leq -1$, respectively $\eta_{\mathrm{gp}} \geq 1$ for producers that provision thermal energy for the purpose of cooling.

Similarly to the previous remarks on modeling generic consumers, temperature-dependent conversion efficiencies may be considered by introducing individual conversion efficiencies for each considered inlet or outlet temperature.

Inlet temperature-dependent conversion efficiencies may be expressed as follows for generic producers that generate thermal energy for heating applications:

$$\sum_{i=1}^{N_{\mathrm{f}}} \eta_{\mathrm{gp,in},T_{\mathrm{f},i}} \cdot \dot{m}_{\mathrm{f},i} \cdot c_p\left(T_{\mathrm{f},i}\right) \cdot T_{\mathrm{f},i} + \sum_{i=1}^{N_{\mathrm{r}}} \dot{m}_{\mathrm{r},i} \cdot c_p\left(T_{\mathrm{r},i}\right) \cdot T_{\mathrm{r},i} \stackrel{!}{=} -\dot{E}_{\mathrm{gp,in}}\,. \quad (3.24)$$

Here, the introduced individual conversion efficiencies $\eta_{\mathrm{gp,in},T_{\mathrm{f},i}} \in (0,1]$ allow to represent inlet temperature-dependent producer efficiencies. Conversely, for generic producers that operate as chillers inlet temperature-dependent conversion efficiencies may be represented as follows:

$$\sum_{i=1}^{N_{\mathrm{f}}} \eta_{\mathrm{gp,in},T_{\mathrm{f},i}} \cdot \dot{m}_{\mathrm{f},i} \cdot c_p\left(T_{\mathrm{f},i}\right) \cdot T_{\mathrm{f},i} + \sum_{i=1}^{N_{\mathrm{r}}} \dot{m}_{\mathrm{r},i} \cdot c_p\left(T_{\mathrm{r},i}\right) \cdot T_{\mathrm{r},i} \stackrel{!}{=} \dot{E}_{\mathrm{gp,in}}\,. \quad (3.25)$$

Here, the individual factors $\eta_{\mathrm{gp,in},T_{\mathrm{f},i}}$ ought to be defined greater or equal to 1.

Outlet temperature-dependent conversion efficiencies of generic prosumers may be similarly represented by:

$$\sum_{i=1}^{N_{\mathrm{f}}} \dot{m}_{\mathrm{f},i} \cdot c_p\left(T_{\mathrm{f},i}\right) \cdot T_{\mathrm{f},i} + \sum_{i=1}^{N_{\mathrm{r}}} \eta_{\mathrm{gp,out},T_{\mathrm{r},i}} \cdot \dot{m}_{\mathrm{r},i} \cdot c_p\left(T_{\mathrm{r},i}\right) \cdot T_{\mathrm{r},i} \stackrel{!}{=} -\dot{E}_{\mathrm{gp,in}}\,, \quad (3.26)$$

with $\eta_{\mathrm{gp,out},T_{\mathrm{r},i}} \geq 1$ for heaters, whereby a higher value of $\eta_{\mathrm{gp,out},T_{\mathrm{r},i}}$ indicates a lower conversion efficiency, i.e. a higher consumption of primary energy. Conversely, for chillers:

$$\sum_{i=1}^{N_{\mathrm{f}}} \dot{m}_{\mathrm{f},i} \cdot c_p\left(T_{\mathrm{f},i}\right) \cdot T_{\mathrm{f},i} + \sum_{i=1}^{N_{\mathrm{r}}} \eta_{\mathrm{gp,out},T_{\mathrm{r},i}} \cdot \dot{m}_{\mathrm{r},i} \cdot c_p\left(T_{\mathrm{r},i}\right) \cdot T_{\mathrm{r},i} \stackrel{!}{=} \dot{E}_{\mathrm{gp,in}}\,, \quad (3.27)$$

with $\eta_{\mathrm{gp,out},T_{\mathrm{r},i}} \in (0,1]$, a lower value of $\eta_{\mathrm{gp,out},T_{\mathrm{r},i}}$ results in a lowered conversion efficiency.

For most generic producers the temperature operating ranges at each inlet and outlet are well defined in the data sheet of a respective prosumer. Hence, as illustrated for the case of a generic consumer, the considered mass stream temperatures ought to be chosen such that the whole operating range at the inlet and outlet may be accurately represented, or as accurate as the defined layer temperatures allow if the producer is connected to a TES.

3.2.4. Solar Thermal Collectors

Prior to the introduction of the multi-flow constant temperature approach, solar thermal collectors were considered as static thermal energy producers within the previously presented EMS framework. Considering the notion of constant inlet and outlet temperatures and, hence constant mean collector temperature, the expected future thermal energy yield of a solar thermal collector was forecasted independently of the actual operation of the hydronic system it was integrated in, but rather solely based on the expected ambient temperature and solar irradiance (see 2.2.3).

In the multi-flow constant temperature context this separation is no longer possible, considering that the inlet and outlet temperature of a collector may now be modulated and, hence affect the resulting thermal energy yield. However, contrary to a generic producer, the energy output of a solar collector is heavily dependent on outer conditions, namely solar irradiance and ambient temperature, and, hence cannot be freely controlled. To account for this interdependence between the yield of a solar thermal collector, and controllable operation conditions and outer disturbances, the following procedure to determine its expected yield is proposed: First, the expected thermal energy yield for each possible mean collector temperature $\bar{T}_{\mathrm{fl}}$, defined by possible inlet–outlet temperature combinations, is forecast by means of the forecasting method described in 2.2.3. Naturally, only combinations that result in a net energy yield, i.e. where the outlet temperature is greater than the inlet temperature, are considered.

T_f	T_r	$\bar{T}_\mathrm{fl}$
30 °C	45 °C	37.5 °C
30 °C	60 °C	45.0 °C
30 °C	75 °C	52.5 °C
45 °C	60 °C	52.5 °C
45 °C	75 °C	60.0 °C
60 °C	75 °C	67.5 °C

Table 3.1.: Inlet–outlet temperature combinations and the resulting mean collector temperatures.

To illustrate this, consider a solar collector whose inlet and outlet mass stream is approximated by parallel mass streams with temperatures $T_{\mathrm{f},i} \in \{30\,°\mathrm{C}, 45\,°\mathrm{C}, 60\,°\mathrm{C}\}$ respectively $T_{\mathrm{r},i} \in \{45\,°\mathrm{C}, 60\,°\mathrm{C}, 75\,°\mathrm{C}\}$. The considered inlet–outlet combinations for these sets, along with the resulting mean collector temperatures $\bar{T}_\mathrm{fl}$, are shown in Table 3.1. The expected yield is forecast for each of the different mean collector temperatures (taking into account the meteorological forecasts of ambient temperature and solar irradiance) using (2.7). The actual yield can then be determined by the optimizer by attributing weights to the individual inlet–outlet temperature pairs and the corresponding yield $\dot{E}_{\mathrm{solar},p}$. They are represented by auxiliary continuous variables z_p for each pair $p = 1, \ldots, N_\mathrm{pair}$ of inlet–outlet temperatures, $T_{\mathrm{f},p}$ and $T_{\mathrm{r},p}$, where N_pair denotes the number of considered inlet–outlet pairs. These weights have to sum up to one at each time instance if the solar collector is operational, i.e. if a mass stream is pumped through it. Otherwise, more than or not all of the available energy would be transported out of the solar collector. The latter mode of operation of the collector, so-called yield shedding, must be a conscious decision and should be handled outside of the solar collector model by means of a auxiliary modeled controllable thermal energy sink.

The energy yield of the solar collector $\dot{E}_\mathrm{solar}$, thus, simply is:

$$\dot{E}_\mathrm{solar} = \sum_{p=1}^{N_\mathrm{pair}} z_p \cdot \dot{E}_{\mathrm{solar},p}\,, \qquad \sum_{p=1}^{N_\mathrm{pair}} z_p = \delta_\mathrm{solar}\,. \tag{3.28}$$

Here, δ_{solar} is an auxiliary binary variable which represents whether the solar collector is operational, $\delta_{\text{solar}} = 1$, or not, $\delta_{\text{solar}} = 0$.

Each inlet–outlet temperature pair is uniquely linked to a mass flow rate via the corresponding predicted solar gain:

$$\dot{m}_p = z_p \cdot \frac{\dot{E}_{\text{solar},\,p}}{c_p(T_{\text{r},\,p}) \cdot T_{\text{r},\,p} - c_p(T_{\text{f},\,p}) \cdot T_{\text{f},\,p}} \tag{3.29}$$

The combined collector yield $\dot{E}_{\text{solar}}$ needs to be transferred out of the collector by means of the actual in- and outflowing mass streams, hence requiring:

$$\dot{E}_{\text{solar}} \overset{!}{=} \sum_{i=1}^{N_{\text{f}}} \dot{m}_{\text{f},\,i} \cdot c_p\left(T_{\text{f},\,i}\right) \cdot T_{\text{f},\,i} + \sum_{i=1}^{N_{\text{r}}} \dot{m}_{\text{r},\,i} \cdot c_p\left(T_{\text{r},\,i}\right) \cdot T_{\text{r},\,i}\,. \tag{3.30}$$

As the final step, the inlet- and outlet mass flow rates need to be determined from the pair mass flows rates $\dot{m}_p$. Therefore, the following constraints need to be met:

$$\dot{m}_{\text{f},\,i} \overset{!}{=} -\sum_{p \,\in\, \mathcal{P}_{T_{\text{f},\,i}}} \dot{m}_p\,, \qquad\qquad \dot{m}_{\text{r},\,i} \overset{!}{=} \sum_{p \,\in\, \mathcal{P}_{T_{\text{r},\,i}}} \dot{m}_p\,. \tag{3.31}$$

Here, the sets $\mathcal{P}_{T_{\text{f},\,i}}$, respectively $\mathcal{P}_{T_{\text{r},\,i}}$, comprise the indices of all inlet-outlet temperature pairs that consider the inlet temperature $T_{\text{f},\,i}$ respectively the outlet temperature $T_{\text{r},\,i}$.

In the vast majority of real-world applications a solar thermal collector is connected to a TES either directly or by means of a heat exchanger. Hence, the choice of considered inlet and outlet temperatures is typically dependent on the considered storage layer temperatures. In general, the considered outlet temperatures should be chosen depending on the application, i.e. whether the solar collector is expected to provide medium and/or high temperature thermal energy, and depending on operation limits defined in the data sheet of a particular collector. The considered inlet temperatures then may follow by considering all layer temperatures of lower temperature than the highest considered outlet temperature.

3.2.5. Heat Pumps

Heat pumps are characterized by the fact that they reverse the spontaneous/ natural direction of thermal energy transfer by conduction. They absorb thermal energy from a colder body (the source) and discharge it on a hotter body (the sink). According to the *second law of thermodynamics*, this inversion of the natural direction of thermal energy transfer requires an additional input of energy, typically by means of work.

With that said, a general heat pump may be modeled similar to a generic producer, where a *coefficient of performance* (COP) is defined instead of an efficiency factor η. It relates the net amount of thermal energy $\dot{E}_{\mathrm{hp,sink}}$ transferred to the thermal sink with the net amount of energy transferred by work $\dot{W}_{\mathrm{hp,in}}$ into the heat pump:

$$\mathrm{COP} = \left| \frac{\dot{E}_{\mathrm{hp,sink}}}{\dot{W}_{\mathrm{hp,in}}} \right| . \tag{3.32}$$

Hence, an energy balance equation similar to (3.22) may be constructed for a generic heat pump:

$$\dot{E}_{\mathrm{hp,sink}} = u_{\mathrm{hp}} \cdot y_{\mathrm{hp}}^{\max} \stackrel{!}{=} \sum_{i=1}^{N_{\mathrm{f}}} \dot{m}_{\mathrm{f},i} \cdot c_p\left(T_{\mathrm{f},i}\right) \cdot T_{\mathrm{f},i} + \sum_{i=1}^{N_{\mathrm{r}}} \dot{m}_{\mathrm{r},i} \cdot c_p\left(T_{\mathrm{r},i}\right) \cdot T_{\mathrm{r},i} . \tag{3.33}$$

The maximum thermal output power of the heat pump $y_{\mathrm{hp}}^{\max}$ is again set to be negative for cooling applications. The control input of the heat pump is restricted, $u_{\mathrm{hp}} \in [0,1]$. The necessary input energy for the heat pump operation can be defined with respect to the COP:

$$\dot{E}_{\mathrm{hp,sink}} \stackrel{!}{=} -\mathrm{COP} \cdot \dot{W}_{\mathrm{hp,in}} . \tag{3.34}$$

In reality, the COP of a heat pump is not a constant, but instead heavily dependent on operational and environmental conditions. For example, the efficiency of any heat pump is significantly influenced by the chosen temperature operating point. An increased temperature difference between the thermal source and sink will typically lower the COP.

A well-known example for this is the vapor-compression air source heat pump, which is commonly installed in residential and commercial buildings to provide space heating and cooling. This type of heat pump uses the ambient air as its thermal source (heating) respectively sink (cooling), thus its COP inherently varies significantly with the time of day and time of year. Hence, for modern air source heat pump space heating applications it is not uncommon to observe a varying COP in the range of $2 - 6$ in a single heating-season, depending on the outside temperature and the thermal energy demand.

This temperature dependency has to be considered specifically for each investigated heat pump, as it varies depending on the utilized heat pump technology and the properties of the thermal source (temperature, humidity for air source heat pumps, etc.). However, once the dependence of the COP on the inlet and outlet temperature is known, it may be considered in a similar way as varying efficiencies in the case of the generic producer or the solar thermal collector.

Absorption Chiller

A water-fired absorption heat pump (absorption chiller for short) needs to be modeled in a slightly different way. The energy here is not provided by means of work such as electric energy, but a high temperature fluid, hence heat. Therefore, in- and outflowing mass streams need to be considered as opposed to simple energy flows.

Absorption chillers are typically used for cooling applications. A high temperature fluid (the heat source) provides the necessary energy to regenerate an absorption solution that is used to cool a refrigerant. The combined absorbed thermal energy is dissipated by a third loop of heat-transfer medium whose temperature is typically stabilized by a controllable heat sink, e.g. a cooling tower. For the hydronic system comprising the three loops the overall energy balance of the absorption chiller can be stated as follows:

$$\dot{E}_{\text{gen}} + \dot{E}_{\text{evp}} + \dot{E}_{\text{abs}} \stackrel{!}{=} 0\,. \tag{3.35}$$

Here, $\dot{E}_{\text{gen}} < 0$ denotes the thermal energy that is absorbed from the high temperature loop (generator), $\dot{E}_{\text{evp}} < 0$ denotes the thermal energy absorbed from the refrigerant loop (evaporator) and $\dot{E}_{\text{abs}} > 0$ denotes the thermal energy that is transferred out of the chiller by means of the cooling loop (absorber).The latter usually has a temperature neither high enough for heating, nor low enough for cooling, and is thus considered waste heat.

The efficiency of the absorption chiller is again expressed via the COP, which relates the amount of obtained thermal energy for cooling at the evaporator with the thermal energy absorbed in the generator:

$$\text{COP} = \left| \frac{\dot{E}_{\text{evp}}}{\dot{E}_{\text{gen}}} \right| . \tag{3.36}$$

Conversely to the COP of heat pumps used for space heating that use the ambient surroundings as their thermal source, for the absorption heat pump it is typically smaller than one, e.g. 0.7, considering that the required high temperature thermal input energy $\dot{E}_{\text{gen}}$ usually has to be generated by a thermal energy producer within the hydronic system and the thermal energy in the cooling loop is as aforementioned considered waste heat.

The amount of absorbed thermal energy in the generator and the evaporator, and thus the COP, is typically found to strongly depend on the inlet temperature of the high temperature mass stream feeding the generator. The outlet temperature of the refrigerant at the evaporator is typically controlled internally, hence it may be assumed to be constant. Likewise, the inlet and outlet temperature at the absorber may be assumed constant since they can be controlled by the connected thermal energy sink. This last assumptions is necessary to sufficiently simplify available general models describing the behavior of an absorption chiller in order to use them as prediction models within an MPC-driven EMS.

Given the above assumptions, an absorption chiller can be represented by only considering the generator inlet temperature as the dominant modulable variable that defines the operation of the absorption chiller. The relationship between the generator inlet temperature and the thermal energy absorbed at the generator and evaporator, given a defined evaporator outlet and absorber

inlet temperature, is typically found in the data sheet of an absorption chiller.

Therefore, a simplified absorption chiller prediction model may be constructed, where the temperature dependence of the absorbed energy at the generator $\dot{E}_{\text{gen}}$ may be expressed as:

$$\begin{aligned}\dot{E}_{\text{gen}} &= \delta_{\text{chiller}} \cdot \sum_{i=1}^{N_{\text{f,gen}}} \dot{E}_{\text{gen},\,T_{\text{f,gen},i}} \cdot \frac{\dot{m}_{\text{f,gen},i}}{\dot{m}_{\text{gen,nom}}} \\ &\stackrel{!}{=} \sum_{i=1}^{N_{\text{f,gen}}} \dot{m}_{\text{f,gen},i} \cdot c_p\left(T_{\text{f,gen},i}\right) \cdot T_{\text{f,gen},i} + \sum_{i=1}^{N_{\text{r,gen}}} \dot{m}_{\text{r,gen},i} \cdot c_p\left(T_{\text{r,gen},i}\right) \cdot T_{\text{r,gen},i}\,.\end{aligned} \tag{3.37}$$

Here, $\dot{E}_{\text{gen},\,T_{\text{f,gen},i}}$ denotes the nominal absorbed thermal power at a generator inlet temperature of $T_{\text{f,gen},i}$ that is defined within the data sheet of an absorption chiller. Furthermore, the nominal mass flow rate through the generator, which is also typically defined within the data sheet of an actual absorption chiller, is denoted by $\dot{m}_{\text{gen,nom}}$. The return temperature is fixed, considering that $\dot{E}_{\text{gen}}$ is defined by the generator inlet temperature only, but might lie between the defined return mass stream temperatures $T_{\text{r,gen},i}$. Therefore, the sum is still formulated for the return mass streams, such that the mass flow rates will automatically adjust so that the appropriate temperature will be represented.

A binary variable δ_{chiller} representing whether the absorption chiller is *on* or *off* is introduced as well. It is necessary because the mass flow rates $\dot{m}_{\text{f,gen},i}$ cannot simply be reduced to zero. In order to ensure that the actual generator mass flow rate does not deviate too much from its nominal value, which otherwise would entail significant model errors, the following constraint is defined:

$$\dot{m}_{\text{gen}}^{\text{min}} \leq -\sum_{i=1}^{N_{\text{f,gen}}} \dot{m}_{\text{f,gen},i} \leq \dot{m}_{\text{gen}}^{\text{max}}\,. \tag{3.38}$$

Here, the admissible deviation is expressed by means of an absolute lower and upper bound, denoted by $\dot{m}_{\text{gen}}^{\text{min}}$ respectively $\dot{m}_{\text{gen}}^{\text{max}}$.

Many actual absorption chillers are controlled by means of an internal two-point controller, whereby the mass flow rate at the generator is not

modulated, but rather the associated pump is either switched *on* or switched *off*. In this case the above constraint may also be defined as an equality constraint, enforcing the combined mass flow rate through the generator to be equal to the rated nominal mass flow rate.

The absorbed thermal power $\dot{E}_{\text{evp}}$ at the evaporator may be expressed with respect to the generator inlet temperature s.t.:

$$\begin{aligned}\dot{E}_{\text{evp}} &= \delta_{\text{chiller}} \cdot \sum_{i=1}^{N_{\text{f,gen}}} \dot{E}_{\text{evp},\, T_{\text{f,gen},i}} \cdot \frac{\dot{m}_{\text{f,gen},i}}{\dot{m}_{\text{gen,nom}}} \\ &\overset{!}{=} \sum_{i=1}^{N_{\text{f,evp}}} \dot{m}_{\text{f,evp},i} \cdot c_p\left(T_{\text{f,evp},i}\right) \cdot T_{\text{f,evp},i} + \sum_{i=1}^{N_{\text{r,evp}}} \dot{m}_{\text{r,evp},i} \cdot c_p\left(T_{\text{r,evp},i}\right) \cdot T_{\text{r,evp},i} \,.\end{aligned} \tag{3.39}$$

As previously discussed, the absorbed thermal power at the evaporator is defined by the generator inlet temperature. The generator inlet temperature-dependent absorbed energy at the evaporator is denoted by $\dot{E}_{\text{evp},\, T_{\text{f,gen},i}}$. Specific values for it are typically defined within the data sheet of an absorption chiller. The total amount of absorbed power at the evaporator $\dot{E}_{\text{evp}}$ is defined by the weighted sum of these data sheet values. Although, the temperature at the outlet of the evaporator is usually assumed constant, given that it is typically internally controlled, a sum over several $\dot{m}_{\text{f,evp},i}$ is considered in the above equation, given that the layer temperatures of a storage that may be connected to the evaporator may not necessarily match this constant temperature.

Last, the energy transferred to the cooling loop $\dot{E}_{\text{abs}}$, which is defined through (3.35), has to be expressed by means of associated in- and outflowing mass streams:

$$\dot{E}_{\text{abs}} \overset{!}{=} \dot{m}_{\text{abs}} \cdot \left(-c_p\left(T_{\text{f,abs}}\right) \cdot T_{\text{f,abs}} + c_p\left(T_{\text{r,abs}}\right) \cdot T_{\text{r,abs}}\right) \,. \tag{3.40}$$

Considering that both the inlet ($T_{\text{f,abs}}$) and the outlet temperature ($T_{\text{r,abs}}$) of the absorber are assumed to be constant, only the mass flow rate $\dot{m}_{\text{abs}} > 0$ has to be determined such that the absorbed energy at the evaporator and the generator is transferred out of the chiller through the cooling loop, to be subsequently dissipated at a connected thermal energy sink.

The internal electrical energy consumption of the chiller (necessary to power the internal circulation pumps) is not explicitly considered in the presented prediction model. It is usually constant if the chiller is switched on, however, its contribution to the overall energy balance is negligible. If the cost of the consumed electricity should be considered, an auxiliary continuous variable describing this power consumption has to be introduced. It may then be defined as a constant, nominal power consumption value multiplied by the binary variable δ_{chiller}.

3.2.6. Distributors and Switches

In practical hydronic system applications, valves and fittings, such as tee-pieces, are used to distribute a mass stream of heat-transfer medium from one prosumer to other prosumers. Many valves are nowadays remotely controllable by a central process control system, and therefore need to be included in the prediction model of a hydronic system. Two distinct prosumers, *switches* and *distributors*, are used to represent valves and fittings in the EMS.

Distributors redistribute mass streams from N_{i} inlets among N_{o} outlets. They are represented mathematically by the following constraints for the combined set of considered distributor temperatures $\mathcal{T}$:

$$\sum_{i=1}^{N_{\text{i}}} \dot{m}_{\text{f}_{i,j_i}} + \sum_{o=1}^{N_{\text{o}}} \dot{m}_{\text{r}_{o,k_o}} \overset{!}{=} 0\,, \quad \text{for every } T_c \in \mathcal{T} \text{ with } T_{\text{f}_{i,j_i}} = T_{\text{r}_{o,k_o}} = T_c\,. \tag{3.41}$$

The above equality constraints enforce that all the mass streams entering the distributor at a certain temperature T_c through any of the inlets, must be redirected onto a set of equivalent outflowing mass streams with equal temperature. The set of considered temperatures $\mathcal{T}$ comprises all temperatures for which at least one inlet or outlet mass stream enters, respectively exits, the distributor. Therefore, if for any mass stream entering the distributor at a given temperature there is no exiting mass stream defined with equal temperature or vice versa, the above constraints enforces the mass flow rate of said mass stream to be zero at all times. Such a distributor only makes physical sense if all outlets have an intersection of considered parallel mass

stream temperatures, and if all inlet temperatures are part of the combined set of all outlet temperatures.

A *switch* connects one mass stream to one of several other mass streams. The direction is irrelevant: it can, thus, be either an input selector or an output selector. For the example of a switch with a single inlet and N_o outlets this gives:

$$-\dot{m}_{\mathrm{f},i} \stackrel{!}{=} \sum_{o=1}^{N_\mathrm{o}} \dot{m}_{\mathrm{r}_o,j_o}\,, \quad \text{for every } i = 1,\ldots,N_\mathrm{f}, \quad \text{and} T_{\mathrm{f},i} = T_{\mathrm{r}_o,j_o}\,. \tag{3.42}$$

In order to enforce that mass streams exit the switch through exclusively one outlet, *special ordered sets of type 1* (SOS1) constraints have to be defined. These constraints indicate to the optimizer that only one element out of a set of optimization variables, or linear expressions of optimization variables, may be non-zero. Hence, for the discussed single inlet, multiple outlets switch, the following SOS1 constraints need to be defined:

$$\mathrm{SOS1}\left(\left\{\sum_{i=1}^{N_{\mathrm{r}_1}} \dot{m}_{\mathrm{r}_1,i}\,,\ \ldots\ ,\ \sum_{i=1}^{N_{\mathrm{r}_{M_o}}} \dot{m}_{\mathrm{r}_{N_o},i}\right\}\right)\,. \tag{3.43}$$

Here N_{r_o} denotes the number of considered parallel mass streams at the o-th outlet. Only a single sum can then be greater than zero.

For the multiple inlets, single outlet case, the constraints may be defined in a similar way, but for the combined mass flow rates at the inlets instead of the outlets.

3.2.7. Connections

Within the multi-flow constant temperature context, mass balance between the source and the sink port of a connection generally does not infer energy balance. Thus, the representation of connections within hydronic systems needs to be adapted with respect to the model presented in Chapter2 Section 2.2.2. For the case of ideal connections, it is no longer sufficient that both source and sink port are of the same type, i.e. describing a mass stream

of the same heat-transfer medium, but rather they must, now, describe the medium at the same temperatures as well. Therefore, an ideal connection may be expressed by the following constraint within the multi-flow constant temperature context:

$$\dot{m}_{\mathrm{f},i} + \dot{m}_{\mathrm{r},j} \overset{!}{=} 0 \quad \text{for every } T_c \in \mathcal{T} \text{with } T_{\mathrm{f},i} = T_{\mathrm{r},j} = T_c\,. \tag{3·44}$$

The set $\mathcal{T}$ comprises the considered temperatures of the parallel mass streams at both the source and the sink of the connections. Any parallel mass streams that are considered at either the source or sink, for which no counterpart at equal temperature is defined on the other side of the connection will, thus, be set to zero. Therefore, valid connections may only be defined between source and sink ports whose considered temperature sets have a *non*-empty intersection.

With the consideration of multiple temperatures, temperature-dependent thermal losses that occur along a connection may now be modeled. In order to represent these losses, the mass flow rates of the considered parallel source mass streams entering the connection at a given temperature are not set equal to the mass flow rates of parallel sink mass streams of equivalent temperature. Instead, each parallel source mass stream is split up among the sink mass stream at equal and the sink mass stream at the adjacent temperature that is closer to the ambient temperature. By varying the relative magnitude of the mass flow rates of the two sink mass stream contributions, temperature-dependent losses may be represented for each source mass stream. Naturally, it is only possible to represent thermal energy losses if for each temperature considered at the source there actually is an equivalent temperature, as well as an adjacent temperature considered at the sink. Otherwise, depending on their temperature, thermal energy losses may not be represented for all source mass streams.

If the discussed requirement is met for a given connection, each source mass stream may be split into two fictitious sink mass streams, which can be mathematically expressed as follows:

$$\begin{aligned} -\alpha_c \cdot \dot{m}_{\mathrm{f},i} &= \dot{m}_{\mathrm{r},j,i} \\ (-1+\alpha_c) \cdot \dot{m}_{\mathrm{f},i} &= \dot{m}_{\mathrm{r},j+\tau_\mathrm{s},i} \end{aligned} \quad \text{for every } T_c \in \mathcal{T} \text{with } T_{\mathrm{f},i} = T_{\mathrm{r},j} = T_c\,. \tag{3·45}$$

Here, the mass flow rate $\dot{m}_{\mathrm{r},j,i}$ represents the contribution of the i-th source mass stream to the j-th sink mass stream. The index of the adjacent sink temperature is determined through τ_s, which is defined to be -1 if the respective T_c is greater than the ambient temperature and 1 if T_c is smaller than the ambient temperature, assuming that the temperatures of the mass streams at the sink are ordered in an ascending manner. The loss factor α_c is naturally constrained to $\alpha_c \in [0,1]$ and should depend on the feed temperature $T_{\mathrm{f},i} = T_c$, the ambient temperature T_{amb} and the adjacent temperature $T_{\mathrm{r},j+\tau_s}$. The combined mass flow rates of the sink mass streams are defined as follows:

$$\dot{m}_{\mathrm{r},j} \stackrel{!}{=} \sum_{i \in \mathcal{P}_j} \dot{m}_{\mathrm{r},j,i} \,, \tag{3.46}$$

where the set $\mathcal{P}_j$ comprises all source mass stream indices i that contribute to the j-th sink mass stream.

For a given source mass stream temperature T_c, the obtained thermal energy losses $\dot{E}_{\mathrm{loss},c}$ should be proportional to the temperature difference to the surroundings

$$\dot{E}_{\mathrm{loss},c} = k_{\mathrm{loss}} \cdot (T_c - T_{\mathrm{amb}}) \,, \tag{3.47}$$

where k_{loss} is a design parameter which represents the surface area of the pipe and its thermal conductivity. This expression, however, in contrast to (3.45) does not depend on the mass flow rate $\dot{m}_{\mathrm{f},i}$. Hence, the actual goal of obtaining thermal losses proportional to the mixed temperature

$$\dot{E}_{\mathrm{loss}} = k_{\mathrm{loss}} \left(\frac{\sum_{i=1}^{N_{\mathrm{f}}} \dot{m}_{\mathrm{f},i} \cdot T_{\mathrm{f},i}}{\sum_{i=1}^{N_{\mathrm{f}}} \dot{m}_{\mathrm{f},i}} - T_{\mathrm{amb}} \right) \,, \tag{3.48}$$

and independent of the overall mass flow rate is still not possible with this approach.

As a result of this, the coefficients α_c need to be chosen carefully and individually for every mass stream of every connection, considering that for each parallel source mass stream the respective temperature difference to the adjacent temperature may be different. Additionally, one has to note that depending on the physical parameters of the connection and the defined adjacent temperature, the actually occurring thermal energy

losses may exceed the losses that can be represented according to the above method. In that case one may resolve said issue by choosing, if possible, a different temperature then the next adjacent sink temperature within the constraint (3.45).

3.3. Integration of the Multi-Layer Thermal Storage Model with Constant Temperature Levels

Besides the presented multi-flow constant temperature prediction models, the multi-layer constant temperature thermal storage prediction model presented in 2.3.1 needs to be integrated into the existing EMS framework.

In order to use the presented continuous-time model within the EMS framework, it first needs to be discretized, considering that the use of MPC infers the use of discrete time system models. However, this discretization is not trivial considering the discrete states of the model, namely whether a given layer currently resides at a given outlet, which layer currently is in contact with the face sides of the storage and the instantaneously viable triplet configurations that are all represented by associated binary indicator variables. In light of the typically used sampling periods employed within actual EMS applications for hydronic systems, and depending on the physical dimensions of the modeled TES, multiple discrete state changes may frequently occur within a single discrete time step. Therefore, between two discrete time instances multiple layers may be available at a respective outlet, several layers may lose thermal energy trough any of the face sides of the storage and some triplet configurations may become viable as others diminish. In order to prevent infeasibilities of the EMS optimization problem, the implications of these occurring state switches need to be accurately considered within the discrete time model of the multi-layer sensible heat storage. To achieve this, the presented definitions of the introduced binary indicator variables will have to be adapted to the discrete-time case. Consequently, additional continuous- and binary-valued auxiliary variables and mixed-integer constraints need to be introduced to consider the occurring state

changes between two adjacent time instances. For further information on the specifics of the proposed discretization scheme and the resulting modified mixed-propositional logic statements, defining the respective indicator variables of the multi-layer storage model, the interested reader is redirected to the article [17].

In order to integrate the arising mixed-logical continuous propositions into the MPC optimization problem, the given propositions need to be expressed by means of mixed-integer linear inequalities which then can be posed as constraints. To efficiently realize this transformation, several methods are proposed in literature, some of which are briefly summarized in Appendix A Section A.3 or discussed in more detail in e.g. [14]. The different methods diverge in the number of auxiliary continuous and binary variables as well as the number of additional mixed-integer constraints that are introduced to represent different logic and mixed-logic propositions. Therefore, the chosen method may significantly affect the complexity of the resulting MILP. This is due to first, the varying number of introduced binary variables which potentially may increase the optimization problem complexity exponentially. Second, different mixed-integer constraints, that are used to represent particular propositions, may entail different solution spaces during integer relaxation, which is typically part of optimization algorithms for MILP. As a rule of thumb, larger solution spaces may slow down optimization, and hence entail larger solving times.

During the course of this thesis an approach based on the *conjunctive normal form* (CNF) of a propositional logic statement was utilized. This approach may be summarized as follows: First, each continuous operating event that is part of a mixed-logical propositional statement is represented by means of an auxiliary binary variable. By then substituting the events by means of the auxiliary binary variables a *Boolean function* is obtained. Subsequently, this function is then expressed by means of its equivalent CNF, which can be computed by several methods or utilizing readily available free online tools (e.g. [8]). The resulting CNF then by definition is a logical disjunction of so-called *maxterms*, which themselves are disjunctions of binary variables and possibly their respective negations. Therefore, a CNF may be easily transformed into a set of mixed-integer constraints by simply enforcing that the sum of all variables within each maxterm is greater or equal to one. Given the simplicity of this approach, any logical or mixed-logical expression

may be expressed by means of equivalent mixed-integer constraints in an automated way. However, depending on the considered propositions, the illustrated method may potentially not result in the minimal amount of introduced binary variables or the most compact solution space.

By employing the proposed discretization scheme and utilizing the illustrated CNF method to express propositions by means of constraints, a usable prediction model for the multi-layer sensible heat storage with constant temperatures is obtained. The last issue that remains to be addressed, before the model may be utilized within the existing EMS framework, is model initialization and correction, i.e. how the individual layer heights are initialized and corrected based on available measurements. Typically the state of a sensible heat storage is determined by means of measuring the temperature within the storage, i.e. one or several temperature sensors are mounted along the vertical axes of the storage. To obtain an equivalent set of layer heights from these measurements, the available measurements are first interpolated (e.g. as proposed in [29]) to obtain a continuous vertical temperature profile. Based on said profile, the internal energy or exergy of the storage can be computed and the layer heights of the associated model chosen such that, either the internal energy or exergy is preserved. Naturally for more than two considered layers within the storage model, the individual layer heights are not uniquely defined by the total internal energy or exergy. To determine the appropriate layer heights of the prediction model the iterative method proposed in [31] is utilized. Within this method the computed exergy, rather than the internal energy, is used as the layer heights defining quantity, as it leads to more realistic results. This method was implemented into the existing EMS framework and is utilized to compute the initial layer heights, and to subsequently correct prediction errors of the future storage state by means of the most recent temperature measurements.

Last, one main noteworthy difference between the proposed prediction model and the one that was implemented in the EMS framework has to be discussed to understand the following discussion of the conducted case study. Within the proposed multi-layer constant temperature thermal storage prediction model, the authors define that one of the considered layer temperatures has to be equal to the ambient temperature. However, this definition may prove to be bothersome in an actual EMS application, where the temperature of the ambient surroundings of a TES may significantly

vary with respect to the time of year or even the time of day. The treatment of this physical reality is not considered within the article, and hence unclear, given that layer temperatures are set to be constant over time, and hence may not be frequently redefined. Within the chosen implementation of the proposed multi-layer constant temperature prediction model no layer is defined with specifically ambient temperature, rather each storage model is defined to have at least one layer with a temperature exceeding, and one with a temperature inferior to the expected value range of the ambient temperature. This implies that ambient losses may occur for every considered layer, whereby the resulting height reductions of each layer entail height increases of the adjacent layers whose temperature is closer to the current ambient temperature.

With the discussed prediction models implemented in the considered EMS framework, a representative case study was conducted to verify and analyze the made framework modifications with respect to physical sanity of the results and potential EMS performance benefits. The next chapter will discuss the set-up of this case study as well as the obtained results.

4. Validation: Industrial Winery

The following case study concerns the design of an EMS for an industrial winery whose, formerly strictly conventional, means of thermal energy generation have recently been extended with a renewable source in the form of a solar thermal collector array and an absorption chiller which can use high temperature thermal energy — e.g. from the solar thermal collector array — to provide thermal energy for cooling purposes.

The objective of the EMS is to intelligently incorporate the newly added components. Its operational targets are to maintain process stability whilst shifting the provision of energy from the formerly utilized conventional energy carriers, namely *liquefied petroleum gas* (LPG) and electrical power, towards the installed renewable means of thermal energy generation. The operational strategy devised by the EMS is expected to reduce the operational costs, considering that solar thermal energy after initial installation costs is considered free of charge, as well as reduce the overall emissions of greenhouse gases associated with the operation of the plant.

Unfortunately, only very limited actual process data was made available by the operators of the plant during the period in which this thesis was conducted. Hence, several assumptions regarding e.g. the typical demand profiles of the thermal loads or their specific parameters and operating specifications had to be made to parameterize the prediction models. In spite of those assumptions, the conducted case study should nevertheless facilitate the validation of the enhanced and newly integrated prediction models, as well as allow for evaluating the potential performance benefits and drawbacks entailed by the usage of the respective models in an EMS.

4.1. Plant Set-Up

The investigated plant comprises two distinct geographical production sectors, which will be referred to as *West Wing* and *East Wing*. A schematic layout of the energy provision system in both production sectors indicating the installed prosumers, the available interfaces to external energy sources, the available connections between the sectors and the individual prosumers, as well as the considered heat-transfer medium temperatures for modeling the hydronic subsystem of the plant is depicted in Figure 4.1. Every connection between components is defined to be uni-directional, whereby the considered direction of energy or mass flow is indicated by an arrow.

Each individual production sector is concerned with heating and cooling processes and, hence each comprises a distinct high temperature (*HT*) and low temperature (*LT*) sensible heat storage. These are connected to the respective thermal loads and available thermal energy producers in each sector. Notably, the thermal load denoted by the label *Pipe Cleaning* can be fed by either one of the two high temperature TES.

From the perspective of the EMS, one high temperature (*Vats*) and two distinct low temperature thermal energy loads (*Vats* and *Office*) are distinguished in the East Wing. In the West Wing four high temperature (*Barrels*, *Office*, *DHW* and *Maintenance*) and two distinct low temperature thermal energy consumer (*Barrels* and *Office*) are distinguished. The prosumer denoted by *Dryer* represents an adsorption dryer, hence it is defined as a consumer of both high and low temperature thermal energy. Thermal loads for heating and cooling that are identified by means of the same label in each production sector, describe the same physical system component, whose thermal energy demand for heating and cooling, however, can be assumed independent, and, hence be considered by means of two distinct consumer models for the sake of simplicity.

As illustrated in the schematic, each thermal load is defined with individual temperature specifications, hence a varying number of inlet and outlet temperatures are considered within their respective prediction models. These specifications are inferred from the functionality of the individual components for the operation of the plant, which will be discussed in the following.

High temperature thermal energy is provided either by a LPG boiler or the newly installed solar thermal collector array, which consists of 20 individual evacuated-tube collectors. Whilst the LPG boiler is defined to provision thermal energy at high temperatures, the solar collector array may also provide thermal energy at a medium temperature level. Both energy producers are connected to both high temperature TES in the two production sectors by means of a controllable three-way valve. Hence, at each specific time instance each thermal energy producer may only charge one of the storages. These considered valves are modeled by means of *Switch* prosumers which are depicted by a multiplexer symbol in the illustrated plant layout.

Distributor prosumers are used to aggregate inflowing energy and mass streams that stem from different prosumers in order to subsequently redirect them between several outflowing streams. In the illustrated plant layout, they are not specifically shown but are used wherever several mass streams or energy flows, stemming from different prosumers, enter the port of a specific prosumer. Likewise, they are used for mass streams or energy flows that exit a specific prosumer port and are distributed among several receiving ports.

In contrast to high temperature thermal energy for heating, low temperature thermal energy for cooling is generated individually by separate producers within each production sector. In the East Wing, cooling is exclusively provided by the newly installed absorption chiller, whereas in the West Wing an electrically powered compression chiller is utilized. In order to provide low temperature thermal energy, the generator of the absorption chiller needs to be connected to a high temperature thermal energy source. Thus, the generator is connected to the high temperature TES in the East Wing. The waste heat of the absorption chiller is fed to a connected cooling tower, whose feed and return temperature are set constant in accordance with the typical operating point of the absorption chiller.

The energy demand of the plant as a whole — and of each respective production sector — varies greatly with respect to the time of year, given that the production of wine inherently depicts strong seasonal dependencies with respect to the individual production steps that occur subsequently after the time of grape harvest. For a better intuition and understanding of

the following proceedings, the operation of the plant over the course of a typical yearly production cycle is sketched in the following.

The production cycle of a new wine vintage commences with the grape harvest, which typically begins in early September and may last until mid-October. During that time period, the harvested grapes are gradually transported from the vineyards to the neighboring plant, where they are processed and subsequently stored in large vats, located in the East Wing. During this first storage phase, the process of alcoholic fermentation is initiated. To ensure a controlled progression of the fermentation and subsequently a high quality of the resulting end product, the temperature of the vats needs to be stabilized at 30 °C. Alcoholic fermentation is an exothermic process, therefore heating and/or cooling of the vats may be necessary depending on the ambient temperature and the stage of the fermentation process.

By mid-November the process of alcoholic fermentation is considered to be completed and the grapes are transferred into the West Wing, where they are put into wooden barrels for further storage. During the first few weeks of this second storage period malolactic fermentation commences, which requires the stabilization of the room temperature of the warehouse containing the barrels to a value of 17 °C. After mid-December the process of malolactic fermentation fades out and the temperature of the warehouse is controlled to be around 15 °C for the remainder of the storage period.

Whilst the temperature stabilization and control of the wine-making process requires the main share of the used thermal energy, additional thermal energy is required for the climatization of the office areas within both production sectors. For the office in the East Wing only thermal energy for cooling during the summer and early autumn months is required. In addition, thermal energy is also required for domestic hot water (DHW) provision within the sanitary facilities (West Wing), the humidity control of storage cellars (West Wing), as well as maintenance tasks, namely pipe cleaning (both sectors) and the operation of a steam cleaner (West Wing).

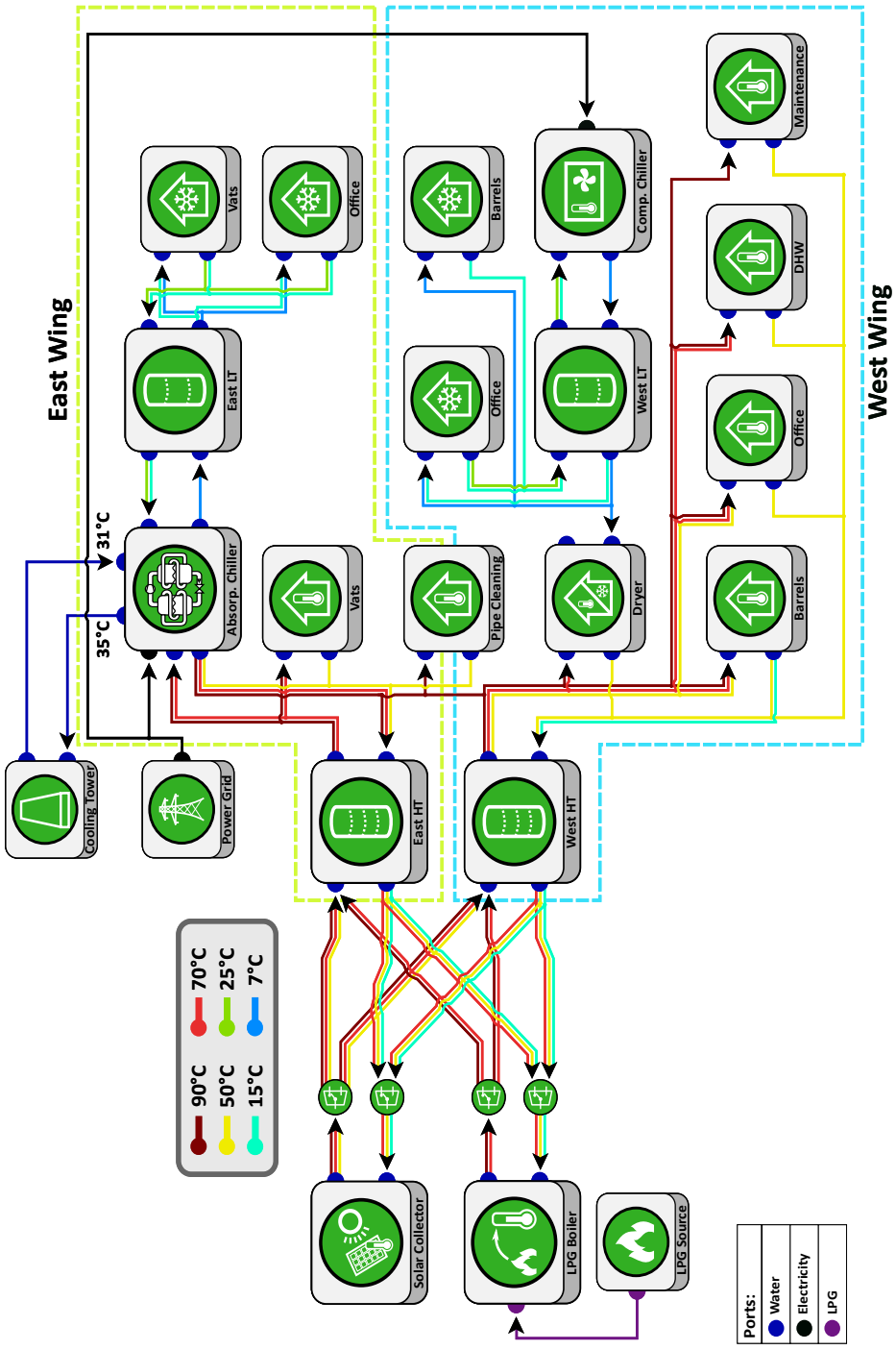

Figure 4.1.: Layout of the industrial winery from the perspective of the EMS.

4.2. Test Data

Considering the lack of informative actual process data, fictional test data sets to validate the designed EMS controller were constructed based on the available plant and process information. These data sets concern those quantities that are typically assumed known or forecast within the existing EMS framework, namely weather data, load profiles of the thermal loads and the yield profile of the solar thermal collector.

In order to obtain accurate past weather data for the known location of the plant, the *Photovoltaic Geographical Information System* (PVGIS) [6] developed by the *European Commission Joint Research Centre* was utilized. The PVGIS provides free to use web applications that allow to obtain accurate weather, solar irradiance and solar system energy production data for most geographical locations on earth based on satellite measurements. Since the investigated plant is located in southern Europe, the weather data was extracted from the PVGIS-*SARAH* database, which provides weather data on an hourly basis and with a high spatial resolution for the time period from the year 2005 until the year 2016. In addition, the PVGIS applications allow to consider potential shading effects by the surrounding horizon, and furthermore to consider the orientation of the investigated collector array within the provided data sets for the solar irradiance. Both effects were considered within the obtained test data set for this case study in order to obtain the best possible approximation of the actual weather conditions and consequently the solar thermal energy yield at the location of the plant.

Based on the obtained weather data, the expected thermal energy yield during the time for which weather data is available, was estimated by (2.7). The effective collector area, the optical efficiency and the loss coefficients of the collector were defined according to the data sheet of the installed collectors. These parameters of the considered evacuated-tube solar thermal collector array are shown in Table 4.1.

For simplicity, the mean collector temperature was defined constant over the entire time range, namely $\bar{T}_{\mathrm{fl}} = 55\,^{\circ}\mathrm{C}$, which is roughly the median value of all considered mean collector temperature values within the given set-up (see Figure 4.1).

N_{coll}	A_{coll}	η_{o}	k_1	k_2	α	β
20	$3.26\,\text{m}^2$	76.7 %	$1.6\,\text{W}\,\text{K}^{-1}\,\text{m}^{-2}$	$0.006\,\text{W}\,\text{K}^{-2}\,\text{m}^{-2}$	0°	0°

Table 4.1.: Parameters of the considered solar thermal collector array. The collectors are mounted flat on an even surface, hence the slope α and azimuth β are 0°. The total collector array size is obtained by multiplying the area of a single collector A_{coll} by the total number of installed collectors N_{coll}.

Load profiles for the individual thermal loads were constructed based on the ambient temperature data and the limited process data that was available. These known process data quantities are: a rough approximation of the aggregated monthly thermal energy demand for heating and cooling of the overall plant; the approximate distribution of the thermal energy demand among the different processes within the plant with respect to the time of year; and: some typical temperature set-points of the involved processes. Considering that some thermal loads, namely domestic hot water provision and thermal energy for maintenance tasks, are not expected to correlate in any meaningfully way with the outside ambient temperature, their respective load profiles were constructed based on randomly distributed usage intervals during the typical usage period, and with an educated guess on the usage frequency of said prosumers.

The resulting profiles of the energy demand of the thermal loads and the yield of the solar collector for the years 2015 and 2016 are depicted in Appendix B in Figure B.1 to Figure B.8.

4.3. Simulation

Based on the constructed test data set, a numerical simulation was conducted to validate the functionality of an EMS that uses the newly integrated prediction models. In order to obtain representative and informative results the simulation was conducted over the course of one representative day that displayed considerable and varying thermal energy demand, for both heating and cooling, in both production sectors by a large number of active prosumers, as well as noticeable solar thermal collector yield. This test

scenario should showcase the potential of the new EMS by requiring it to consider the varying utilization of different prosumers and the occurring high thermal energy yield of the solar thermal collector array to subsequently plan the dispatch of the available backup energy generation and the charge and discharge of the available energy storage units accordingly. As a result, the considered TES are expected to display fluctuating SOC, given that the demand for thermal energy is likely not coherent with the availability of solar thermal energy. Considering the underlying multi-layer model representation of the TES, this circumstance is expected to potentially result in various changes of the discrete state of the model which naturally complicates the EMS optimization problem. This complexity will likely result in higher optimization problem solving times, thus, providing a good indication of the implications of the increased model complexity on running times.

Given the above considerations, October 3rd, 2016 was chosen for the numerical simulation. The expected load profiles of the considered consumers and the expected solar collector energy yield on that and the adjacent days are depicted in Figure B.9 until Figure B.16.

The conducted numerical simulation was set up as follows: First, considering that the respective load profiles were artificially constructed based on obtained past weather data, as opposed to given by actual measurement data, the expected thermal demand for each thermal load over the respective prediction horizon was not forecasted. Instead, the computed load profiles were treated deterministically, i.e. the thermal energy demand of each load was set to follow the artificially generated demand profile.

Second, the expected solar thermal collector yield necessarily had to be forecasted, considering that multiple inlet and outlet temperatures are considered within the prediction model, and hence the solar collector yield depends on the operation of the plant. In order to obtain reasonable forecast results, the computed solar thermal collector yield, weather and mean collector temperature data for the past 90 days were used to initialize and train the multi-linear regression forecasting algorithm by means of computing the respective hourly regression coefficients for each day of the week. With the respective regression coefficients computed, inlet-outlet temperature-dependent solar yield forecasts were obtained as part of the

prediction phase of the EMS according to the method presented in Chapter 3 Section 3.2.4.

Third, the following parameters for the controllable thermal energy generators within the plant were defined. The LPG boiler is defined through its maximum and minimal power output of 100 kW respectively 10 kW, and its constant conversion efficiency of $\eta = 0.85$. The thermal energy output of the electrically powered compression chiller is bound between 57 kW and 5 kW. The COP of the chiller is defined to be a constant $\text{COP} = 2.5$, i.e. the thermal energy provided for cooling is 2.5 times higher than the consumed electrical energy of the compressor. Similarly, the COP of an absorption chiller defines how much energy for cooling is provided — absorbed at the evaporator — per unit of absorbed high temperature thermal energy at the generator. Both, the amount of absorbed energy at the generator and at the evaporator depend on the temperature of the mass stream at the inlet of the generator. For the specific chiller installed in the plant this dependency is depicted in Figure 4.2. It is expressed by means of *absorption coefficients*, i.e. with respect to the rated standard operation values for the generator energy input and the evaporator cooling capacity. This nominal absorbed thermal energy at the generator is defined to be 40.1 kW respectively 24 kW at the evaporator. The resulting temperature-dependent COP of the absorption chiller is depicted in Figure 4.3. In addition, the data sheet of the absorption chiller defines the nominal generator mass flow rate to be constant at $1.9\,\text{kg}\,\text{s}^{-1}$ during active operation of the chiller.

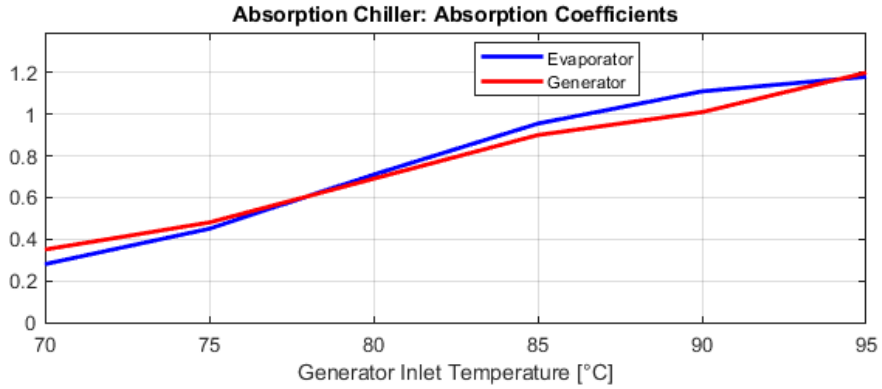

Figure 4.2.: Absorption coefficient vs. generator inlet temperature for the considered absorption chiller.

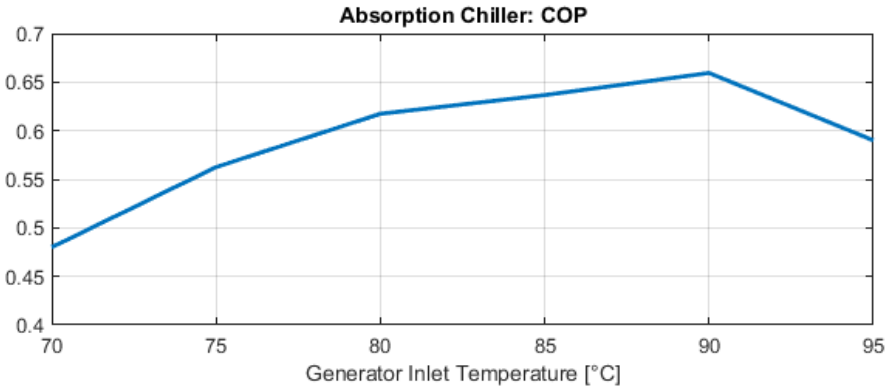

Figure 4.3.: COP vs. generator inlet temperature for the considered absorption chiller.

Last, all four sensible heat storages are modeled with an equal volume of $3\,\mathrm{m}^3$ and a height of 2.5 m. Both high and low temperature storages are defined with equal layer temperatures, namely $T_{\mathrm{hot}} = \{90\,^{\circ}\mathrm{C}, 70\,^{\circ}\mathrm{C}, 50\,^{\circ}\mathrm{C}, 15\,^{\circ}\mathrm{C}\}$ and $T_{\mathrm{cold}} = \{25\,^{\circ}\mathrm{C}, 15\,^{\circ}\mathrm{C}, 7\,^{\circ}\mathrm{C}\}$, and are initialized with the same initial layer heights. Each storage has two inlets/outlets, whereby one pair of inlets and outlets is defined to be located at a height of 0.125 m, i.e. at 5 % of the height of the storage, and the second pair of taps is located at 2.375 m, i.e. at 95 % of the height of the storage.

Considering the rather small size of the thermal storages with respect to the load profiles or the nominal output power of the connected prosumers, and the overall quite complex plant set-up (mainly made complex by the consideration of four individual multi-layer sensible heat storages), a rather short prediction horizon of 6 h, whereby the first hour is partitioned in 15 min and the remaining prediction horizon in 30 min intervals, was chosen for the simulation. In light of this short prediction horizon and the mentioned high complexity of the plant set-up — and hence of the associated optimization problem —, the physical phenomena of axial conduction and ambient thermal energy losses are *not* considered within the prediction models of the TES, given their expected negligible effects. All connections are assumed to be ideal, i.e. lossless.

Given the fact that the control optimization problem in the given case study is a MILP, the acceptable relative tolerance between the optimal solution that

is obtained with relaxation of the integrality constraint of all considered integer optimization variables and the best found integer solution, the so-called *MIP gap* parameter needs to be defined. In the presented case study this parameter was set to 1 %, hence the utilized MILP solver may terminate the search for a better solution as soon as it finds a valid integer solution with an associated cost function value that deviates less than 1 % from the optimal solution of the integrality-relaxed problem.

In order to solve the optimization problem, the commercial solver software *Gurobi* [9] was utilized. The numerical simulation script, as well as the discussed EMS framework are implemented in the *Julia* [4] programming language, a rather novel, high-level mathematical programming language that offers good performance and, through the native *JuMP* [5] package, facilitates the optimization problem definition as well as integration of external numerical solver software such as *Gurobi*.

With the above discussed parameters defined, the simulation was carried out on a *Lenovo T430* Laptop with an integrated *Intel i5-3320* processor, 8 GB of RAM and running *Windows 10*. The obtained simulation results are depicted in Figure B.17 to Figure B.27. The solving time and the MIP gap associated with each solution are depicted in Figure B.28 respectively Figure B.29. To conclude the case study, the remainder of this chapter will present and illustrate the most prominent of the obtained results.

4.4. Simulation Results

The obtained simulation results display several noteworthy features related to the novel prediction models that were used within the designed EMS. The following discussion of the simulated EMS controller behavior will proceed in a chronological manner, starting from the first considered simulation time step at the stroke of midnight.

Initially all thermal storages are initialized to be rather empty (see Figure B.17 to Figure B.20), i.e. they contain little usable energy from the perspective of most of the connected prosumers (with the exception of thermal energy for cooling of the vats or the office facilities, which may

be provisioned at both 7 °C and 12 °C). Therefore, considering the present thermal energy demand to heat the vats in the East Wing (see Figure B.10) and the natural lack of solar irradiance at night, the LPG boiler is switched on continuously on a low setting of on average 14 kW during the early morning hours until roughly 7:15 a.m. to feed the high temperature storage located in the East Wing (see Figure B.25 and Figure B.26).

In the West Wing there is no thermal energy demand until 6 a.m. after which some thermal energy for space heating and domestic hot water provisioning is required (see Figure B.13). Given the predictive capabilities of the utilized EMS, however, no thermal energy from the LPG boiler is fed into the high temperature storage in the West Wing, as the controller anticipates that the current energy within the storage should suffice for the expected demand, until additional thermal energy from the solar collector array is available at a later time of day.

After 7:15 a.m. thermal energy from the solar thermal collectors is first made available (see Figure B.21). It is approximately equally distributed between both high temperature TES until 11:15 a.m. (see Figure B.22). Notably, the high temperature TES in the East Wing is initially fed with predominantly medium temperature thermal energy, given that the solar collector may operate most efficiently in this way and provide the highest instantaneous thermal energy yield. Conversely, the TES in the West Wing is generally fed with slightly higher temperature thermal energy, given the continuing prosumer energy demand in the West Wing sector and considering that the prosumers in the West Wing consume exclusively high temperature thermal energy.

After 11:15 a.m. the thermal energy output of the solar collector is almost continuously fed into the TES in the East Wing at the highest possible outlet temperature of 90 °C. This decision by the EMS is likely motivated by the approaching considerable thermal energy demand for cooling in the East Wing, that, given the operating principle of the utilized absorption chiller, in turn entails a high demand for high temperature thermal energy. To meet this large energy demand for cooling, the LPG boiler is switched on at 14:15 p.m. to provide additional high temperature thermal energy to the generator of the absorption chiller. One noteworthy feature of the obtained absorption chiller operation reference concerns the chosen generator inlet

temperature. Whilst initially the absorption chiller is operated at its most efficient operating point, after 16 p.m. the chiller is operated at its lowest possible temperature setting which, with respect to Figure 4.3, results in a lowered COP of the chiller. This behavior may be explained by the fact that after 16 p.m. the thermal energy demand for cooling in the East Wing sector continuously decreases, and that there is a lot of remaining thermal energy within the high temperature storage at 70 °C.

The thermal energy demand for cooling of the prosumers in the West Wing, that arises in the afternoon hours and remains considerably high until late at night, is provisioned by the installed compression chiller (see Figure B.27), and is, hence, independent of any other energy demand within the plant.

The solving time necessary to obtain a suitable solution to the control optimization problem at each time step is illustrated in Figure B.28. Evidently, the solving time varies greatly (by almost three orders of magnitude) between different optimization iterations, ranging from a few seconds to violating the maximum admissible solving time of 15 min. As one may expect, the solving time steeply increases as soon as the thermal energy demand for cooling in the East Wing comes into scope of the prediction horizon, given the implied coupling of the two TES in the East Wing by means of the absorption chiller, and hence the entailed increased system complexity. Similarly, with the decrease of this energy demand in the late afternoon a notable decrease in solving time is observable.

The MIP gap associated with each solution of the optimization problem is depicted in Figure B.29. Naturally, for the time step where the maximum admissible solving time was violated (13:45 p.m.) a MIP gap higher than the defined upper bound of 1 % is observed.

The following chapter will summarize and discuss the key insights that may be drawn from the obtained results of the presented case study, with respect to the EMS performance benefits and the potential drawbacks that are entailed by the usage of the enhanced prosumer prediction models. Additionally, a brief outlook on necessary future research and development regarding hybrid linear prediction models of prosumers within hydronic system will be given.

5. Conclusion

The obtained case study results clearly illustrate important benefits that may be obtained by using the presented enhanced prosumer prediction models in MPC-driven EMS. Most notably, by considering the temperature-dependent efficiencies/performance of different prosumers in their respective prediction models, the overall plan of operation that is derived by an employed EMS may steer the considered plant in a more energy efficient fashion.

In the presented results this circumstance is exemplary observable in the devised operation strategy for the solar thermal collector, where initially lower temperature thermal energy is provided by the collector to charge both high temperature thermal energy storages at the highest possible energy efficiency. At a later point, the solar thermal collector is then utilized at a more inefficient operating point in order to supply the arising high temperature thermal energy demands. This adaptation of the instantaneous behavior of the solar thermal collector, depending on the expected conditions and utilization of the other prosumers within the system, is beneficial to the overall system efficiency that is entailed by the derived plan of operation. In general, this efficiency increase will be particularly pronounced for prosumers that exhibit a stronger varying temperature-dependent efficiency/performance such as for example flat plate solar thermal collectors, whose respective loss coefficients k_1 and k_2 are much higher than those of evacuated-tube collectors, which were considered as part of the presented case study.

However, in order to truly quantify these performance benefits for a range of different real-world applications, extensive practical tests of EMS that utilize the newly integrated prediction models need to be conducted. These test would also be necessary to assess the model deviation of especially the proposed multi-layer sensible heat thermal storage prediction model and the entailed, potentially adverse, effects on the EMS performance. However,

with respect to the previously utilized prediction models, the proposed enhanced models are expected to significantly better approximate the actual prosumer behavior.

Besides practical validations, extensive additional simulation studies to ensure the practicability of the proposed methods are advised. Especially the range of occurring solving times needs to be investigated, given its potential adverse effects on the stability of a designed controller.

The significantly increased solving times, that are entailed by the usage of the proposed prediction models, namely the multi-layer thermal storage model given the large amount of introduced auxiliary binary variables, are the main drawback of the presented models/methods. The negative consequences of this increased number of binary system variables is expected to be especially notable when hydronic systems with relatively small TES are to be controlled, considering the likely increased frequency of discrete state changes within the associated multi-layer prediction model. Therefore, the proposed prediction model enhancements are expected to be particularly beneficial for plants and applications that comprise a small number of rather large TES, and whose system dimensions justify the increased necessary computing power to solve the control optimization problem.

As a last point, recently significant advancements have been made in the field of optimization algorithm research [2]. Resulting from this, many commercial providers of optimization algorithm software have released novel algorithms that are particularly focused on bilinear problems. Therefore, in the near future it may be no longer necessary to explicitly linearize the phenomenon of energy transfer by convection within the prediction models of prosumers. Following from this, one may then be able to compose generic prosumer prediction models where the specific temperature-dependent behavior of prosumers may be explicitly represented, rather than approximated by the methods that were illustrated in this thesis. However, in the case that these novel bilinear optimization algorithms will, at least initially, fail to provide the necessary performance, it is hoped for that the methods and ideas illustrated in this thesis will prove useful and beneficial to other researchers and engineers that are concerned with the development of MPC-driven EMS for MES.

Appendix

Appendix A.

Model Predictive Control

Model predictive control (MPC) is an optimization-based control strategy that has been increasingly employed since the 1980s and nowadays is considered the quasi-standard solution for advanced process control, especially for chemical and petrochemical plants and processes [20], i.e. processes that are typically characterized by rather slow dynamics. However, in light of the continuing advancements in computer technology and optimization algorithms the scope of potential applications for MPC is ever increasing. Therefore, nowadays MPC is used not only for systems with rather slow dynamics, but also for the real-time control of very agile systems and applications, such as vehicle powertrains or path planning for self-driving cars, or very large and complex systems such as electrical power grids.

A.1. Main Concept

The fundamental control concept of MPC is that based on a discrete-time dynamic model of the plant (*prediction model*), the expected future behavior of the plant is forecast/predicted over a finite time horizon (*prediction horizon*) based on the generalized set of control inputs and taking into account known disturbances (e.g. environmental conditions). Considering the notion of discrete-time models, the future plant behavior is, hence, simulated for a number of specific time instances, whereby the time difference between consecutive instances is referred to as the *sampling period*, which does not necessarily has to be constant. Based on the predicted plant behavior, an

optimization problem is constructed. It is defined by a scalar so-called *cost function*, which describes metrics to evaluate the predicted generalized plant behavior. These metrics, also referred to as *costs*, are typically defined in such a way that a less favorable plant behavior results in higher costs. A typical example of this case would be the consideration of a term describing the absolute divergence of the output of a system from a defined future reference within the cost function. Generally, the solution of the optimization problem is, thus, defined to be the future set of control inputs (actuations) that minimize the defined cost function, i.e. that result in the desired plant behavior, subject to potential constraints concerning e.g. the plants state or the range of admissible values for the control inputs.

Following the solving of the optimization problem and, thus, the computation of the optimal control input series, the first element of the derived control input series is executed as soon as the previous sampling period is expired. Upon said time instance at which the first computed time step becomes active, the current state of the plant is measured or estimated before the prediction and optimization cycle is repeated considering the updated instantaneous plant state, and potential changes in the expected environmental conditions or changes of applicable constraints. Naturally, given the time passed since the previous prediction and optimization cycle, the considered prediction horizon has to be advanced by one time step. In light of this circumstance, the illustrate method is fittingly referred to as the *receding horizon principle*. Consequently, MPC is inherently an adaptive control strategy, meaning that the current control actions are determined considering changing present and expected conditions and events.

To further illustrate the operating principles behind MPC and in order to better understand the entailed implications with respect to general controller design and implementation, the example of a general single input, single output plant, whose output is sought to track a known control reference is discussed. Preliminary to utilizing any MPC strategy a time-discrete dynamic model of the plant has to be derived, which is assumed to be of the form:

$$\mathbf{x}_{k+1} = f\left(\mathbf{x}_k, u_k, \mathbf{w}_k\right) , \tag{A.1}$$

$$y_{k+1} = g\left(\mathbf{x}_k, u_k, \mathbf{w}_k\right) . \tag{A.2}$$

Here, the discrete-time state of the plant at time index k is denoted by $\mathbf{x}_k$, u_k

denotes the considered scalar control input, y_k is the associated scalar plant output and $\mathbf{w}_k$ comprises all external disturbances that are known.

Utilizing a MPC strategy to determine the future time series of control inputs that would make the output of the plant track the defined reference would then entail the following steps: First, the generalized plant output is predicted over the prediction horizon, i.e. the following N_p future time steps, depending on the future series of control inputs and the expected values of the known disturbances. Second, the scalar cost function J is defined with respect to the state, output, input and the known disturbances of the plant, in order to define the objectives and the performance metrics of the controller. Considering that in the discussed general example the goal is for the output of the plant to track a defined control reference r, a reasonable definition of J may be given by:

$$J = \sum_{k=k_0+1}^{k_0+N_\mathrm{p}} Q_k \cdot (y_k - r_k)^2 + R_k \cdot u_k^2 \,. \tag{A.3}$$

Here, k_0 denotes the current time instance and Q_k and R_k are chosen, potentially time-varying, positive weighting coefficients. With respect to (A.3), it is clear that the value of J increases with the future divergence of the output of the plant from the defined reference. Additionally, the value of the cost function is defined to increase with the square of the value of the future control input variable itself.

The first term of J is intuitive and represents the defined reference tracking objective of the controller. However, the second term is motivated by the fact, that besides optimal tracking behavior, one is typically interested in achieving reference tracking with the lowest possible amount of control input actuation. This is due to the fact, that in many control system applications increased actuation is considered to increase equipment wear and tear and/or entails increased cost of operation. Therefore, users and engineers may prefer controllers with potentially slightly lower tracking accuracy but low control actuation over a controller with slightly better tracking behavior though high control actuation. Note, that this implicit limitation of the range of control input values is not directly connected to control input limitations that typically occur in practical applications. These explicit input restrictions should be incorporated in the optimization problem by means

of constraints, rather than through the illustrated optimization incentives which are sometimes referred to as *soft constraints*.

Within the proposed cost function two controller performance metrics are defined, i.e. reference tracking behavior and low control actuation. Hence, the resulting time series of future control inputs may be understood as a trade-off between those metrics. In order to individually specify how this trade-off ought to be made, the defined weighting factors Q and R may be chosen according to the application and preferences of the control systems engineer. Furthermore, their respective time dependence allows for defining them individually for each time step, such that e.g. one can emphasize accurate reference tracking at the end of the prediction horizon, whereas divergences in the near future are to some degree more tolerable.

Generally, many more arbitrary complex terms may be added to a cost function depending on the investigated plant and the defined controller objectives. The illustrated example only serves to convey the general procedure and intuition when constructing the cost function of a model predictive controller.

With the cost function defined, the resulting control optimization problem for the discussed example may be posed as follows:

$$
\begin{aligned}
\min_{u_{k_0+1}, \dots, u_{k_0+N_\mathrm{p}}} \quad & J \,, \\
\text{subject to} \quad & u_\mathrm{min} \leq u_k \leq u_\mathrm{max} \quad \forall\, k \in \{k_0+1, \dots, k_0+N_\mathrm{p}\} \,, \\
& y_\mathrm{min} \leq y_k \leq y_\mathrm{max} \quad \forall\, k \in \{k_0+1, \dots, k_0+N_\mathrm{p}\} \,, \\
& \mathbf{x}_{k_0} \stackrel{!}{=} \mathbf{x}\left(t_0\right) \,, \\
& u_{k_0} \stackrel{!}{=} u\left(t_0\right) \,, \\
& y_{k_0} \stackrel{!}{=} y\left(t_0\right) \,.
\end{aligned}
\tag{A.4}
$$

Here, exemplary constraints on the minimal and respectively maximal value of the input and output of the system are enforced. However, any generic constraint on the state, input or output variables of the system may be defined. The last three equality constraints illustrate the update of the current state, input and output of the system that is carried out at the start of each optimization cycle.

The constructed optimization problem is subsequently solved, typically using specific computer algorithms referred to as *solvers*. The obtained solution, i.e. the series of future control inputs $u^\star = \left[u^\star_{k_0+1}, \ldots, u^\star_{k_0+N_\mathrm{p}}\right]$, may then be considered optimal over the considered prediction horizon with respect to the chosen cost function and the defined constraints.

At time instance $k_0 + 1$ the first entry of $u^\star$ may then be applied to the plant. Afterwards, based on the determined state $\mathbf{x}_{k_0+1}$ and the system output y_{k_0+1} the optimization cycle is repeated for the updated prediction horizon $\left[k_0 + 2, \ldots, k_0 + N_\mathrm{p} + 1\right]$.

Although the obtained series of future control inputs may be defined to be optimal over the prediction horizon with respect to the defined cost function, it is important to emphasize that this notion of optimality does not inevitably entail satisfying controller performance. Satisfying controller behavior for a given application may only be archived if: First, the respective cost function and constraints describe meaningful metrics with which the system behavior can actually be sufficiently evaluated. Second, the defined restrictions allow for feasible solutions of the optimization problem. Besides, considering that it is rather intricate to prove the stability of a model predictive controller careful choice and evaluation of the MPC parameters, i.e. mainly sampling period and length of prediction horizon, is necessary before a controller may be finally deployed. In addition, it may be necessary to define adequate recovery strategies for the case that no feasible solution is found within an optimization iteration, or for the case that optimization solving times exceed the sampling periods at times.

Last, expanding on these brief general remarks on controller performance and stability, the implications of system model accuracy will be briefly discussed here. With respect to the illustrated cost function (A.3) it is apparent, that the accuracy of the utilized prediction model directly affects the solution of the optimization problem, given that the future system output, which is predicted based on the defined model, is directly considered within the cost function. Therefore, only the effects of properties that are captured within the defined prediction model on the output of the system may be assessed when predicting the future plant behavior. Hence, the series of future control inputs is solely determined by the optimizer based on the plant information that is comprised within the defined prediction model and

the enforced constraints. The so derived series of control inputs may prove to be insufficient or potentially completely inadequate if important aspects of the plant dynamics are not captured within the prediction model.

In contrast to decreasing controller performance entailed by insufficient plant prediction models, overly accurate models, i.e. representing non-essential dynamics that are rather irrelevant to the system behavior, may result in complex optimization problems that take a long time to be solved. These potentially increased solving times may entail a necessary increase of the utilized sampling period or a decrease of the chosen prediction horizon, which in turn may both impair the controller performance or stability given the coarser time discretization or shorter system behavior prediction. Considering the above remarks, a trade-off between considered model complexity, chosen sampling time and length of prediction horizon usually needs to be made.

Besides refraining from modeling non-essential plant dynamics, optimizer solving times may potentially also be decreased by restricting the utilized prediction model and cost function to be of a particular system, respectively function, class, such as e.g. linear prediction models and linear cost functions. For this example, the resulting control optimization problem would be classified as a *linear program* (LP), for which specialized and efficient optimization algorithms have been designed. For other classes of optimization problems different solvers exist that differ in their respective solving times and availability, i.e. whether they are open-source or only commercially available. However, as a general rule of thumb the more restrictive an optimization problem class is, e.g. LP are more restrictive than *mixed-integer linear programs* (MILP), the more efficient state-of-the-art numerical solvers may potentially solve the respective optimization problems. Therefore, depending on the application, slight prediction model inaccuracies entailed by a more restrictive class of systems and the resulting system approximations, may be preferable for the benefit of reduced solving times and, hence, potentially decreased sampling periods or increased prediction horizons.

A.2. MPC with hybrid linear prediction models

The main control strategy that is utilized and discussed within this thesis is MPC with hybrid linear prediction models. The term *hybrid* signifies that both continuous- and discrete-valued system variables are considered within the respective prediction models. Whilst linear systems of continuous-valued system variables are typically defined by means of differential or difference equations, depending on whether a physical system is described in continuous or in discrete time, the evolution of discrete-valued systems has to be represented differently, e.g. by means of finite state machines. Combining these two very different classes of systems in a common framework is non-trivial, and hence several modeling frameworks have been devised that each focus on different specific subclasses of hybrid systems and the occurring interactions between the continuous- and the discrete-valued system parts. This strive towards a unifying modeling framework should not be understood as a purely academic curiosity without real practical relevance. In fact considering the past increased integration of computer technology, i.e. inherently discrete-valued systems, into basically every aspect of modern-day infrastructure, including any generic industrial plant and process, a common modeling framework may be inevitably necessary when seeking to adequately model those systems to subsequently control them. Additionally, many processes or machines comprise inherent discrete logic, e.g. a continuous-valued system that is affected by discrete-valued states such as the position of a switch/selector such as the gear lever of a car. A detailed and comprehensive description of these systems is only possible within a modeling framework that considers both continuous- and discrete-valued system components and the interactions between them. In fact, practical examples exist where the lack of proper consideration of these interactions was shown to result in control system instabilities and even complete system failures [21].

A rather famous hybrid system modeling framework that repeatedly is mentioned within this thesis is the *mixed logic dynamical* (MLD) system framework, which was first introduced in [3]. Within this framework the dynamics of a system are described by linear dynamic equations subject to mixed-integer linear constraints. Discrete-valued system components are represented by binary system variables, and are typically defined by means

of logical propositions of other binary variables and operating events, i.e. events that are defined with respect to (in)equality conditions of continuous-valued system variables and represent whether said condition is met or not. In order to integrate these discrete-valued system components into the linear dynamic system, the MLD framework describes systematic methods to reformulate the defining logic propositions into equivalent mixed-integer constraints, to hence obtain a holistic hybrid system representation.

Although model simulation may be complicated by the fact that mixed-integer constraints have to be considered, i.e. that model simulation implies the use of optimization algorithms that solve for integer feasibility, the presented modeling framework lends itself naturally to be used within optimization-based control strategies such as MPC, where the arising constraints may simply be integrated into the control optimization problem. Considering that many energy systems have a substantial amount of inherent logic and hence discrete-valued subsystems, MPC with linear hybrid prediction models — that can be derived using the MLD framework — is frequently used as the control strategy of choice within EMS.

The main question that needs to be answered, however, is how exactly discrete-valued system components can be represented by means of equivalent mixed-integer constraints such that both continuous- and discrete-valued system parts are subsumed within a single equivalent MLD model. This reformulation process is non-trivial. Therefore, the following section is dedicated to briefly illustrate and discuss common methods that facilitate this translation. The following summary of common methods is based on [14], where the interested reader may find a more concise treatment of the topic and specifically the methods only summarized here.

A.3. Reformulating Logic Relations as Constraints

Discrete operating events or states of a system can be represented by means of binary system variables. To illustrate this, one may assign binary indicator variables to represent the truth value of statements which define a state "the boiler is on" or an event "the boiler's power consumption exceeds 5 kW". Compound statements can be constructed by combining individual

statements through operators, which in the context of Boolean algebra are referred to as *connectives*. The set of typically distinguished connectives is shown in Table A.1. The compound statement "the boiler is on *and* its power

Symbol	Connective
$\neg$	logical "not"
$\wedge$	logical "and"
$\vee$	logical "or"
$\oplus$	logical "exclusive or"
$\Longrightarrow$	logical implication
$\Longleftrightarrow$	logical equivalence

Table A.1.: Commonly considered logical connectives.

consumption exceeds 5 kW" can thus be expressed as follows

$$X_1 \wedge X_2 \,, \tag{A.5}$$

where X_1 and X_2 represent the individual atomic statements.

In the context of propositional calculus the introduced variables X_1 and X_2 are referred to as *literals* or *Boolean variables*. Each of these variables naturally has only two possible values, namely `true`, i.e. the statement is true, and `false`, i.e. the statement is false. Therefore, one may introduce the binary variables δ_1 and δ_2 to represent the literals X_1 and X_2, where a value of $\delta_i = 1$ is equivalent to $X_i = \texttt{true}$ and $\delta_i = 0$ is equivalent to $X_i = \texttt{false}$. The logic proposition (A.5) can, hence, be restated as follows:

$$[\delta_1 = 1] \wedge [\delta_2 = 1] \,. \tag{A.6}$$

In order to enforce that this compound statement renders true, one can simply define the following integer linear equality constraint:

$$\delta_1 + \delta_2 \overset{!}{=} 2 \,. \tag{A.7}$$

As a matter of fact, every compound statement that connects two literals by one of the connectives shown in Table A.1 can be similarly enforced by equivalent integer linear constraints. These constraints are illustrated in Table A.2. This observation suggests that one may be able to represent arbitrary

Logic Relation	Integer (In)equality
$\neg X_1$	$\delta_1 \overset{!}{=} 0$
$X_1 \wedge X_2$	$\delta_1 + \delta_2 \overset{!}{=} 2$
$X_1 \vee X_2$	$\delta_1 + \delta_2 \geq 1$
$X_1 \oplus X_2$	$\delta_1 + \delta_2 \overset{!}{=} 1$
$X_1 \implies X_2$	$\delta_1 - \delta_2 \leq 0$
$X_1 \iff X_2$	$\delta_1 - \delta_2 \overset{!}{=} 0$

Table A.2.: Elementary logic propositions and their equivalent representation by means of integer in-/equality constraints.

complex propositional statements by means of integer linear constraints. Therefore, the next subsection will summarize three general methods that may be utilized to facilitate the translation of arbitrary complex propositional statements into equivalent integer linear in- respectively equality constraints.

A.3.1. Translating Generic Logical Propositions into Equivalent Integer Linear Constraints

Generic relations between Boolean variables may be expressed by means of a Boolean formula F:

$$F\left(X_1, \ldots, X_n\right), \tag{A.8}$$

where F defines an arbitrary combination of the literals X_1 to X_n by means of any of the connectives shown in Table A.1. Several different methods exist to enforce the compound statement defined by F to render `true`, i.e. to enforce the Boolean relation:

$$F\left(X_1, \ldots, X_n\right) = \texttt{true}, \tag{A.9}$$

through equivalent integer linear constraints. The most simple and straightforward approach is to separate the Boolean relation (A.9) into elementary compound statements as shown in Table A.2. Subsequently, each elementary

compound statement may be substituted by an auxiliary binary variable and the rules of Table A.2 to reformulate elementary compound statements as integer linear constraints can be applied recursively. Although this method is very simple and may be performed automatically, it potentially introduces a large number of binary variables that, when integrated into an optimization problem, may significantly increase its computational complexity.

A common method that does not require the introduction of auxiliary binary variables is based on the *conjunctive normal form* (CNF) representation of a Boolean formula. A CNF is a *product of sums*, i.e. a logical disjunction of so-called *maxterms* which are conjunctions of literals and negated literals. As a matter of fact, every Boolean formula can be expressed by means of an equivalent CNF, hence this method of representation does not restrict the kinds of Boolean formulas that can be considered. Enforcing that a Boolean formula is true, if the formula is stated in its equivalent CNF can be achieved as follows: Consider the generic CNF

$$\bigwedge_{j=1}^{N} \left(\bigvee_{i \in \mathcal{P}_j} X_i \vee \bigvee_{i \in \mathcal{N}_j} \neg X_i \right) , \tag{A.10}$$

where N denotes the number of maxterms and the sets $\mathcal{P}_j$ and $\mathcal{N}_j$ contain the indices of positive respectively negated literals X_i that are part of the j-th maxterm. Naturally, each maxterm may only comprise either the literal itself or its negation, as otherwise the respective maxterm would always render true. In order to enforce that a CNF evaluates to true, the following integer constraint for each maxterm has to be met:

$$\sum_{i \in \mathcal{P}_j} \delta_i + \sum_{i \in \mathcal{N}_j} (1 - \delta_i) \geq 1 \quad \forall\, j = 1, \ldots, N\,, \tag{A.11}$$

where the binary variables δ_i represent the literals X_i.

The presented CNF method does not introduce any auxiliary binary variables and thus should be generally preferred over the aforementioned substitution method. However, the integer constraints that are derived as part of the illustrated CNF method potentially do not describe the most compact solution space if the used integrality constraint of the binary variables were to be relaxed, i.e. the associated variables were to be treated as continuous

variables that are bounded within the interval $[0, 1]$. The term *compact* hereby refers to the smallest achievable solution space, that is obtained during the relaxation of the binary variables, which still contains all feasible binary variable solutions that render the respective Boolean formula true. A larger solution space potentially entails larger optimization problem solving times, considering that integrality relaxation and subsequent LP solving is a key component of many optimization algorithms for MILP.

To address this issue another reformulation method for logic propositions that does not introduce any auxiliary binary variables and that entails a compact solutions space is discussed in [14]. This method relies on computing the *convex hull* that contains all feasible binary variable solutions, and subsequently expressing the space encompassed by the convex hull as a multi-dimensional polyhedron. The face sides of the obtained polyhedron may then each be expressed by equivalent mixed-integer linear constraints that appropriately define the compact solution space for a given Boolean relation. However, for the modeling tasks that had to be solved as part of this thesis, experimental tests showed no benefits when utilizing this method. Therefore, only the CNF method was utilized.

A.3.2. Translating Generic Mixed Continuous-Logic Propositions into Equivalent Mixed-Integer Linear Constraints

Besides purely logical propositions, when modeling hybrid systems, one is typically also confronted with representing the interaction between the continuous and discrete worlds, namely discrete events that are triggered by continues dynamics, or more accurately binary variables that represent whether linear in-/equality conditions of continuous variables are met or not. As for the purely logical case, the MLD framework provides methods to represent these interactions by means of mixed-integer linear constraints.

The most fundamental interaction between continuous- and discrete-valued variables may be of the form:

$$X \iff [f(x) \leq 0] \ . \tag{A.12}$$

Here, the Boolean variable X evaluates to true if and only if the linear function of the continuous variables x, $f(x)$, is smaller than or equal to zero. This mixed continuous-logic proposition can be expressed by means of mixed-integer constraints as follows:

$$\begin{aligned} f(x) &\leq M - M \cdot \delta \,, \\ f(x) &\geq \epsilon + (m - \epsilon) \cdot \delta \,. \end{aligned} \tag{A.13}$$

This reformulation of (A.12) is commonly referred to as the *big-M* formulation. The identifiers M and m define a upper, respectively lower, bound on the image of the linear function $f : \mathbb{R}^n \mapsto \mathbb{R}$ for a *bounded* domain $x \in \mathcal{X} \subset \mathbb{R}^n$:

$$\begin{aligned} M &:= \max_{x \in \mathcal{X}} f(x) \,, \\ m &:= \min_{x \in \mathcal{X}} f(x) \,. \end{aligned} \tag{A.14}$$

The identifier ϵ in (A.13) denotes a small tolerance value, typically the machine constant, such that the constraint needs not to be formulated as a strict inequality.

Other mixed-integer linear constraints representing fundamental mixed logic-continuous propositions are given in Table A.3.

In order to express compound statements, the state of each operating event (continuous in-/equality condition) can be represented by an auxiliary literal by means of (A.13). As a result, a compound proposition of only Boolean variables is obtained which can be reformulated into equivalent (mixed-)integer linear constraints of binary variables, by means of the previously discussed methods.

Mixed Continuous-Logic Relation	Mixed-Integer Inequalities
$[f(x) \leq 0] \implies X$	$f(x) \geq \epsilon + (m - \epsilon) \cdot \delta$
$X \implies [f(x) \leq 0]$	$f(x) \leq M - M \cdot \delta$
$X \iff [f(x) \leq 0]$	$f(x) \leq M - M \cdot \delta$ $f(x) \geq \epsilon + (m - \epsilon) \cdot \delta$
If X then $z = f(x)$ else $z = 0$	$z \leq \quad M \cdot \delta$ $-z \leq -m \cdot \delta$ $z \leq \quad f(x) - m \cdot (1 - \delta)$ $-z \leq -f(x) + M \cdot (1 - \delta)$

Table A.3.: Elementary mixed logic-continuous relations and their equivalent representation by means of mixed-integer inequalities. The conditional on the lower left corresponds to a product of a binary and a continuous variable $z = \delta \cdot f(x)$.

Appendix B.

Additional Information on the Case-Study

B.1. Load Profiles

In the following figures the computed load and yield profiles for the prosumers are depicted for the years 2015 and 2016. They are educated guesses and based on descriptions of the underlying processes as well as information on the yearly demand, but not on measurements with a high temporal resolution. The considered prosumers are grouped into several categories, whose aggregated thermal energy demand for heating and cooling is shown. Thermal energy demand for cooling is represented by negative values to clearly distinguish between thermal energy demand for heating and cooling.

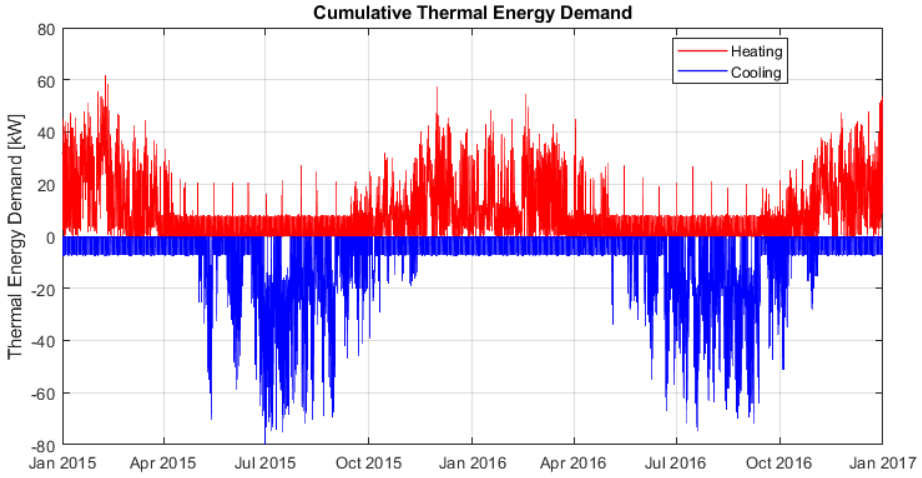

Figure B.1.: Combined thermal energy demand profiles of all considered prosumers.

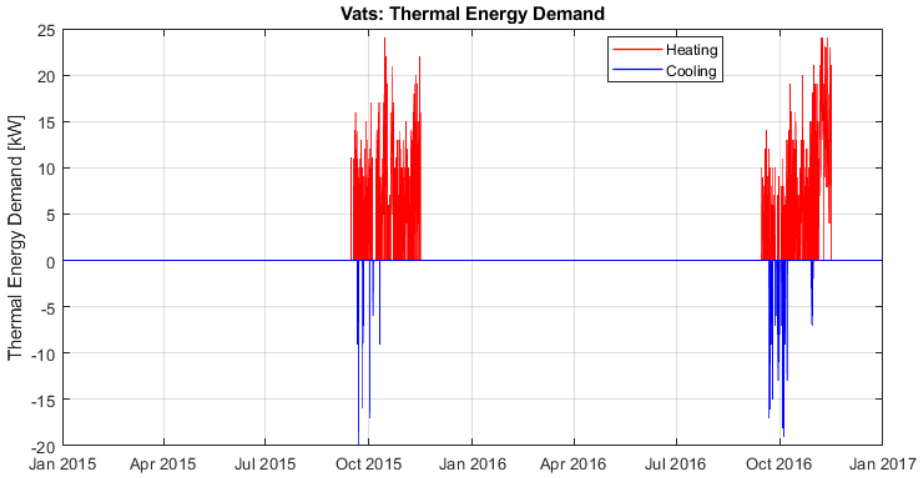

Figure B.2.: Thermal energy demand profile for heating and cooling of the vats. The vats are filled with grape juice after the harvest season and are to be heated to initiate the fermentation process. This process is exothermic, and hence also some thermal energy for cooling is required in order to control the temperature inside of the vats, thus ensuring a good tasting end product.

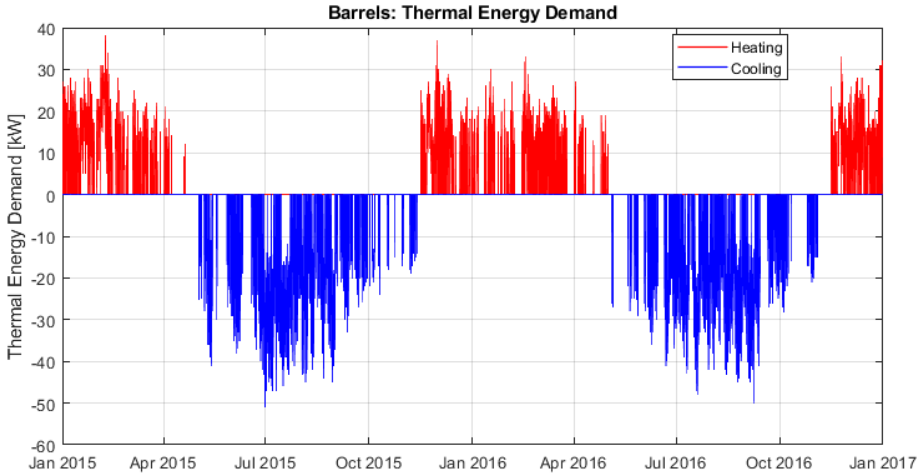

Figure B.3.: Thermal energy demand profile for heating and cooling of the barrels. The fresh wine from the vats is transferred to the barrels and must be kept at a constant temperature during winter (heating) and summer (cooling).

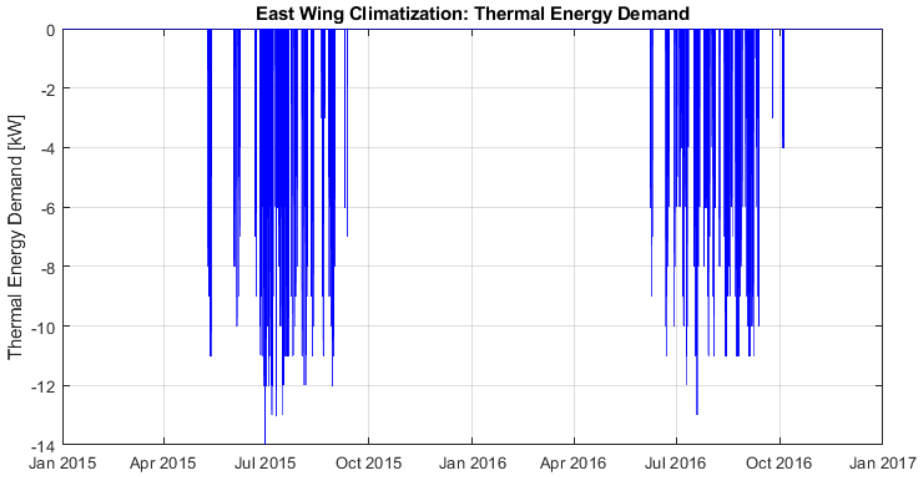

Figure B.4.: Thermal energy demand profile for climatization of the office facilities in the East Wing. Only energy for space cooling during summer is required.

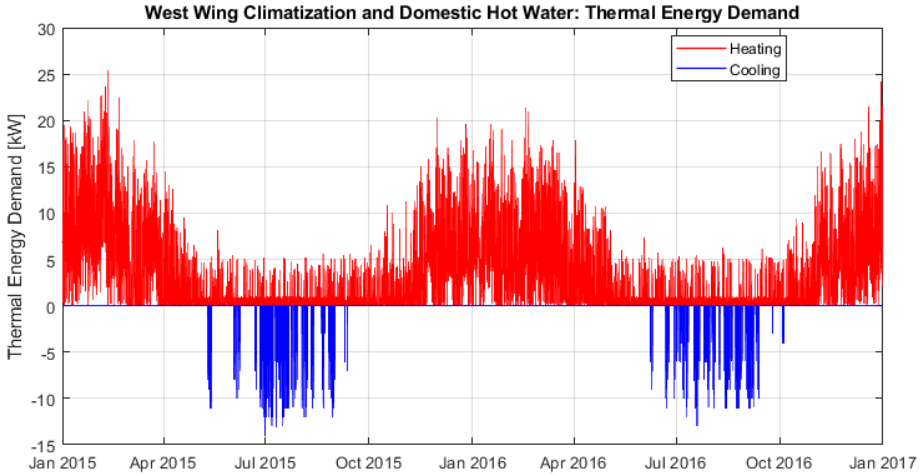

Figure B.5.: Thermal energy demand profile for climatization of the office facilities, and domestic hot water provision in the West Wing. Conversely to the facilities in the East Wing, the office facilities in the West Wing also require thermal energy for space heating in winter.

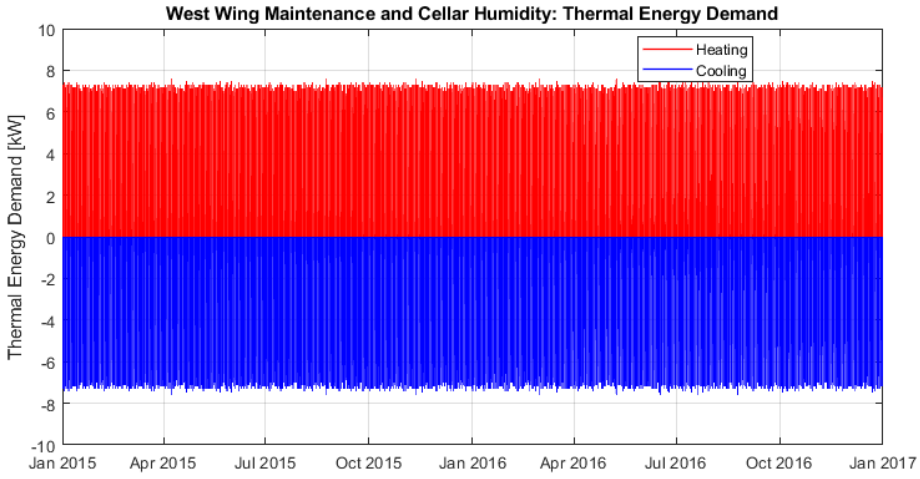

Figure B.6.: Thermal energy demand profile for maintenance tasks and storage cellar humidity stabilization in the West Wing.

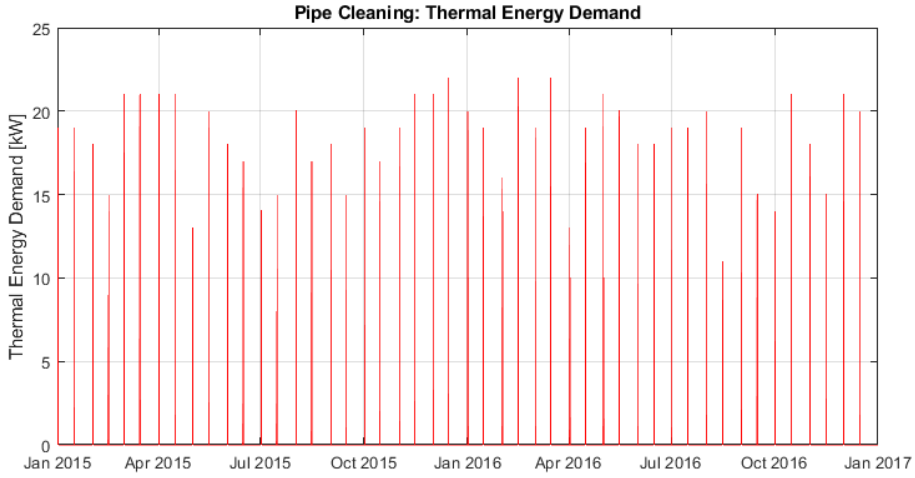

Figure B.7.: Thermal energy demand profile for pipe cleaning.

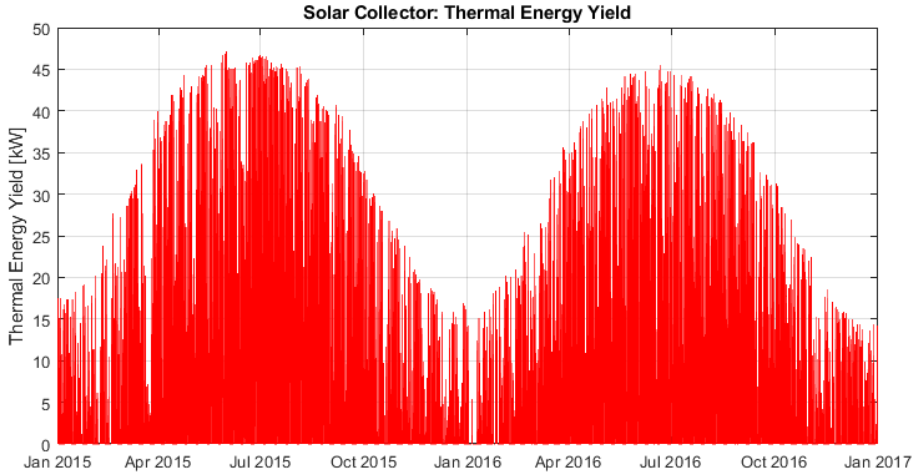

Figure B.8.: Computed thermal energy yield of the installed solar thermal collector array for a mean collector temperature of $\bar{T}_{\mathrm{fl}} = 55\,^{\circ}\mathrm{C}$. The yield was computed according to (2.7), and with the parameters given in Table 4.1.

B.1.1. Simulation Profiles

From the yearly load and yield profiles, October 3rd was used for the actual simulation study. The following figures show the energy demand and yield during this day, along with the adjacent days, in closer detail.

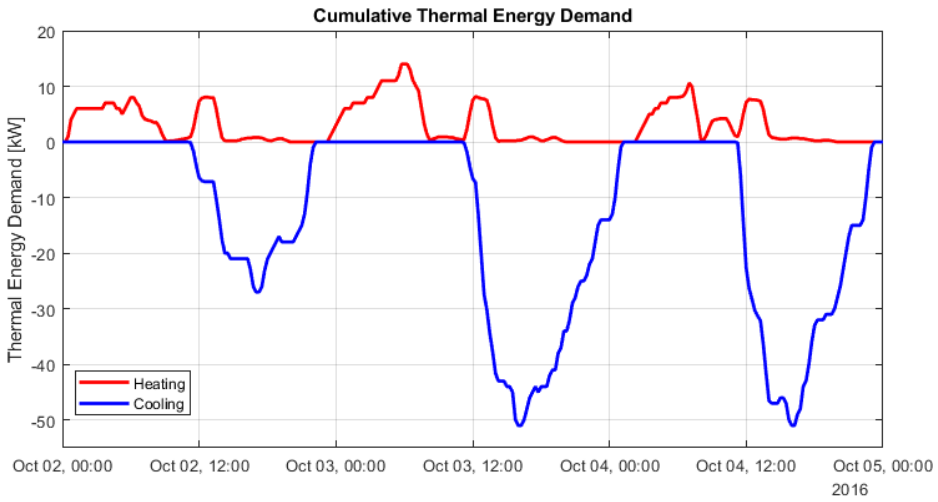

Figure B.9.: Combined thermal energy demand of all considered prosumers between October 2nd and October 4rd of 2016.

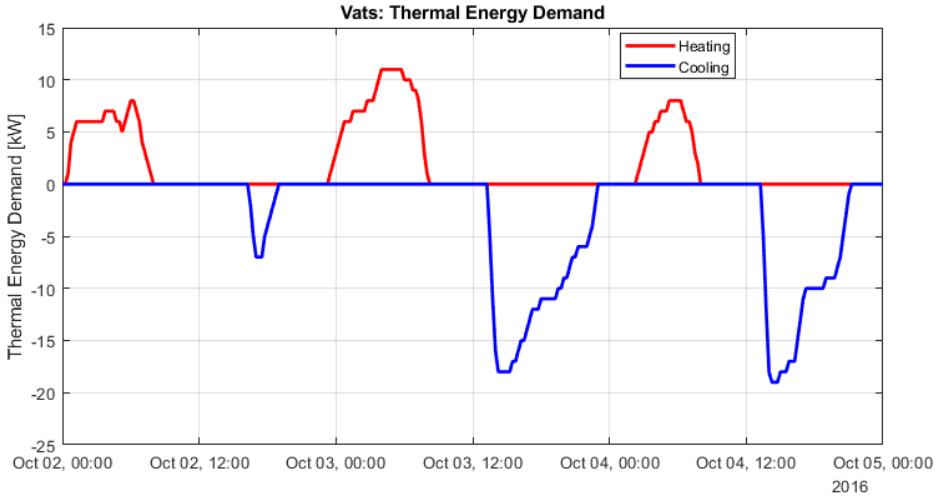

Figure B.10.: Thermal energy demand profile for heating and cooling of the vats between October 2nd and October 4rd of 2016.

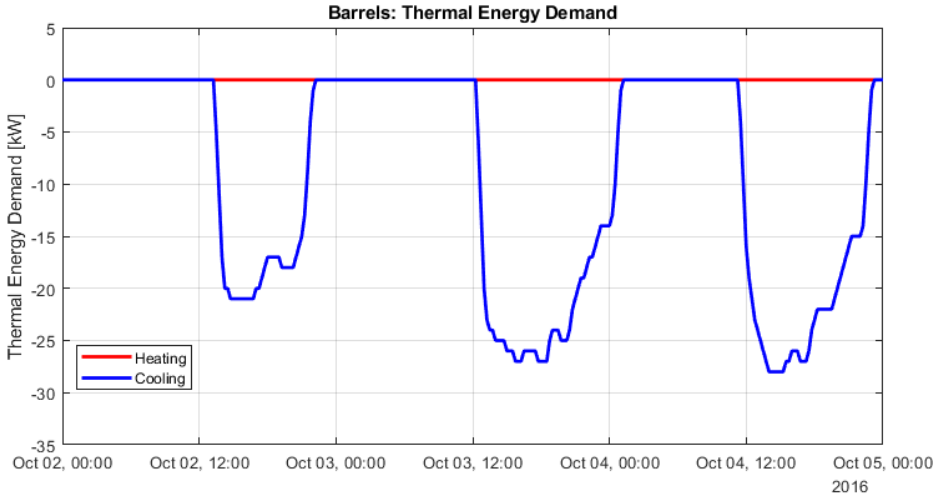

Figure B.11.: Thermal energy demand profile for heating and cooling of the barrels between October 2nd and October 4rd of 2016.

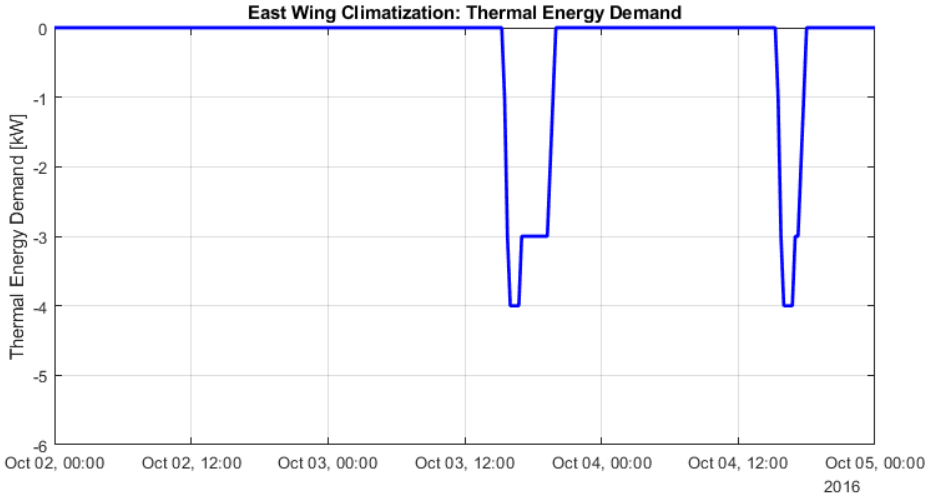

Figure B.12.: Thermal energy demand profile for climatization of the East Wing between October 2nd and October 4rd of 2016.

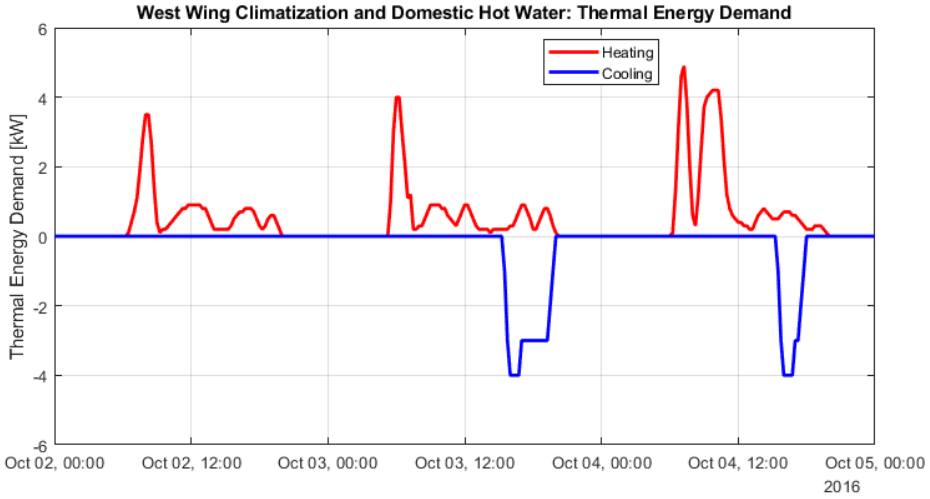

Figure B.13.: Thermal energy demand profile for climatization and domestic hot water provision in the West Wing between October 2nd and October 4rd of 2016.

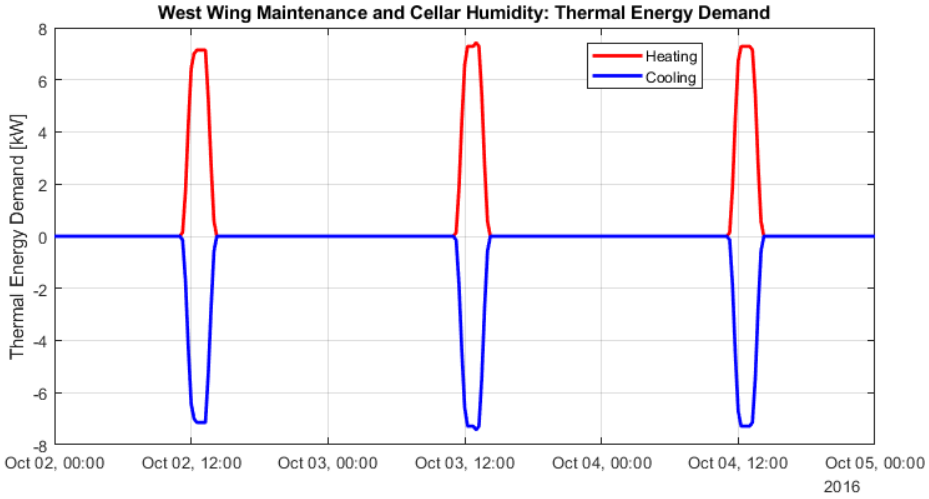

Figure B.14.: Thermal energy demand profile for maintenance tasks and storage cellar humidity stabilization in the West Wing between October 2nd and October 4rd of 2016.

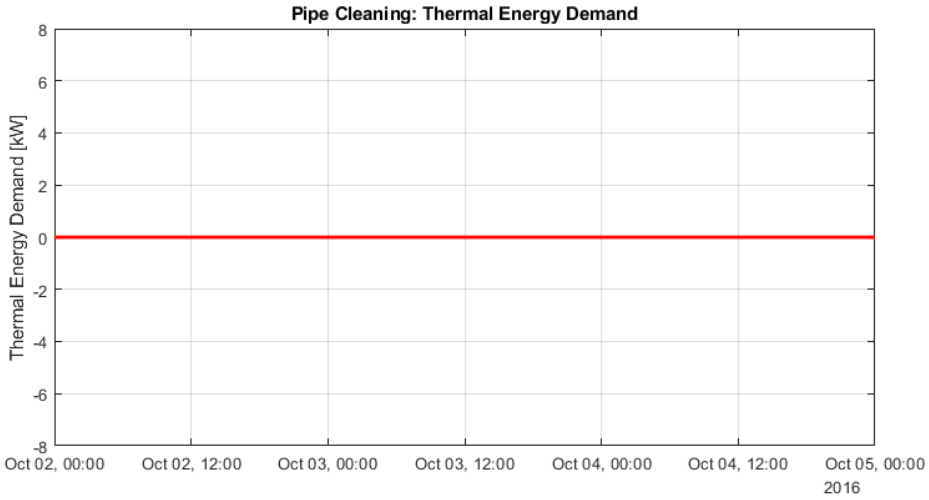

Figure B.15.: Thermal energy demand profile for pipe cleaning between October 2nd and October 4rd of 2016.

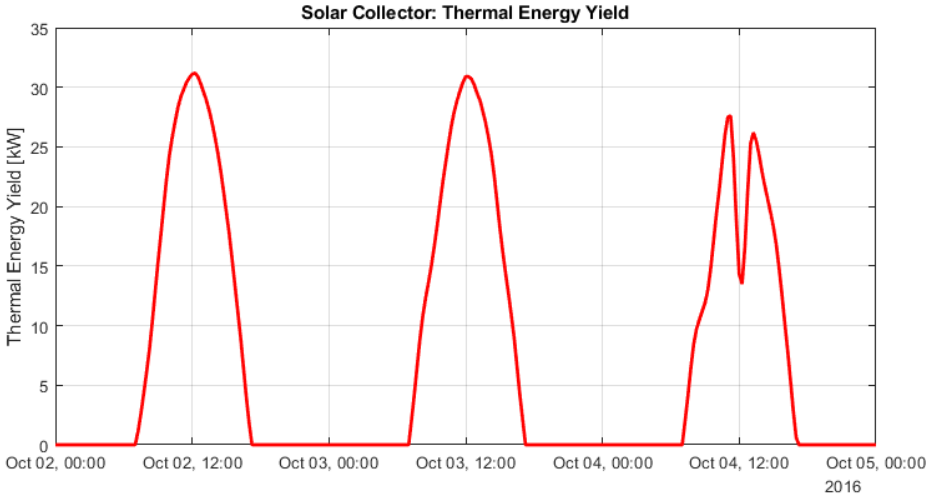

Figure B.16.: Expected thermal energy yield of the installed solar thermal collector array for a mean collector temperature of $\bar{T}_{\mathrm{fl}} = 55\,^{\circ}\mathrm{C}$ between October 2$^{\mathrm{nd}}$ and October 4$^{\mathrm{rd}}$ of 2016.

B.2. Simulation Results

In the following, the simulation results for the conducted case study are depicted. Given the high complexity of the considered plant, the following collection of simulation results is not complete, i.e. only the temporal evolution of the most relevant prosumer variables are shown. These include: the layer heights of the sensible heat storages; the output power of the thermal energy producers; the generator inlet temperature of the absorption chiller; and the mass flow rates through the solar collector and the LPG boiler with the associated production sector origin of the respective mass streams.

B.2.1. Thermal Energy Storages

The following four figures (B.17 to B.20) depict the variation of the layer heights of the sensible heat storages over time. The individual layer heights are depicted in a stacked manner, representing the vertical cross section of the storage. The dashed lines in the figures represent the height of the considered inlet/outlet pairs.

Initially both high temperature TES are rather empty, i.e. the relative height of the two high temperature layers is small compared to the height of the lower temperature layers. Considering that solar energy is not available at night, both storages are discharged in the early morning hours. Given the significant thermal energy demand in the East Wing, the LPG boiler is switched on and feeds the East Wing TES. This results in a depletion of the lowest layer of the storage. The layer at 50 °C at the same time continuously increases in size due to the return flow of the connected and active thermal loads.

Whilst the storage in the West Wing is almost exclusively discharged, the storage in the East Wing is charged with a significant amount of high temperature thermal energy from noon on. At around 15 p.m. the two top layers, hence occupy the entire usable volume of the storage. This energy, however, is completely consumed by the end of the day. At midnight of October 3rd both storages contain little usable energy, with the dominant temperature in the storage being 50 °C.

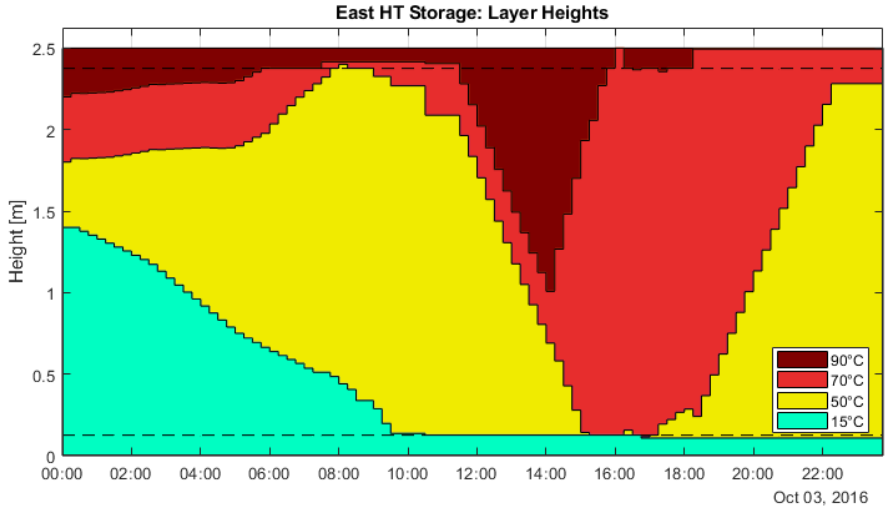

Figure B.17.: Layer heights over time within the high temperature sensible heat storage (East HT) of the East Wing.

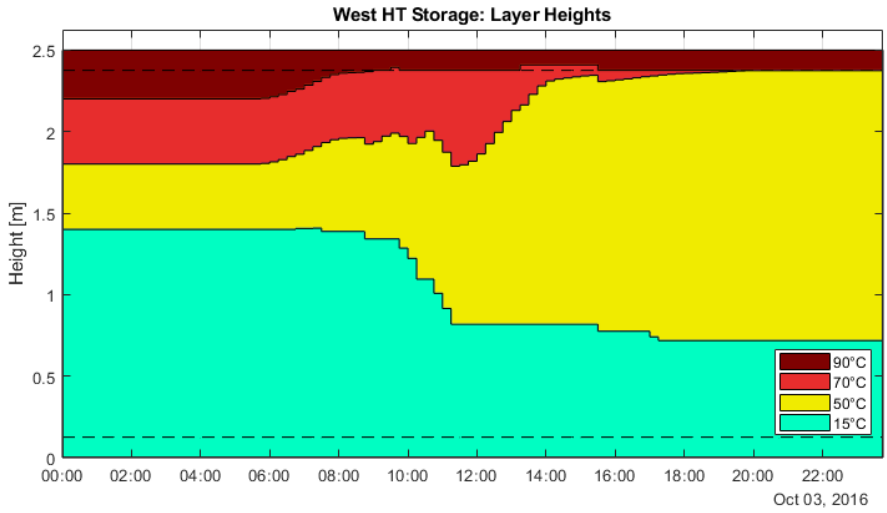

Figure B.18.: Layer heights over time within the high temperature sensible heat storage (West HT) of the West Wing.

Similarly to the high temperature TES, the low temperature TES are rather empty at the beginning of October 3rd. The initial temperature distribution remains unchanged in the early morning hours, considering that no thermal energy demand for cooling occurs in either of the two production sectors.

The TES in the West Wing is charged from around 8 a.m. on by the compression chiller, thus the height of the lowest layer increases gradually following the output power profile of the compression chiller (see Figure B.27). With increasing thermal energy demand after noon the storage is discharged again up until 8 p.m. after which the provided output power of the compression chiller exceeds the thermal energy demand again, thus charging the storage.

The TES in the East Wing remains rather empty the entire time, with small variations depending on whether the output power of the absorption chiller (see Figure B.23) exceeds the thermal energy demand, such as around 4 p.m. At the end of the day, the storage is completely empty, with the top most layer occupying the entire usable volume of the storage.

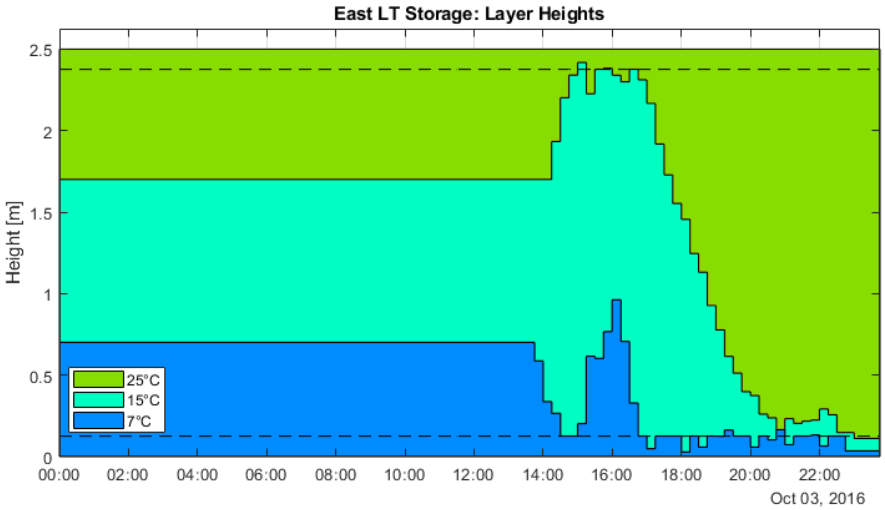

Figure B.19.: Layer heights over time within the low temperature sensible heat storage (East LT) of the East Wing.

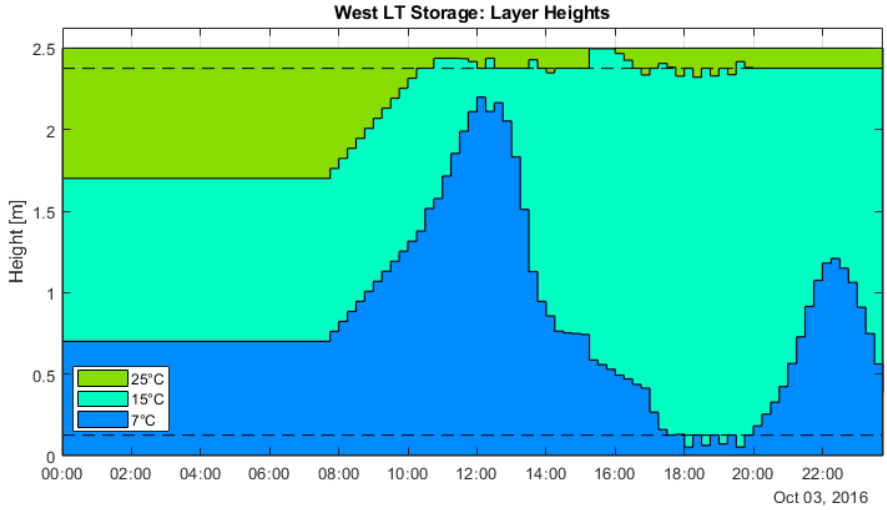

Figure B.20.: Layer heights over time within the low temperature sensible heat storage (West LT) of the West Wing.

B.2.2. Thermal Energy Generators

In the following figures, B.21 to B.27, the most important results for the thermal energy producers are depicted.

Solar Thermal Collector

The thermal energy yield of the solar collector is depicted in Figure B.21. The dashed lines represent the forecasted thermal energy yields for all considered inlet and outlet temperature combinations. The solid line is the actual thermal energy yield that was chosen by the EMS controller by means of selecting the corresponding inlet and outlet temperature.

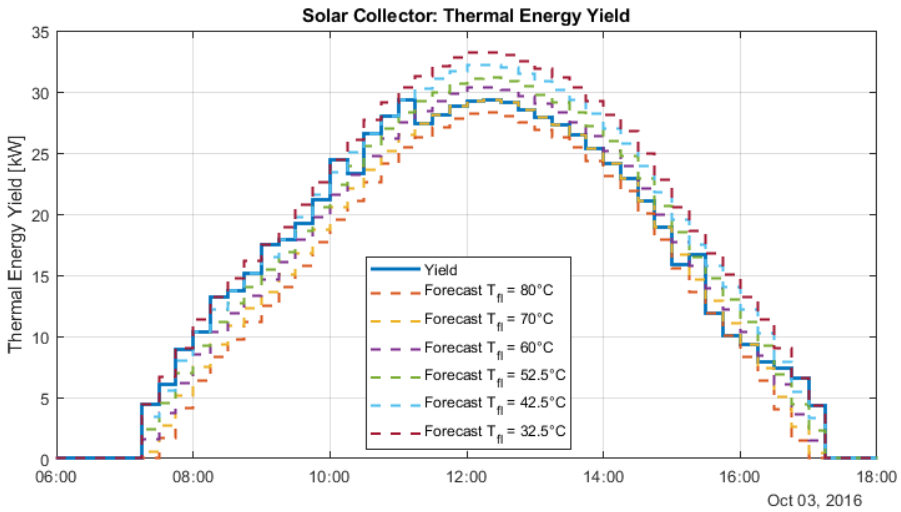

Figure B.21.: Thermal energy yield of the solar collector array.

Figure B.22 depicts the associated mass flow rates at the different considered temperatures at the inlet and outlet of the collector. A yellow background indicates that the source, respectively sink, of the in- and outflowing mass streams of the collector is the high temperature storage in the East Wing, whilst a light blue background indicates that the mass stream stems from, respectively enters, the high temperature storage in the West Wing. Inlet

and outlet mass streams can be distinguished by remembering that outlet mass streams are defined to have positive mass flow rates, whilst inflowing mass streams are set to have negative mass flow rates.

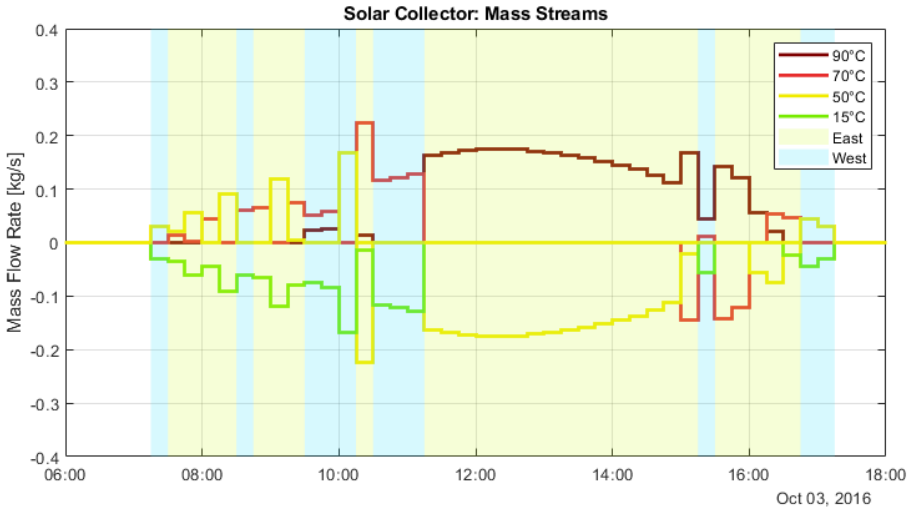

Figure B.22.: Mass flow rates of the considered parallel mass streams at the inlet and outlet of the solar thermal collector array.

Absorption Chiller

The absorbed thermal energy at the generator and the evaporator of the absorption chiller are depicted in Figure B.23. The associated generator inlet temperature is illustrated in Figure B.24.

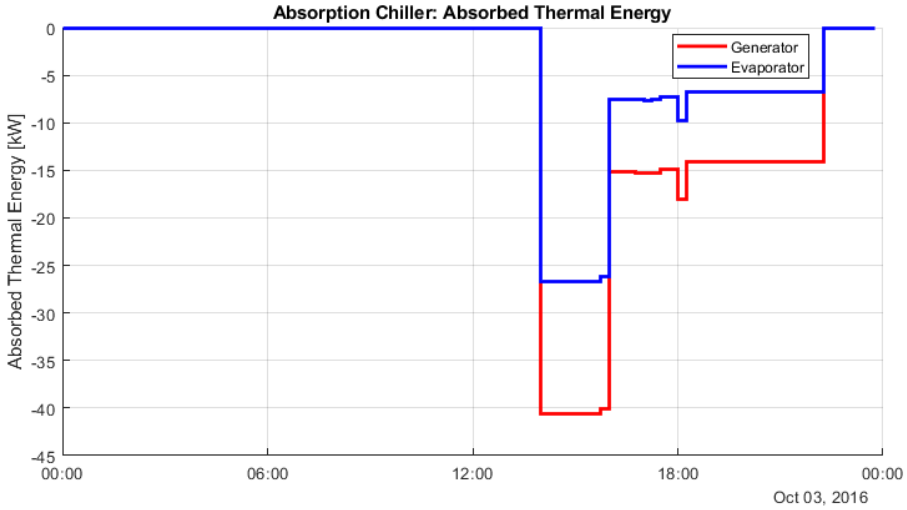

Figure B.23.: Absorbed thermal energy at the generator and evaporator of the absorption chiller.

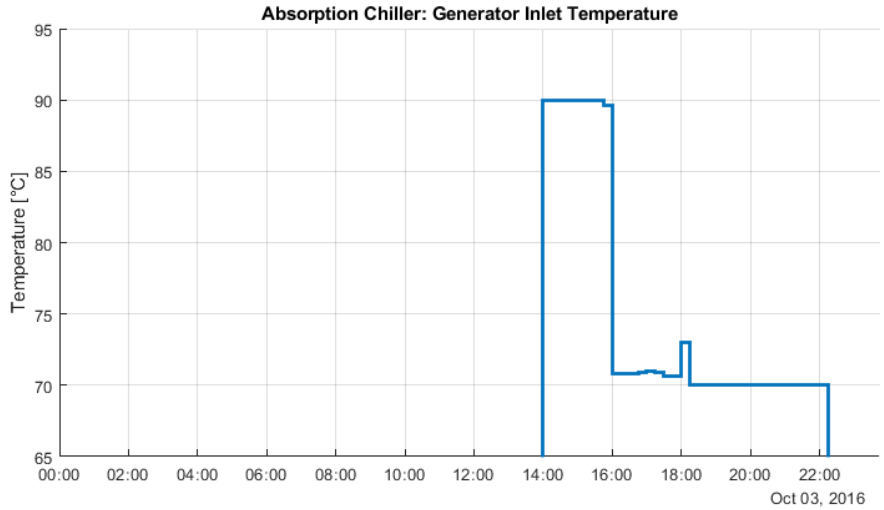

Figure B.24.: Mixed temperature of the parallel mass streams entering the generator inlet of the absorption chiller.

LPG Boiler

The output power of the LPG boiler is depicted in Figure B.25. The associated mass flow rates of the parallel mass streams at the inlet respectively outlet of the boiler are depicted in Figure B.26.

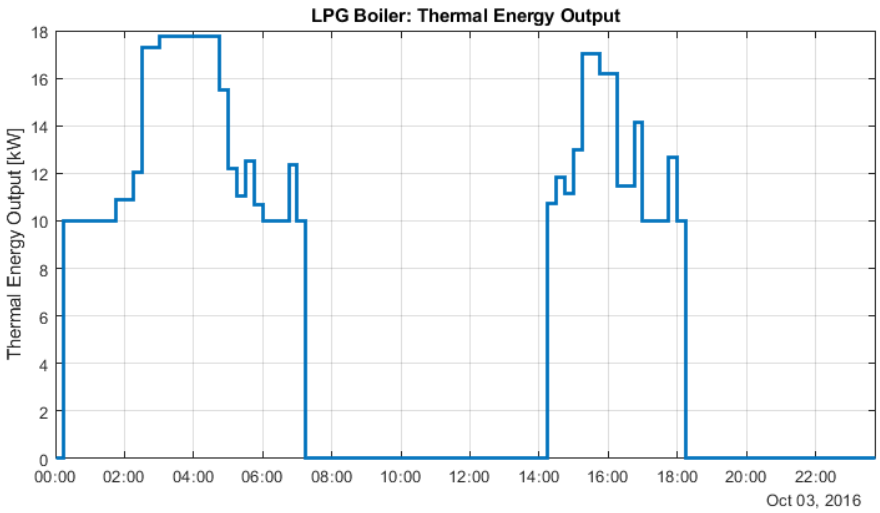

Figure B.25.: Thermal energy output of the LPG boiler.

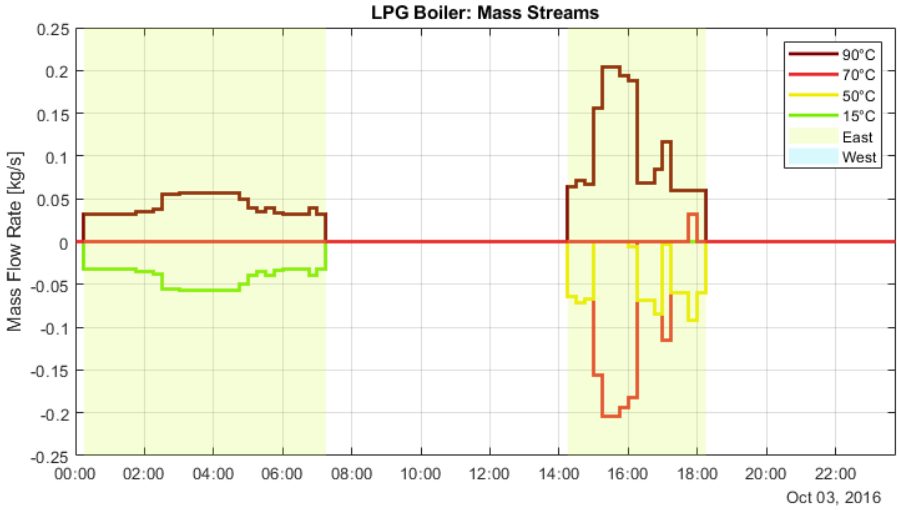

Figure B.26.: Mass flow rates of the considered parallel mass streams at the inlet and outlet of the LPG boiler.

Compression Chiller

The output power of the compression chiller is depicted in Figure B.27.

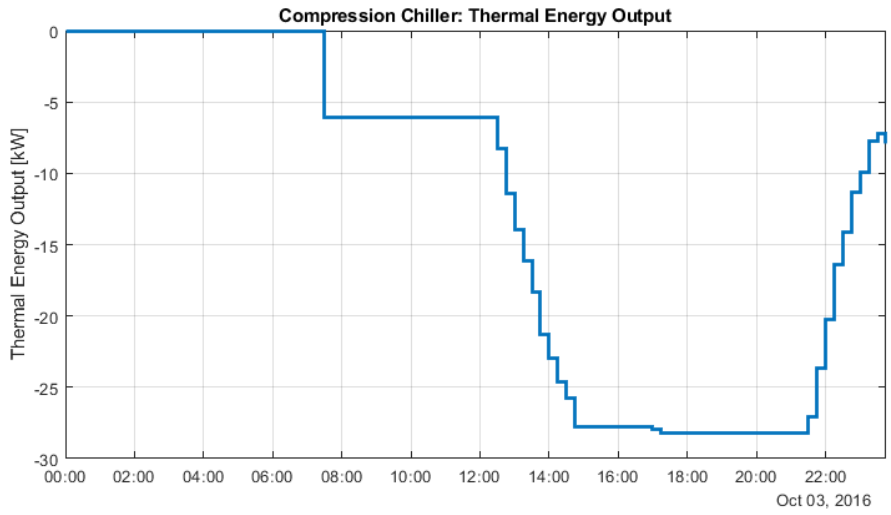

Figure B.27.: Thermal energy output of the compression chiller.

B.2.3. Optimization Parameters

Solving Time

The necessary time to solve each optimization problem in each MPC iteration is depicted in Figure B.28. The solving time is illustrated with respect to the first time step of the considered prediction horizon (x-axis). The dashed line indicates the maximal admissible solving time of 15 min.

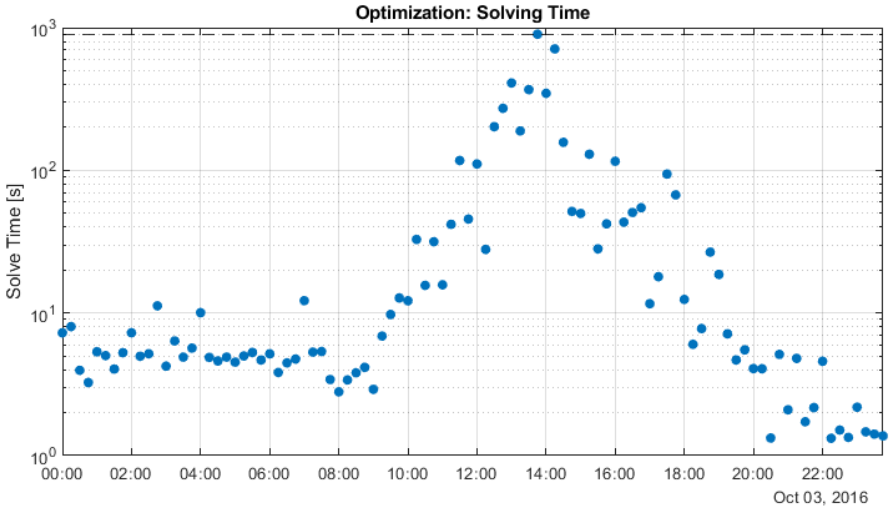

Figure B.28.: Solving times of the control optimization problem.

MIP Gap

The MIP gap associated with each obtained solution is illustrated in Figure B.29, whereby the dashed line indicates the defined maximum admissible MIP gap of 1 %. The optimization ran into a timeout just before 14 : 00 o'clock and was stopped, which led to a higher MIP gap than allowed.

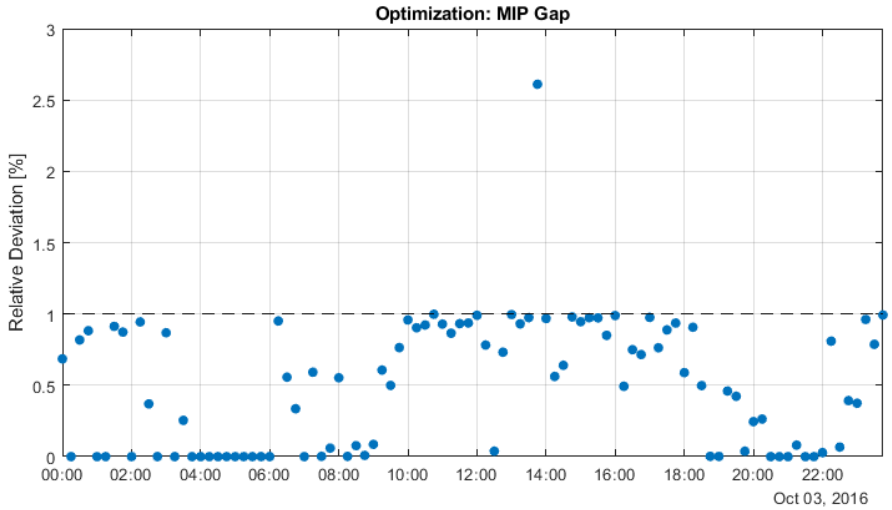

Figure B.29.: Relative deviation of each obtained solution to the optimization problem from the integer integrality relaxed solution (MIP gap).

Bibliography

[1] URL: http://lpsolve.sourceforge.net/5.1/absolute.htm (visited on 09/01/2020) (cit. on p. 31).

[2] Tobias Achterberg and Ali Towle. *Gurobi Webinar: Non-Convex Quadratic Optimization*. URL: https://www.gurobi.com/resource/non-convex-quadratic-optimization/ (cit. on p. 108).

[3] Alberto Bemporad and Manfred Morari. "Control of systems integrating logic, dynamics, and constraints." In: *Automatica* 35.3 (Mar. 1999), pp. 407–427. DOI: 10.1016/s0005-1098(98)00178-2 (cit. on pp. 22, 23, 117).

[4] Jeff Bezanson et al. "Julia: A fresh approach to numerical computing." In: *SIAM review* 59.1 (2017), pp. 65–98. URL: https://doi.org/10.1137/141000671 (cit. on p. 103).

[5] Iain Dunning, Joey Huchette, and Miles Lubin. "JuMP: A Modeling Language for Mathematical Optimization." In: *SIAM Review* 59.2 (2017), pp. 295–320. DOI: 10.1137/15M1020575 (cit. on p. 103).

[6] European Commission Joint Research Centre. *Photovoltaic Geographical Information System*. Version 5.1. 2001. URL: https://ec.europa.eu/jrc/en/pvgis (cit. on p. 98).

[7] Tobias Fleiter et al. *Profile of heating and cooling demand in 2015*. Research rep. Version D 3.1. Heat Roadmap Europe, 2017. URL: https://heatroadmap.eu/wp-content/uploads/2018/09/3.1-Profile-of-the-heating-and-cooling-demand-in-the-base-year-in-the-14-MSs-in-the-EU28-2.pdf (cit. on p. 1).

[8] Christian Gottschall. *Logic calculator*. Apr. 9, 2020. URL: https://www.erpelstolz.at/gateway/formular-uk-zentral.html (visited on 09/01/2020) (cit. on p. 89).

[9] LLC Gurobi Optimization. *Gurobi Optimizer Reference Manual*. 2020. URL: http://www.gurobi.com (cit. on p. 103).

[10] *IEC 61970: Energy management system application program interface (EMS-API)*. Tech. rep. International Electrotechnical Commission, Dec. 7, 2005 (cit. on p. 16).

[11] Peter Kovacs. *A guide to the standard EN 12975*. Tech. rep. Version Deliverable D2.3. QAiST - IEE/08/593/SI2.529236, 2012. URL: http://www.estif.org/fileadmin/estif/content/projects/QAiST/QAiST_results/QAiST%20D2.3%20Guide%20to%20EN%2012975.pdf (cit. on pp. 9, 28).

[12] Pierluigi Mancarella. "MES (multi-energy systems): An overview of concepts and evaluation models." In: *Energy* 65 (Feb. 2014), pp. 1–17. DOI: 10.1016/j.energy.2013.10.041 (cit. on p. 18).

[13] M.C. McManus. "Environmental consequences of the use of batteries in low carbon systems: The impact of battery production." In: *Applied Energy* 93 (May 2012), pp. 288–295. DOI: 10.1016/j.apenergy.2011.12.062. URL: https://www.sciencedirect.com/science/article/pii/S0306261911008580 (cit. on p. 2).

[14] Domenico Mignone. "Control and estimation of hybrid systems with mathematical optimization." en. PhD thesis. 2002. DOI: 10.3929/ETHZ-A-004279802 (cit. on pp. 89, 118, 122).

[15] Michael Moran. *Principles of Engineering Thermodynamics*. Vol. 7. Singapore: Wiley, 2012. ISBN: 9780470918012 (cit. on pp. 65, 67).

[16] A. Moser et al. "A MILP-based modular energy management system for urban multi-energy systems: Performance and sensitivity analysis." In: *Applied Energy* 261 (Mar. 2020), p. 114342. DOI: 10.1016/j.apenergy.2019.114342. URL: https://www.sciencedirect.com/science/article/pii/S030626191932029X (cit. on pp. 19, 40).

[17] Daniel Muschick et al. "A multi-layer model of stratified thermal storages for MILP-based energy management systems." In: *Not yet published* (2021) (cit. on pp. iii, v, 11, 15, 45, 89).

[18] Thomas Nigitz and Markus Gölles. "A generally applicable, simple and adaptive forecasting method for the short-term heat load of consumers." In: *Applied Energy* 241 (May 2019), pp. 73–81. DOI: 10.1016/j.apenergy.2019.03.012 (cit. on pp. 27, 29).

[19] Lanre Olatomiwa et al. "Energy management strategies in hybrid renewable energy systems: A review." In: *Renewable and Sustainable Energy Reviews* 62 (Sept. 2016), pp. 821–835. DOI: 10.1016/j.rser.2016.05.040 (cit. on p. 18).

[20] S.Joe Qin and Thomas A. Badgwell. "A survey of industrial model predictive control technology." In: *Control Engineering Practice* 11.7 (July 2003), pp. 733–764. DOI: 10.1016/s0967-0661(02)00186-7 (cit. on p. 111).

[21] Arian J. van der Schaft and Hans Schuhmacher. *An Introduction to Hybrid Dynamical Systems*. 2000 (cit. on p. 117).

[22] Thomas Schütz, Rita Streblow, and Dirk Müller. "A comparison of thermal energy storage models for building energy system optimization." In: *Energy and Buildings* 93 (Apr. 2015), pp. 23–31. DOI: 10.1016/j.enbuild.2015.02.031 (cit. on pp. 44, 46).

[23] David Steen et al. "Modeling of thermal storage systems in MILP distributed energy resource models." In: *Applied Energy* 137 (Jan. 2015), pp. 782–792. DOI: 10.1016/j.apenergy.2014.07.036 (cit. on p. 43).

[24] United Nations. *Kyoto Protocol*. Dec. 11, 1997. URL: https://unfccc.int/kyoto_protocol (cit. on p. 1).

[25] United Nations. *Paris Agreement*. New York, Dec. 12, 2015. URL: https://unfccc.int/process-and-meetings/the-paris-agreement/the-paris-agreement (cit. on p. 1).

[26] Viktor Unterberger et al. "Adaptive Methods for Energy Forecasting of Production and Demand of Solar Assisted Heating Systems." English. In: *ITISE 2018 International Conference on Time Series and Forecasting*. Vol. 1. Sept. 2018, pp. 170–181 (cit. on pp. 27, 29).

[27] Luca Urbanucci, Francesco D'Ettorre, and Daniele Testi. "A Comprehensive Methodology for the Integrated Optimal Sizing and Operation of Cogeneration Systems with Thermal Energy Storage." In: *Energies* 12.5 (Mar. 2019), p. 875. DOI: 10.3390/en12050875 (cit. on p. 10).

[28] Sharon J. Wagner and Edward S. Rubin. "Economic implications of thermal energy storage for concentrated solar thermal power." In: *Renewable Energy* 61 (Jan. 2011), pp. 81–95. DOI: 10.1016/j.renene.2012.08.013 (cit. on p. 2).

[29] Joko Waluyo and Mohd Abd Majid. "Temperature Profile and Thermocline Thickness Evaluation of a Stratified Thermal Energy Storage Tank." In: *International Journal of Mechanical and Mechanics Engineering* (Feb. 2010). URL: https://www.researchgate.net/publication/277735695_Temperature_Profile_and_Thermocline_Thickness_Evaluation_of_a_Stratified_Thermal_Energy_Storage_Tank (cit. on p. 90).

[30] Muhammad Fahad Zia, Elhoussin Elbouchikhi, and Mohamed Benbouzid. "Microgrids energy management systems: A critical review on methods, solutions, and prospects." In: *Applied Energy* 222 (July 2018), pp. 1033–1055. DOI: 10.1016/j.apenergy.2018.04.103 (cit. on p. 18).

[31] Sandra Zlabinger. "Schichtspeichermodellierung als Grundlage für die Entwicklung modellprädiktiver Regelungen von Wärmeversorgungssystemen." MA thesis. Technische Universität Graz. URL: https://permalink.obvsg.at/tug/AC15366852 (cit. on pp. 11, 54, 90).